TESI DOCTORAL

Títol	**Channel sounding and physical layer definition for the HF long-haul radio link between Antarctica and Spain**
Realitzada per	**Marcos Antonio Hervás García**
en el Centre	**Escola Tècnica Superior d'Enginyeria Electrònica i Informàtica La Salle**
i en el Departament	**Comunicacions i Teoria del Senyal (DCTS)**
Dirigida per	**Dr. Joan Lluis Pijoan Vidal** i **Dra. Rosa Maria Alsina Pagès**

C. Claravall, 1-3
08022 Barcelona
Tel. 936 022 200
Fax 936 022 249
E-mail: urlsc@sec.url.es
www.url.es

Thesis for the degree of Doctor of Philosophy

Channel sounding and physical layer definition for the HF long-haul radio link between Antarctica and Spain

MARCOS ANTONIO HERVÁS GARCÍA

ENGINYERIA I ARQUITECTURA LA SALLE

UNIVERSITAT RAMON LLULL

December 2015

Channel sounding and physical layer definition for the HF long-haul radio link between Antarctica and Spain
PhD program: Information Technologies and its Management, ©

Marcos Antonio Hervás García

Departamento de Comunicaciones
y Toría de la Señal (DCTS)

Enginyeria i Arquitectura La Salle
Universitat Ramon Llull
c/Quatre Camins, 30,
08022, Barcelona

Supervisors: Dr. Joan Lluís Pijoan and Dra. Rosa-Ma Alsina-Pagès

A Celia.
A mi hermana Elia.
A mis padres, Antonio y Milagros,
os debo lo que soy, gracias.

Abstract

La comunicación por rebote ionosférico en la banda de HF se presenta como un buen candidato en el establecimiento de llamadas y transmisión de datos en aplicaciones militares, países en vías de desarrollo, catástrofes naturales o como sistema de *backup* gracias a la sencillez del despliegue del sistema y al bajo coste que supone. Los estándares actuales de comunicaciones HF definen *bit rates* entre 75 y 12.800 bps, dependiendo de las condiciones del canal, empleando un ancho de banda de 3 kHz. Los últimos avances incluyen funcionalidades de *Automatic Link Establishment* (ALE) y *Automatic Repeat Request* (ARQ), permitiendo establecer el enlace de comunicación y solicitando la retransmisión de datos cuando un paquete se haya perdido de manera automática, sin la necesidad de que el usuario sea un técnico experto.

En este proyecto se han definido dos objetivos científicos: *i)* estudiar la variabilidad de este canal ionosférico HF durante un ciclo solar completo y *ii)* proponer una nueva capa física adaptada a este canal. Esta tecnología se emplea como sistema de transmisión de los datos de los sensores instalados en la *Antarctic Station Juan Carlos I* (ASJI) por la comunidad científica desplazada a la isla y Cambrils (España). Estableciendo un radio enlace unidireccional de 12.760km. El sistema implementado es de muy baja potencia, 200 W, empleando un sencillo monopolo en transmisión debido a las restricciones medioambientales impuestas por el tratado antártico. Se han revisado los distintos estándares de HF para poder desplegar éste radio-enlace, sin embargo, ninguno de ellos cumple con los bajos niveles de SNR observados. Por lo tanto, se debe diseñar un nuevo esquema de modulación para poder establecer la comunicación.

Esta tesis aplica los sondeos de banda estrecha y banda ancha para el estudio de la variabilidad del canal, aplicándolos a la campaña 2013-2014 y obteniendo los resultados de ésta para mantener la serie histórica. Para la propuesta de capa física, se estudian técnicas de modulación *multi carrier* y de espectro ensanchado, a partir de resultados previos, y se analizan y prueban diversas técnicas de *single carrier*. Finalmente, se han definido dos es-

quemas de modulación de capa física para emplear en condiciones de canal pobre y moderado.

Keywords: High Frequency (HF), Ionospheric Communications, Hostile Channels, Sounding, Direct-Sequence Spread Spectrum (DSSS), Orthogonal Frequency Division Multiplexing (OFDM), Single Carrier Frequency Domain Equalization (SC-FDE), Single Carrier Frequency Division Multiplexing Access (SC-FDMA).

Agradecimientos

En primer lugar deseo expresar mi agradecimiento al director de esta Tesis, Dr. Joan Lluis Pijoan, por haber confiado en mí y haberme instado a realizar esta Tesis Doctoral, así como por sus consejos, recomendaciones y dedicación.

De mi etapa realizando proyectos de transferencia de tecnología, me gustaría agredecerle a Ricard Aquilué el haberme transmitido su pasión por las FPGAs, el desarrollo de proyectos de *Hardware*, el gusto por la buena comida japonesa, así como tantos ratos divertidos. A Xavier Rosell y a Albert-Miquel Sánchez, agradecerles los buenos momentos que me han hecho pasar en el restaurante, y el apoyo en los no tan divertidos y estresantes. Sois muy grandes todos.

A David Badia, por todos los consejos de EMC, gastronomía, batallitas variadas, ser cómplice en las escursiones a la cafetería a media tarde, y sobretodo por saber escuchar y aconsejar. Al resto de los antárticos, de los que en un momento u otro he aprendido algo, sobretodo a Martí Salvador, por haber trabajado conmigo codo con codo durante tanto tiempo, y habernos sentado a discutir una y mil veces el análisis de los resultados obtenidos y la propuesta de nuevas pruebas durante incontables horas. En lo personal, por el gran amigo que has sido y eres, llegando incluso a compartir vivienda.

A Àlex Barco, por el apoyo, las sesiones de auto-ayuda y las risas, por compartir preocupaciones e inquietudes así como esa preciada base de datos de buenos restaurantes de Barcelona, gracias por compartirla ”en parte”, en definitiva por ser como eres. A Ferran, que en un corto periodo de tiempo, has demostrado ser una gran persona. A Àngels Aragonés y Joan Navarro por compartir inquietudes y preocupaciones en este amplio periodo de tiempo, así como comentarios picantes y con mala idea, sois muy grandes tanto como personas como investigadores.

Dicen que los últimos serán los primeros, en este caso es cierto, quiero agradecer a la co-directora de esta Tesis, Dra. Rosa Maria Alsina-Pagès, por haber encontrado en ella no solo un ejemplo de rigor científico, sino un apoyo en cada uno de los momentos en los que la he necesitado. Gracias Rosa.

Sobre el autor

Marcos Hervás obtuvo una Ingeniería Técnica de Telecomunicaciones con especialidad en imagen y sonido en la Universidad de Alicante en el año 2008. En el año 2010 obtuvo una Ingeniería Superior de Telecomunicaciones en la Escuela de Ingeniería de La Salle, Universidad Ramon Llull. Desde el año 2011 al 2015 estuvo trabajando en el área de transferencia de tecnología realizando proyectos de electrónica, también de investigador desarrollando su tesis doctoral y como docente, focalizado en comunicaciones inalámbricas, canales hostiles y *Software Defined Radio* (SDR).

Recopilación de Contribuciones

Esta tesis es un compendio de las contribuciones más relevantes del autor. El trabajo desarrollado en las siguientes tres contribuciones resumen las tareas realizadas durante su proyecto de investigación:

- Hervás, M., Pijoan, J. L., Alsina-Pagès, R. M., Salvador, M., and Badia, D. (2014). Single-carrier frequency domain equalisation proposal for very long haul HF radio links. *Electronics Letters*, 50(17):1252–1254.

- Hervás, M., Alsina-Pagès, R. M., Pijoan, J. L., Salvador, M., and Badia, D. (2015). Advanced modulation schemes for an Antarctic Long Haul HF Link. Performance comparison between SC-FDE, OFDMA and SC-FDMA in a hostile environment. *Telecommunication Systems*, doi: 10.1007/s11235-015-0110-x.

- Hervás, M., Alsina-Pagès, R.M., Orga, F., Altadill, D., Pijoan, J.L. and Badia, D. (2015). Narrowband and Wideband Channel Sounding of an Antarctica to Spain Ionospheric Radio Link. *Remote Sensing*, 7:11712–11730.

El trabajo realizado en esta tesis se enmarca dentro del proyecto de investigación CTM2010-21312-C03, con el título “Monitorizado y análisis de características geomagnéticas e ionosféricas en la Base Antártica Juan Carlos I. Series históricas, modelado y

predicción de perturbaciones ionosféricas y geomagnéticas". Este se realizó en colaboración con el Instituto Universitario Observatorio del Ebro (OE) y el Departamento de Matemática Aplicada IV de la Universidad Politécnica de Cataluña (UPC). La finalidad del cual es la de diseñar un radio modem capaz de enviar los datos de los sensores geomagnéticos distribuidos por la isla de Livingston (Antártida) del Observatorio del Ebro a Cambrils (España) mediante rebote ionosférico. Además de mantener la serie histórica de los sondeos ionosféricos que se han realizado durante los últimos 11 años. Del sondeo oblicuo de la campaña 2012/2013 se ha publicado el siguiente congreso, el cual es un trabajo previo del artículo publicado en la *Remote Sensing* mencionado anteriormente:

- Hervás, M., Alsina-Pagès, R.M., Orga, F., Pijoan, J.L., Badia, D. and Altadill, D. (2015). Narrowband and Wideband Channel Sounding of an Antarctica to Spain Ionospheric Radio Link. *1st Electronic Conference on Remote Sensing*, 22 June–5 July, Sciforum Electronic Conference Series, 1, d003, doi:10.3390/ecrs-1-d003.

Además de realizar sondeo oblicuo, también se ha realizado sondeo vertical en el observatorio del Ebro para estudiar las capacidades de un enlace vertical, *Near Vertical Incidence Skywave* (NVIS), que aglutinase la información de los distintos sensores. De este estudio se ha publicado el siguiente congreso:

- Hervás, M., Pijoan, J. L., Alsina-Pagès, R. M., Salvador, M., and Altadill, D. (2013). Channel sounding and polarization diversity for the NVIS channel. In Proceedings Nordich HF conference, Farö.

En cuanto al estudio de nuevos esquemas de modulación, además de configuraciones basadas en *single carrier* y *multi carrier*, se han probado esquemas basados en espectro ensanchado. Los resultados de estas pruebas están publicados en el siguiente journal:

- Alsina-Pagès, R. M., Salvador, M., Hervás, M., Berguedà, P., Pijoan, J. L., and Badia, D. (2015). Spread spectrum high performance techniques for a long haul high frequency link. *IET Communications*, 9(8):1048–1053.

Finalmente, se ha realizado algún test para demodular datos transmitidos mediante modulación en fase y cuadratura aplicando *Cellular Neural Networks* sin la necesidad de ecualización. Estos resultados se han publicado en el siguiente congreso:

- Alsina-Pagès, R.M., Hervás, M., Vilasís-Cardona, X., Vinyoles-Serra, M. (2014). QPSK demodulation using Cellular Neural Networks, *14th International Workshop on Cellular Neural Networks*, Notre Dame, 29-31 July, IEEE, 1–2, doi:10.1109/CNNA.2014.6888622.

Tabla de Contenidos

Lista de Figuras

Lista de Tablas

Glosario

AD	*Analog to Digital*
ALE	*Automatic Link Establishment*
ARQ	*Automatic Repeat Request*
ASJI	*Antarctic Station Juan Carlos I*
AWGN	*Additive White Gaussian Noise*
BER	*Bit Error Rate*
CDF	*Cummulative Density Function*
CP	*Cyclic Prefix*
CW	*Continuous Wave*
DA	*Digital to Analog*
DCTS	*Departamento de Comunicaciones y Teoría de la Señal*
DS-SS	*Direct-Sequence Spread Spectrum*
EVM	*Error Vector Magnitude*
FED-STD	*Federal Standard*
FFT	*Fast Fourier Transform*
FLA	*Frequency of Large Availability*
FOT	*Frequency of Optimum Transmission*
FPGA	*Field Programmable Gate Array*
GPS	*Global Positioning System*
GRECO	*Grupo de investigación de electrónica y comunicaciones*
GR-SETAD	*Grupo de investigación de sistemas electrónicos, telecomunicaciones y análisis de datos*
HF	*High Frequency*
HTM	*High Throughput Mode*
IBI	*Interblock Interference*
IBO	*Input Back-Off*
ICI	*Inter Carrier Interference*
IONCAP	*Ionospheric Communications Analysis and Prediction Program*

ISI	*Inter Symbol Interference*
ITU-R	*International Telecommunication Union - Radiocommunication Sector*
LFDMA	*Localized FDMA*
LQA	*Link Quality Analysis*
LUF	*Lowest Usable Frequency*
MIL-STD	*Military Standard*
MET	*Máster de Ingeniería de Telecomunicaciones*
MMSE	*Minimum Mean Square Error*
MUF	*Maximum Usable Frequency*
NVIS	*Near Vertical Incidence Skywave*
OFDM	*Orthogonal Frequency Division Multiplexing*
OIS	*Oblique Ionospheric Sounding*
OTAN	*Organización del Tratado del Atlántico Norte*
PAPR	*Peak-to-Average Power Ratio*
PCIe	*Peripheral Component Interconnect Express*
PN	*Pseudo Noise*
PTS	*Partial Transmit Sequence*
PSK	*Phase Shift Keying*
QAM	*Quadrature Amplitude Modulation*
RRC	*Root-Raised Cosine*
RM	*Robust Mode*
SC-FDE	*Single Carrier Frequency Domain Equalization*
SC-FDMA	*Single Carrier Frequency Division Multiple Access*
SDR	*Software Defined Radio*
SIR	*Signal to Interference Ratio*
SLM	*Selected Mapping*
SNR	*Signal to Noise Ratio*
SSB	*Single Side Band*
SSN	*Sun Spot Number*
STANAG	*Standardization Agreement*
TI	*Tone Injection*
TR	*Tone Reservation*
UMLCAR	*University of Massachusetts Lowell's Center for Atmospheric Research*
USB	*Universal Serial Bus*
VIS	*Vertical Incidence Sounding*
VOACAP	*Voice of America Coverage Analysis Program*

ZF	*Zero Forcing*
ZP	*Zero Padding*
3GPP	*3rd Generation Partnership Project*

Parte I

Introducción

Capítulo 1

Marco de trabajo, motivación y metas

En este capítulo el autor presenta los proyectos en los cuales ha estado involucrado así como las trabajos realizados durante su etapa de investigación. También se realiza una breve revisión del estado del arte que ha motivado la investigación recogida en esta tesis doctoral. Finalmente, se presentan los objetivos de dicho trabajo.

1.1 Marco de trabajo

El trabajo de investigación realizado por el autor empieza en 2011 como Ingeniero Técnico de Telecomunicaciones en el Departamento de Comunicaciones y Teoría de la Señal (DCTS) de la escuela de ingeniería La Salle - Universidad Ramon Llull. Como miembro del Grupo de Investigación de Electrónica y Comunicaciones (GRECO), ha participado en diversos proyectos relacionados con el diseño de electrónica de altas prestaciones, comunicaciones digitales y transferencia de tecnología a empresas, así como en varios proyectos de investigación.

En la fase final de su tesis doctoral ha formado parte del Grupo de Investigación de Sistemas Electrónicos, Telecomunicaciones y Análisis de Datos (GR-SETAD), ya que a partir de enero de 2014, debido a una reorganización de los grupos de investigación, el grupo pasó a formar parte del GR-SETAD, participando principalmente en proyectos de investigación.

Desde Septiembre de 2010 a Junio de 2011 trabajó en el diseño de una plataforma digital con arquitectura *Software Defined Radio* (SDR) llamada IRIS [1]. Dicha plataforma emplea una *Field Programmable Gate Array* (FPGA) como núcleo central de procesado del fabricante Xilinx, 2 conversores duales *Analog to Digital* (AD) y *Digital to Analog* (DA), diversos periféricos y buses de entradas/salidas como PCI-e, USB on the go, Gigabit Ethernet, entre

otros. Dicho proyecto se realizó como proyecto final de carrera de la titulación de Ingeniería de Telecomunicaciones del autor y fue financiado mediante un proyecto interno de La Salle. Actualmente se utiliza como recurso docente en uno de los casos del Máster de Ingeniería de Telecomunicaciones (MET). El trabajo recogido en el *technical report* [1] está en revisión en el *International Journal of Electrical Engineering Education*.

Entre 2011 y 2013 participó en un proyecto de transferencia de tecnología para la empresa Testmotors, donde se realizaba la monitorización de multitud de sensores en *Real Time* para el control preventivo de fallos en motores eléctricos, se realizó tanto la electrónica, la cual estaba basada en una FPGA como unidad de procesado, como el *Firmware* del producto. Este proyecto fue financiado por la empresa Testmotos bajo el código de proyecto SASME.

En Febrero de 2013 se incorporó en el proyecto conocido como **Proyecto Antártico**. Dicho proyecto tenía como objetivos el sondeo de banda estrecha y de banda ancha del canal ionosférico entre la Antártida y Cambrils (España), durante un ciclo solar completo, así como la transmisión de los datos de los sensores distribuidos por la Base Antártica Española Juan Carlos I (ASJI). Dichos datos son recopilados por la comunidad científica desplazada a la isla, y la transmisión se realiza mediante rebote ionosférico con técnicas que emplean muy baja potencia utilizando la frecuencia óptima en base a los sondeos realizados previamente. El proyecto ha sido financiado por el gobierno español CTM2010-21312-C03, CTM2009-13843-C02, CGL2006-12437-C02 y REN2003-08376-C02, y por la Universidad Ramon Llull 2014-URL-Trac-018 y 2015-URL-Proj-041.

1.2 Motivación

En esta sección se ha recopilado información de los hechos históricos más relevantes de las radiocomunicaciones, además del estudio del comportamiento de la ionosfera así como los estándares de comunicación que han ido apareciendo en la banda de *High Frequency* (HF), 3-30 MHz.

1.2.1 Hechos históricos más relevantes

En [2] se considera la publicación de James Clerk Maxwell en 1873 del *Treatise on Electricity and Magnetism* [3] como el nacimiento de las comunicaciones *Wireless*, ya que este trabajo sentó las bases teóricas de la propagación electromagnética moderna. Sin embargo, no fue hasta el año 1888 cuando se detectaron las primeras ondas radio por Heinrich Rudolph

Hertz, quien demostró que las perturbaciones generadas en una *Spark Coil* experimentaban el mismo comportamiento definido por Maxwell.

Dicho trabajo inspiró a Nikola Tesla y a Guglielmo Marconi a experimentar con la telegrafía inalámbrica empleando código Morse. Marconi consiguió enviar mensajes mediante un radio enlace de unos pocos km en 1896. Pese a que se pensaba que los radio-enlaces requerían de visión directa, descartando las comunicaciones *over the horizon*, en 1901 detectó una señal telegráfica transmitida a 3000 km de distancia.

Edward Appleton dio respuesta al porque se podía recibir señales en cualquier punto del planeta pese a la no visión directa. Appleton [4] descubrió que existía una región de la atmósfera cargada con partículas ionizantes (ionosfera), la cual tiene la capacidad de reflejar algunas ondas incidentes. A mediados de la década de los años 20, aplicando dicha teoría se desarrollaron mecanismos de medida y predicción de las propiedades reflectoras de la ionosfera. En la II Guerra Mundial se estableció el primer radio enlace de alto alcance permitiendo comunicaciones entre tierra, mar y aire. El establecimiento de dichos radio enlaces requería de técnicos expertos con años de experiencia, que conocían los efectos que producía la variabilidad de la ionosfera en dicha propagación.

Con la aparición de las comunicaciones por satélite en los años 60, el interés por las comunicaciones HF cayó, quedando relegado su uso en sistemas de *backup*. Sin embargo, en la última década, el interés por parte de la comunidad científica en las comunicaciones HF se ha incrementado, ya que además de sistema de *backup* es un buen candidato para el establecimiento de redes de comunicaciones en países en vías de desarrollo y en situaciones de emergencias debido a catástrofes naturales [5]. Dicho interés ha provocado la aparición de sistemas *Automatic Link Establishment* (ALE), dicho sistema permite utilizar una radio HF de igual manera que un teléfono móvil convencional, no requiriendo de un técnico experto en el establecimiento de la llamada.

1.2.2 Canal ionosférico

La ionosfera es la región de la atmósfera comprendida entre los 50 y 500 km de altura, esta contiene gases de diferente composición y densidad, dependiendo de la altura y el tiempo pueden ser ionizados por la radiación solar [6]. Esta actividad provoca la aparición de electrones libres que se liberan de los átomos o moléculas neutras, convirtiendo a estos en átomos o moléculas ionizadas, este gas recibe el nombre de plasma. Los electrones liberados se mueven libremente produciendo que las ondas electromagnéticas incidentes se

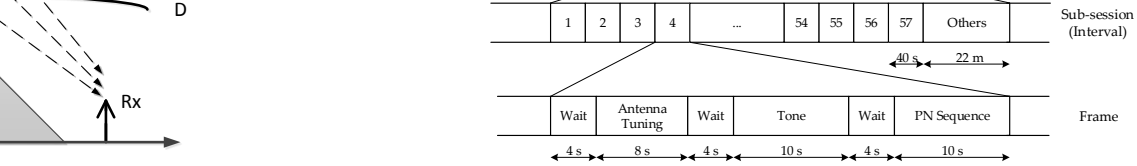

reflejen volviendo hacia la Tierra como puede verse en la Fig. 1.1. Además de la ionización producida por la radiación solar, el campo magnético terrestre, la posición interplanetaria y otras perturbaciones afectan a dicha ionización.

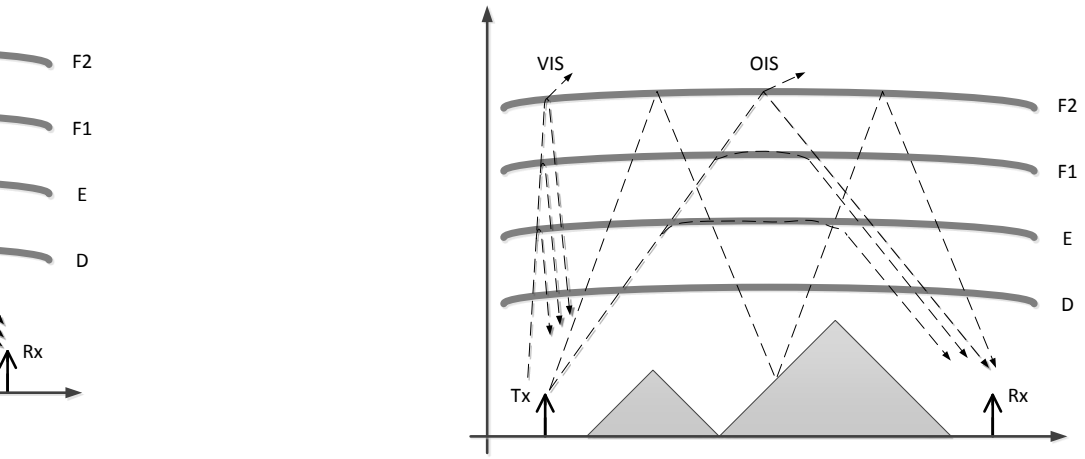

Fig. 1.1 Ejemplo de rebote ionosférico en las distintas capas de la ionosfera para la propagación vertical (VIS) y oblicua (OIS)

Elementos que afectan a la ionosfera

La radiación solar es la encargada de la formación de la ionosfera, principalmente los rayos X y la luz ultravioleta. Uno de los fenómenos solares más importantes en dicha ionización es el número de manchas solares o *Sun Spot Number* (SSN) [6], el SSN mide el número de estas manchas solares sobre la superficie solar. El SSN tiene una periodicidad media de 10.7 años, que se conoce como ciclo solar, cuando este número es elevado, la ionización también lo es.

Otro efecto derivado de la actividad solar que afecta a la formación de la ionosfera es el viento solar [6]. El viento solar está formado por un plasma que se ha separado del sol siguiendo unas lineas de campo magnético, dichas líneas de campo son diferentes en función de la posición de la Tierra respecto al sol. Cuando dicho plasma llega a la Tierra interacciona con el campo magnético, deformándolo, de esta manera se modifican las propiedades de la ionosfera.

El campo magnético terrestre, que está desplazado 11° respecto al eje de rotación de la Tierra, interacciona con el plasma dando lugar al magnetoplasma. El magnetoplasma produce oscilaciones tanto en los iones como los electrones por la fuerza de Lorentz a una cierta frecuencia conocida como *gyrofrequency* convirtiendo la ionosfera en un medio

Tabla 1.1 Distancia (en km) de las distintas capas de la ionosfera

Región	*Altura* (km)
D	50-90
E	90-140
F1	140-210
F2	$\geq$210

anisótropo [6]. Estas oscilaciones producen que la onda electromagnética se separe en dos, una polarizada a izquierdas respecto al campo magnético conocida como ordinaria (O) y otra polarizada a derechas conocida como extraordinaria (X). Dicha separación tiene las siguientes consideraciones:

- Las ondas O y X tienen trayectorias diferentes y se reflejan a diferentes alturas.
- La absorción que provoca la ionosfera en la onda X es mayor en que la O.

Morfología

La ionosfera se divide en capas que coinciden con las regiones que poseen picos de densidades de electrones libres [7]. Chapman propuso un modelo para estimar la densidad de electrones libres en función de la altura [8], ya que la composición de esta, gases y moléculas, dependen de la altura. Las partículas más pesadas se encuentran con mayor frecuencia cerca de la Tierra, mientras que las más ligeras están a mayor distancia del planeta.

Las regiones de la ionosfera reciben el nombre de capa D, E, F1 y F2 [9] y su altura puede consultarse en la tabla 1.1, dependiendo de la literatura revisada dicha altura puede verse alterada ligeramente.

Al igual que la ionización de la ionosfera, el comportamiento de dichas capas se ve alterado en función de la estación del año, así como de la hora del día y la latitud, ya que de ésta depende la intensidad de la radiación solar, variando en función del punto del ciclo solar. Por todo ello, se dice que la morfología de la ionosfera presenta variaciones intra-diarias, estacionales y geográficas con un periodo medio de 11 años. Las particularidades más relevantes de cada capa, desde el punto de vista de las telecomunicaciones, se resumen a continuación [2].

- La capa D es la región más interna de la ionosfera, se ioniza durante las horas del día, alcanzando su máximo nivel cuando el sol está en su zenit y se disipa rápidamente cuando el sol se pone.

- La capa E alcanza su nivel de ionización máximo a mediodía, comienza a disiparse cuando el sol se pone y alcanza su valor de ionización mínimo a medianoche. Ocasionalmente se forman nubes irregulares de gases ionizados, que se conoce como la capa E esporádica E_s, esta capa es capaz de reflejar señales desde la parte alta de la banda de HF en adelante.

- La capa F es la región más ionizada de la ionosfera, la recombinación de iones y electrones se realiza muy lentamente a estas alturas, por lo tanto, las propiedades de la ionización se mantienen después de ponerse el sol. Durante las horas del día se pueden distinguir dos capas, F1 y F2. La capa F1 solo existe durante las horas del día y es prácticamente inexistente en invierno. La capa F2 alcanza su máximo nivel de ionización a mediodía y permanece cargada durante la noche, gradualmente se descarga hasta alcanzar su mínimo, justo antes del alba.

Durante las horas del día se requiere que la frecuencia de la onda electromagnética sea lo suficientemente elevada como para penetrar las capas D y E, pero no tanto como para penetrar la capa F, ya que sino no se alcanzaría el rebote ionosférico. El rango de frecuencias que suele cumplir esta restricción está comprendido entre 10 y 20 MHz. Dichas frecuencias suelen penetrar la capa F durante las horas nocturnas, por lo tanto, el rango de frecuencias empleado está comprendido entre 3 y 8 MHz.

Las capas D y E absorben o debilitan la señal, por lo tanto, en invierno cuando la radiación solar es menor, esta no alcanza suficientemente dichas capas y la ionización es menor, permitiendo que señales de menor frecuencia se propaguen fácilmente hasta alcanzar la capa F, dando lugar a comunicaciones de gran alcance.

Durante los mínimos de SSN las frecuencias por encima de 20 MHz no se pueden emplear debido al bajo nivel de ionización de las capas E y F.

Parametrización, caracterización y sistemas de predicción de la propagación HF

Debido a la variabilidad de la ionosfera y al efecto que esta produce sobre la propagación, se han definido parámetros de optimización del uso de frecuencias.

- La mayor frecuencia que puede usarse para establecer un canal de comunicaciones ionosférico HF se conoce como la *Maximum Usable Frequency* (MUF) [6], frecuencias mayores penetran la ionosfera y se propagan por el espacio.
- A bajas frecuencias, el nivel de absorción de la capa D aumenta, llegando a absorber por completo la onda electromagnética. La frecuencia a la que esto ocurre se conoce con el nombre de *Lowest Usable Frequency* (LUF) [6]. Se define una ventana de utilización entre la LUF y la MUF.
- *Frequency of Optimum Transmission*(FOT) [6], es aquella que produce un nivel de señal en recepción máximo, suele estar al 85% de la MUF.

Dispersión temporal [10]: La dispersión temporal es la medida del ensanchamiento temporal que experimenta un pulso al viajar a través del medio. En concreto, corresponde al intervalo de retardo que provoca que la función de autocorrelación de la respuesta impulsional del canal sea diferente de cero, o en la práctica, superior a un cierto umbral.

Principalmente hay dos causas que provocan dicho ensanchamiento temporal [11].

- *Multipath Spread*. La señal transmitida puede seguir varias trayectorias hasta llegar al punto de recepción, esto es debido a que puede reflejarse en diversas capas, es decir, a diferentes alturas produciendo diferentes tiempos de llegada, además la separación de la onda electromagnética en ordinaria y extraordinaria debido al campo magnético también produce que la señal se refleje a diferentes alturas. Por último, si el transmisor y el receptor están situados a poca distancia, se puede producir la recepción de la *ground wave*, esta onda llegaría al receptor antes que las rebotadas en la ionosfera debido a que la distancia recorrida es menor.
- *Delay Spread*. El índice de reflexión de la ionosfera depende de la frecuencia, por lo tanto, cuando la señal transmitida tiene un ancho de banda grande, cada frecuencia puede experimentar velocidades de propagación y trayectorias diferentes, produciendo que en recepción la señal llegue en instantes de tiempo diferente.

El ensanchamiento temporal, cuando el ancho de banda de la señal transmitida es mayor que la inversa del *Multipath Delay Spread* [12], contribuciones agregadas del *Multipath Spread y del* Delay Spread, o ancho de banda de coherencia del canal, produce interferencia inter-simbólica (ISI) ya que la señal experimenta los efectos de un canal no plano. En recepción, el *multipath Spread* puede reducirse transmitiendo a frecuencias cercanas a la MUF, ya que la onda se reflejaría solamente en la capa F2.

Dispersión frecuencial [10]: La dispersión frecuencial pretende medir la rapidez con la que el canal varía. El *Doppler Spread* corresponde al rango de frecuencias de la transformada de Fourier en el dominio del tiempo de la función de autocorrelación de la respuesta impulsional del canal diferente de cero, o en la práctica, mayor a un cierto umbral. El *Doppler Spread* es inversamente proporcional al tiempo de coherencia del canal [12], que define el tiempo durante el cual el canal puede considerarse estático.

El *Doppler shift* es la medida del desplazamiento frecuencial respecto a la frecuencia de transmisión de la señal recibida. Principalmente, este efecto puede observarse ya que las capas no son estáticas, es decir, la altura a la que están presentes se desplaza, produciendo el conocido efecto Doppler en recepción. El *Doppler Shift* produce rotaciones en la constelación y es especialmente relevante en la puesta del sol y al amanecer, cuando las capas se mueven a mayor velocidad.

Existen programas de predicción de la propagación. Los más usados son el *Ionospheric Communications Analysis and Prediction* (IONCAP) y el *Voice of America Coverage Analysis Program* (VOACAP). Estos sistemas de predicción están basadas en datos históricos y no tienen en cuenta las condiciones actuales de la ionosfera. Para producir una predicción más precisa de la ionosfera se emplean sondeadores ionosféricos [13]. De hecho, los sistemas HF más avanzados hacen uso de la técnica de *Link Quality Analysis* (LQA), que consiste en emplear estaciones transmisoras y receptoras para medir la calidad del canal automáticamente.

Sondeo de canal

El conocimiento que se tiene del canal ionosférico se ha obtenido gracias al estudio de la estructura de la ionosfera por medio de sondeo ionosférico. Las diferentes técnicas empleadas para realizar dichos estudios están recopiladas en [14]. Las características de mayor relevancia medidas de la propagación ionosférica respecto a una señal de referencia se citan a continuación [6]: *i)* tiempo de propagación, *ii)* fase, *iii)* variaciones de frecuencia, *iv)* medidas de polarización y *v)* ángulo de llegada.

El equipo convencional para medir la altura virtual de la ionosfera es un radar que realiza un barrido de frecuencia llamado ionosonda [6]. El sondeo se puede realizar tanto vertical como oblicuamente, en función de la distribución geográfica del conjunto transmisor/receptor y de la orientación de las antenas (su directividad). Estos sondeos son de gran relevancia desde el punto de vista de telecomunicaciones, ya que coinciden con los dos tipos de radio-

enlaces de comunicaciones HF mediante rebote ionosférico existentes, es decir, *Near Vertical Incidence Skywave* (NVIS) y oblicuo *(Sky wave)*, respectivamente.

Algunos grupos de investigación emplean la señal obtenida por la red *Global Positioning System* (GPS) para dotar de más información a los equipos convencionales de sondeo ionosférico. La técnica empleada consiste en medir las características no deseadas de las señales de los satélites en recepción, tales como desfase, *Multipath Delay Spread* y *Doppler Spread*. Entre otras, uno de las instituciones socias del concierto del proyecto antártico está realizando estas labores, concretamente el Departamento de Matemática Aplicada IV de la UPC. A continuación se hace referencia a algunos de los proyectos de mayor relevancia en el ámbito de las comunicaciones ionosféricas que se han realizado durante los últimos años.

En los últimos años las zonas polares han resultado ser de gran interés para los científicos desde un punto de vista de comunicaciones ionosféricas, ya que no se dispone de suficiente infraestructura para dar cobertura con otras tecnologías como las comunicaciones VHF. En [15] se presentan las medidas de densidad de electrones sobre parches de ionización empleando 2 GPS en Canadá, se atribuyen los picos observados al aumento del *Sun Spot Number*, y debido a este incremento de ionización la máxima frecuencia máxima de recepción aumenta. En [16], se incluye la aparición de estos parches de ionización, propios de los polos, en el modelado del área de cobertura para obtener una simulación mas real que la que se puede realizar con el VOACAP. En [17, 18] se presentan los resultados de las observaciones del efecto Doppler y el *time of flight*, así como el incremento de la frecuencia máxima disponible para transmitir debido a estos parches, estas observaciones se han realizado en distintos instantes de tiempo del ciclo solar.

En colaboración con la NASA, en [19–22] se presena un experimento en el que se ha enviado un cohete capaz de ionizar la región inferior de la capa F2 de la ionosfera de manera artificial, los resultados presentados estudian como el plasma inyectado afecta a la propagación de la señal de las comunicaciones ionosféricas, para realizar estos estudios se ha empleado el sondeo mediante GPS, y el oblicuo y vertical empleando digisondes DPS-4D.

En [23, 24] se presenta una modificación sobre los sistemas de sondeo actual, analizando la señal OFDM empleada en el sistema de difusión DRM en la bada por debajo de los 30 MHz. Se incrementa así el número de datos de que dispone la ionosonda para extraer los resultados del estado actual de la ionosfera.

1.2.3 Estandarización de la capa física

La creación de estándares de comunicaciones HF por el gobierno Americano, *Military Standard* (MIL-STD) y *Federal Standard* (FED-STD), la OTAN, *Standardization Agreement* (STANAG) y otras organizaciones han influenciado en la proliferación de esta tecnología. Estos estándares pretenden obtener la inter-operabilidad entre diferentes sistemas, ya que definen la forma de onda y los protocolos de comunicaciones. Parte del trabajo que recoge esta tesis consiste en el estudio de formas de ondas candidatas (esquemas de modulación) para la definición de la capa física de un enlace de gran alcance con 4-5 *hops* [25], por ello se realizará un repaso de los estándares de capa física más relevantes en las comunicaciones HF.

El primer paso para la estandarización de la capa física comenzó en las décadas de los 70s y 80s del siglo pasado, cuando la industria militar definió como forma de onda una *single carrier Phase-Shift Keying* (PSK), la cual fue incluida en el estándar STANAG 4285 [26] en 1989 y en el MIL-STD-188-110A [27] con alguna modificación en 1991. Los estándares actuales de capa física de comunicaciones HF son *i)* MIL-STD-188-110B [28], *ii)* MIL-STD-188-141B [29], *iii)* STANTAG 4285 [30], *iv)* STANAG 4539 [31] y v) FED-STD-1052 [32]. Estos estándares definen por completo los esquemas de modulación y la codificación de canal que puede ser empleada. A continuación se definen las particularidades de aquellos de mayor relevancia.

STANAG 4285

El STANAG 4285 emplea una modulación BPSK, QPSK u 8-PSK sobre una portadora de 3 kHz de ancho de banda, alcanzando un *throughput* de 1200, 2400 y 3600 bps de datos codificados, respectivamente. La estructura de la trama de transmisión está dividida en 256 segmentos, cada uno de estos segmentos contiene un preámbulo de 80 símbolos (secuencias m de 31 chips) y 4 bloques de 32 símbolos de datos intercalados con 3 bloques de 16 símbolos de *training*. Este estándar emplea un código de canal convolucional con *code rate* 1/2 y un *constraint length* de 7, y un *interleaver* con dos profundidades, 0.8 s y 10.24 s.

MIL-STD-188-110A

El MIL-STD-188-110A [27] es similar al STANAG 4285, aunque incluye algunas características que mejoran las prestaciones respecto al anterior. El uso de preámbulos más grandes aportan más robustez en escenarios en los que las condiciones del canal sean pobres. Además, el hecho de emplear una estructura de trama distinta le permite trabajar con peores condiciones de *Delay Spread* y *Doppler Spread*. Sin embargo, este se comporta peor que

el STANAG 4285 en canales con grandes *fadings*. Este estándar define los siguientes *data rates*: 75, 150, 300, 600, 1200, 2400 y 4800 bps.

La transmisión en modo robusto alcanza 75 bps empleando una modulación de secuencia directa empleando códigos Walsh, dicha técnica se emplea en el estándar STANAG 4415. Esta técnica agrupa los bits de dos en dos y selecciona uno de los 4 *codewords* ortogonales de longitud 4 para cada agrupación. A continuación transmite dicho *codeword* 8 veces consecutivas obteniendo una secuencia de 32 símbolos modulada mediante una 8-PSK. A continuación se enumeran las prestaciones mínimas requeridas por el estándar, empleando el modo de *interleaving* mas profundo (4.8 ms), con el código convolucional definido en el STANAG 4285.

- El módem alcanzará un *Bit Error Rate* (BER) inferior a 10^{-3} con -9 dB de SNR (3 kHz) para un canal con ruido blanco gausiano con un único path (sin *fadings*).

- El módem alcanzará un BER inferir a 10^{-4} con una SNR entre 0 y -1 dB (3 kHz) para un canal con dos paths, los cuales poseen un *Multipath Delay Spread* máximo de 10 ms y un *Doppler Spread* entre 0.5 y 50.0 Hz

- El módem se sincronizará y suministrará un BER inferior a 10^{-5} cuando el *Multipath Delay Spread* sea inferior a 10.0 ms y el *Doppler Spread* entre 2 y 20 Hz para un nivel de SNR igual a 0 dB (3 kHz).

- El módem mantendrá un BER inferior a 10^{-4} con un nivel de SNR de 10 dB cuando el *signal to interference ratio* (SIR) sea de -6, -25 y -40 dB para interferencias del tipo *self interference*, *Single Side Band (SSB) voice* y *Continuous Wave (CW)*, respectivamente.

MIL-STD-188-110B [28]

A mediados de la década de los 90s, el objetivo principal de las entidades estandarizadoras no fue el de buscar la inter-operabilidad entre sistemas, sino el maximizar la eficiencia espectral respecto a la obtenida con los estándares actuales (STANAG 4285 y MIL-STD-188-110A). Para ello se emplearon constelaciones mas complejas (QPSK, 8-PSK, 16-QAM, 32-QAM y 64-QAM) llegando a alcanzar un *throughput* de 12800 bps. Las nuevas formas de onda se detallan en el STANAG 4539 y en el apéndice C del estándar MIL-STD-188-110B, el cual detalla las *waveforms* cuyo *data rate* es mayor a 2400 bps. Este define 3200, 4800, 6400, 8000 y 9600 bps con codificación de canal y 12800 bps sin codificación.

FED-STD-1052 [32]

Este estándar define la misma capa física que el MIL-STD-188-110A (*single tone*).

MIL-STD-188-141B [29]

El apéndice B de este estándar define las formas de onda para usar el ALE de 3^a generación.

En la tabla 1.2 se recogen las principales características de los estándares de mayor relevancia, mencionados anteriormente.

Tabla 1.2 Características de los principales estándares HF de la capa física

Standard Publication	year	Bandwidth and code rate	Modulation	Bit rate [bps]
STANAG 4285	1989	2400 baud/s, 1/2	2,4,8-PSK	1200/2400/3600
MIL-STD-188-110A	1991	2400 baud/s, 1/2,1/4,1/8	Walsh, 2,4,8-PSK	75/150-600/1200/2400
STANG 4415	2000	2400 baud/s, 1/2	Walsh	75
MIL-STD-188-110B	2000	2400 baud/s, 3/4	4,8-PSK, 16,32,64-QAM	3200-12800
STANAG 4539	2000	2400 baud/s, 3/4	4,8-PSK, 16,32,64-QAM	3200-12800

1.3 Objetivos

Las comunicaciones HF son una buena alternativa para la transmisión de datos en áreas remotas, donde el uso de satélites es muy costosa o la cobertura de estos no cubre estas áreas el 100% del tiempo. La Salle ha estado involucrada en el proyecto antártico (CTM2010-21312-C03) durante los últimos 11 años. El proyecto presenta dos objetivos científicos: *i)* obtener un conocimiento profundo de la variabilidad del canal ionosférico en enlaces HF de muy larga distancia durante un ciclo solar completo y *ii)* la propuesta de una nueva capa física adaptada a dicho tipo de canales. Como aplicación práctica se pretende transmitir, empleando dichas comunicaciones, los datos de los sensores geomagnéticos distribuidos por la isla de Livingston en la Antártida, más concretamente en la base antártica española Juan Carlos I. Actualmente los datos de los sensores se envían diariamente a España empleando satélites geostacionarios, sin embargo, el establecimiento del enlace no es siempre posible debido a problemas de cobertura.

Este tesis es la continuación del trabajo de otros investigadores. Vilella realizó los primeros sondeos y propuso un primer esquema de TX [33, 34]. Deumal estudió las técnicas de reducción de PAPR que se deben utilizar en modulaciones multiportadora con limitación de potencia [35]. Ads analizó los sondeos en toda la banda de HF, tanto en banda ancha

como estrecha y propuso mejoras en dichos sondeos [36]. Bergadà dio un paso adelante proponiendo nuevos esquemas de modulaciones multiportadora [37].

Uno de los objetivos de este proyecto es el establecimiento de un enlace ionosférico de 12.760 km entre la base Juan Carlos I y Cambrils (España), para la transmisión de estos datos. En la Fig. 1.2 puede observarse la trayectoria que debe seguir la onda electromagnética propagada desde el transmisor hasta el receptor.

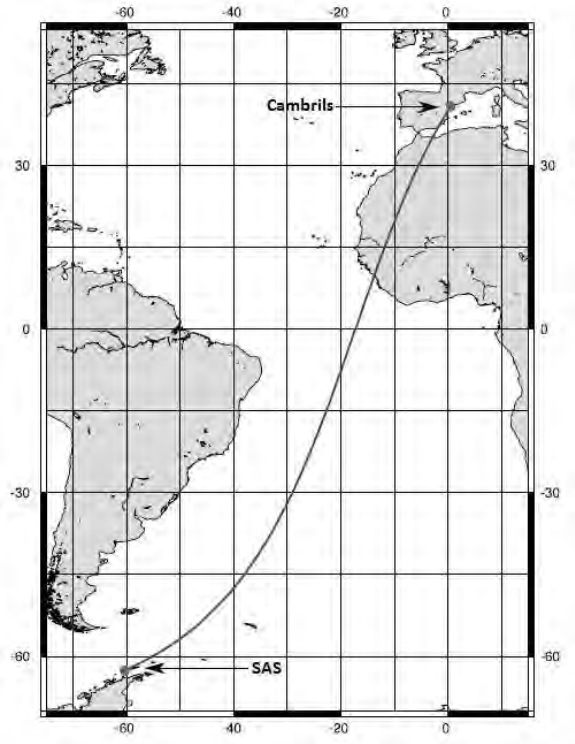

Fig. 1.2 Trayectoria descrita por la onda electromagnética entre la ASJI y Cambrils

El enlace debe tener las siguientes características:

- Este enlace debe ser capaz de transmitir un *throughput* de 5040 bits cada hora para enviar una trama INTERMAGNET (red global de observatorios que monitorizan el campo magnético terrestre) IMF v2.83 cada 12 minutos. Cada trama INTERMAGNET tiene una longitud de 126 bytes.
- El *bit rate* necesario para realizar dicha transmisión debe ser de almenos 8.2 bps para enviar los 5040 bits dentro del intervalo de 10 minutos de que se dispone para la transmisión de datos.

- El retardo máximo de la transmisión de los datos no puede exceder 24 horas.

Debido a que el enlace no está disponible durante el 100% del tiempo, cada INTERMAGNET se envía 3 veces dentro de su slot de transmisión de 10 min, además, en cada slot se envían los datos de las últimas 12 horas para aumentar la probabilidad de recepción correcta cuando el canal no este disponible durante 12 horas seguidas. Esta redundancia impone una restricción de *throughput* de 302.4 bps.

El hecho de instalar un sistema de transmisión en la ASJI impone unas restricciones que limitan las prestaciones del sistema a diseñar. La ASJI solo está abierta durante el verano austral, es decir, entre noviembre y marzo, donde el suministro de energía es limitado. Por lo tanto, la potencia máxima está limitada a 250 W durante el verano austral. Durante el invierno austral la base permanece cerrada y la energía es suministrada por baterías alimentadas mediante generadores eólicos y placas solares.

Por otro lado, debido a la regulación vigente en la Antártida, con restricciones medioambientales, no es posible la instalación de antenas directivas, ya que requieren grandes estructuras. Por lo tanto, el sistema actual utiliza un monopolo de 7.5 m que presenta una ganancia entre -5 y 0 dB con un ángulo de elevación de aproximadamente 10°C. La obtención de dicho ángulo de elevación se ha conseguido mediante la instalación de 32 radiales de 10 metros cada uno que mejoran el plano de tierra.

El sistema de comunicación HF implementado es un enlace unidireccional, por lo tanto no se pueden implementar las técnicas de *Automatic Repeat Request* ARQ y ALE que utilizan los estándares actuales. El sistema debe ser capaz de seleccionar la frecuencia o rango de frecuencias con mayor disponibilidad empleando el mejor esquema de modulación basándose en datos históricos. Por este motivo se han realizado sondeos de canal durante estos 11 años, que corresponde con la duración media de un ciclo solar. Para ello se han realizado *i)* sondeos de banda estrecha que nos permiten obtener las frecuencias con mejor disponibilidad y *ii)* sondeos de banda ancha para obtener las figuras de *Multipath Delay Spread*, *Doppler Spread* y SNR del canal en función de la hora y la frecuencia. En 2008 y 2009, Vilella definió tanto el sondeo de banda estrecha como de banda ancha, así como los requisitos del sistema, y los resultados obtenidos de los sondeos de esas campañas en [33, 34]. En 2013 Ads presentó una mejora sobre el sondeo de banda estrecha en [36], incluyendo un enventanado como filtro, ya que este canal es muy ruidoso y altamente interferido.

Los estándares de comunicación HF en modo robusto requieren un mínimo de 0 dB de SNR para un ancho de banda de 3 kHz. Estos niveles de SNR no son comunes debido a las restricciones ambientales (tipo de antena) y de potencia (250 W) de nuestro sistema. Se considera que los requerimientos mínimos de estándares actuales no cumplen con las condiciones de este enlace. Por lo tanto, se debe definir una capa física en base a la información recopilada en los sondeos de todo el ciclo solar.

Los esquemas de modulación propuestos hasta el momento están basados en la modulación *Direct Sequence Spread Spectrum* (DS-SS) y modulaciones multi-portadora, los cuales ofrecen un *throughput* insuficientes para la transmisión de estos datos. Para el caso de DS-SS se obtuvieron configuraciones con *throughputs* entre 7.94 y 16.3 bps, mientras que para la OFDM entre 71 y 125 bps. Bergadà presentó en [38] los esquemas DS-SS *signaling* y *Orthogonal Frequency Domain Multiplexing* (OFDM) como propuestas de capa física. Por este motivo se han focalizado los esfuerzos en el diseño de esquemas de modulación con *throughputs* mas elevados.

En este trabajo se pretende avanzar en la obtención de dos propuestas de capa física definiendo dos modos de operación, *i) robust mode* (RM) y *ii) high throughput mode* (HTM). El esquema de modulación estudiado para el RM está basado en una modulación de espectro ensanchado DS-SS, dicha modulación emplea un ancho de banda mucho mayor del necesario, por lo tanto, la eficiencia espectral y la densidad espectral de potencia son bajas, reduciendo la interferencia sobre otros usuarios o sistemas. Los esquemas de modulación estudiados para el HTM están basados en la modulación *Single Carrier Frequency Domain Multiplexing Access* (SC-FDMA), que es una variante de la OFDM convencional, que obtiene unos valores de *Peak to Average Power Ratio* (PAPR) mucho menores. También se ha estudiado el uso de la *Single Carrier Frequency Domain Equalisation* (SC-FDE), que es una SC-FDMA con un único usuario.

Referencias

[1] M. Hervás, R.M. Alsina-Pagès, J.L. Pijoan, S. Martí, and D. Badia. IRIS: A software defined radio platform for educational purposes. Technical report, La Salle, URL, 2014.

[2] Harris Corp. *Radio Communications: In the Digital Age*. HF Technology, 2005.

[3] J.C. Maxwell. *A Treatise on Electricity and Magnetism*, volume 1. 1873.

[4] E.V. Appleton and M.A.F. Barnett. On some direct evidence for downward atmospheric reflection of electric rays. *Proceedings of the Royal Society of London. Series A, Containing Papers of a Mathematical and Physical Character*, pages 621–641, 1925.

[5] L.K. Comfort and T.W. Haase. Communication, coherence, and collective action the impact of hurricane katrina on communications infrastructure. *Public Works management & policy*, 10(4):328–343, 2006.

[6] K. Davies. *Ionospheric radio*. Peter Peregrinus Ltd, 1996.

[7] E.E. Johnson, R.I. Desourdis, G. Earle, J.C. Ostergaard, and S Cook. *Advanced high-frequency radio communications*. Artech House Telecommunications Library, 1997.

[8] S. Chapman. The absorption and dissociative or ionizing effect of monochromatic radiation in an atmosphere on a rotating earth part II. Grazing incidence. In *Proceedings of the Physical Society*, volume 43, pages 26–45, 1931.

[9] R. Silberstein. The origin of the current nomenclature for the ionospheric layers. *Journal of Atmospheric and Terrestrial Physics*, 13(3-4):382, 1959.

[10] J.G. Proakis and D.G. Manolakis. *Digital communications*, volume 3. McGraw-Hill, 1995.

[11] P.S. Cannon. Ionospheric propagation and modelling for modern HF communication systems. In *Proceedings Nordich HF conference*, Farö, 1998.

[12] B. Sklar. Rayleigh fading channels in mobile digital communication systems. ii. mitigation. *Communications Magazine, IEEE*, 35(7):102–109, 1997.

[13] B.W. Reinisch, I.A. Galkin, G.M. Khmyrov, A.V. Kozlov, I.A. Lisysyan, K. Bibl, G. Cheney, D. Kitrosser, S. Stelmash, K. Roche, et al. Advancing digisonde technology: the dps-4d. In *Radio Sounding and Plasma Physics, AIP Conference Proceedings*, volume 974, pages 127–143, 2008.

[14] R.D. Hunsucker. Radio techniques for probing the terrestrial ionosphere. In *Springer-Verlag*, New York, USA, 1990.

[15] D.R. Siddle, A.J. Stocker, E.M. Warrington, N.Y. Zaalov, and M.J. Homam. Simultaneous observations of transionospheric and hf ionospheric propagation within the polar cap. *Radio Science*, 48(5):564–572, 2013.

[16] J.S. Naylor, E.M. Warrington, N.Y. Zaalov, and A.J. Stocker. Hf propagation modelling within the polar ionosphere. In *Ionospheric Radio Systems and Techniques (IRST 2012), 12th IET International Conference on*, pages 1–5. IET, 2012.

[17] A.J. Stocker, E.M. Warrington, and D.R. Siddle. Observations of doppler and delay spreads on hf signals received over polar cap and trough paths at various stages of the solar cycle. *Radio Science*, 48(5):638–645, 2013.

[18] A.J. Stocker, D.R. Siddle, E.M. Warrington, N.Y. Zaalov, M.J. Homam, D.H. Boteler, D.W. Danskin, G. De Franceschi, and S.E. Ascaneus. Oblique propagation of hf signals in the polar cap ionosphere. In *Antennas and Propagation (EuCAP), 2013 7th European Conference on*, pages 2694–2698. IEEE, 2013.

[19] D.R. Joshi, K.M. Groves, W.J. McNeil, R.G. Caton, R.T. Parris, T.R. Pedersen, P.S. Cannon, M.J. Angling, and N.K. Jackson-Booth. Hf propagation effects caused by an artificial plasma cloud in the ionosphere. In *AGU Fall Meeting Abstracts*, volume 1, page 3922, 2014.

[20] K.M. Groves, R.G. Caton, T.R. Pedersen, R.T. Parris, Y. Su, P.S. Cannon, N.K. Jacksonbooth, M.J. Angling, and J.M. Retterer. The metal oxide space clouds (mosc) experiment: High frequency (hf) signatures and interactions with the ambient ionosphere. In *AGU Fall Meeting Abstracts*, volume 1, page 05, 2013.

[21] R.G. Caton, T.R. Pedersen, R.T. Parris, K.M. Groves, P.A. Bernhardt, and P.S. Cannon. First look at results from the metal oxide space cloud (mosc) experiment. In *AGU Fall Meeting Abstracts*, volume 1, page 2011, 2013.

[22] N. Jackson-Booth, P. Cannon, M. Angling, R. Caton, K. Groves, T. Pedersen, R. Parris, and Y. Su. Preliminary hf results from the metal oxide space cloud (mosc) experiment. In *General Assembly and Scientific Symposium (URSI GASS), 2014 XXXIth URSI*, pages 1–4. IEEE, 2014.

[23] J. Mlynarczyk, P. Koperski, and A. Kulak. Multiple-site investigation of the properties of an hf radio channel and the ionosphere using digital radio mondiale broadcasting. *Advances in Space Research*, 49(1):83–88, 2012.

[24] Z. Zhao, X. Wan, D. Zhang, and F. Cheng. An experimental study of hf passive bistatic radar via hybrid sky-surface wave mode. *Antennas and Propagation, IEEE Transactions on*, 61(1):415–424, 2013.

[25] J. Perkiomaki. HF Propagation Prediction and Ionospheric Communication Analysis, 2003.

[26] Standardization Agreement 4285. Characteristics of 1200/2400/3600 Bits per Second Single Tone Modulators/Demodulators for HF Radio Links. Technical report, North Atlantic Treaty Organization Std, 1989.

[27] MIL-STD-188-110A. Interoperability and Performance Standards for data modems. Technical report, Department of Defense, USA, 1991.

[28] MIL-STD-188-110B. Interoperability and Performance Standards for data modems. Technical report, Department of Defense, USA, 2000.

[29] MIL-STD-188-141B. Interoperability and Performance Standards for Medium and High Frequency HF Radio Equipment. Technical report, Department of Defense, USA, 1999.

[30] Standardization Agreement 4285. Characteristics of 1200/2400/3600 Bits per Second Single Tone Modulators/Demodulators for HF Radio Links. Technical report, North Atlantic Treaty Organization, 1989.

[31] Standardization Agreement 4539. Technical Standards for Non-Hopping HF Communications Waveforms. Technical report, North Atlantic Treaty Organization, 2000.

[32] FED-STD-1052. elecommunications: HF Radio Modems. Technical report, U.S. Army Soldier Systems Cente, 1990.

[33] C. Vilella, D. Miralles, and J.L. Pijoan. An Antarctica-to-Spain HF ionospheric radio link: Sounding results. *Radio Science*, 43(4), 2008.

[34] C. Vilella, D. Miralles, D. Altadill, F. Acosta, J.G. Solé, J.M. Torta, and J.L. Pijoan. Vertical and oblique ionospheric soundings over a very long multihop HF radio link from polar to midlatitudes: Results and relationships. *Radio Science*, 44(2), 2009.

[35] M. Deumal, A. Behravan, and J.L. Pijoan. On cubic metric reduction in ofdm systems by tone reservation. *Communications, IEEE Transactions on*, 59(6):1612–1620, 2011.

[36] A.G. Ads, P. Bergadà, C. Vilella, J.R. Regué, J.L. Pijoan, R. Bardají, and J. Mauricio. A comprehensive sounding of the ionospheric HF radio link from Antarctica to Spain. *Radio Science*, 48(1):1–12, 2013.

[37] P. Bergadà, R.M. Alsina-Pagès, J.L. Pijoan, M. Salvador, J.R. Regué, D. Badia, and S. Graells. Digital transmission techniques for a long haul HF link: DSSS versus OFDM. *Radio Science*, 49, 2014.

[38] P. Bergadà, M. Deumal, C. Vilella, J.R. Regué, D. Altadill, and S. Marsal. Remote sensing and skywave digital communication from antarctica. *Sensors*, 9(12):10136–10157, 2009.

Capítulo 2

Trabajo de investigación

En este capítulo se describe el trabajo realizado por el autor durante la fase de investigación de su tesis doctoral. Dicho trabajo puede dividirse en dos bloques, *i)* sondeo de canal y *ii)* técnicas de transmisión.

Ha habido dos líneas de estudio dentro del grupo de investigación, por un lado se han realizado sondeos de banda ancha y banda estrecha para generar conocimiento de este canal de comunicaciones a lo largo de todo un ciclo solar, y por otro lado se han probado nuevos esquemas de modulación para realizar la transmisión de datos entre la Antártida y España mediante rebote ionosférico. En cuanto a los sondeos de banda estrecha y banda ancha, la técnica de análisis de estos se presentó en [1]. Más adelante, se introdujeron mejoras respecto al sondeo de banda estrecha [2], aplicando el filtrado paso bajo mediante enventanado y dividiendo la recepción en 14 slots de tiempo, 4 s de silencio para medir la potencia de ruido y 10 s para la potencia de señal. Sin embargo, en esta tesis se ha modificado el filtrado realizado en el análisis de banda estrecha, ya que el enventanado que se estaba realizado poseía un ancho de banda mucho mayor a los 10 Hz especificados, además se ha realizado dicho tipo de sondeo para la campaña 2013-14. En cuanto al estudio de nuevos esquemas de modulación, se habían realizado tests previos empleando modulaciones multiportadora (OFDM) y sistemas de espectro ensanchado definiendo un esquema llamado signaling basado en DS-SS [3]. Las contribuciones en esta tesis doctoral al respecto del estudio de esquemas de modulación, han sido realizar un estudio en profundidad de modulaciones single-carrier (SC-FDE [4] y SC-FDMA [5]) y colaborar en la definición de las pruebas de esquemas basados en la modificación de signaling [6].

El estudio sobre esquemas de modulación para realizar la transmisión de datos entre la Antártida y cualquier otro punto del mundo no ha sido realizado por ningún otro grupo de

investigación. Sin embargo, se han desempeñado multitudes de sondeos ionosféricos tanto verticales como oblicuos, para detectar como algunos fenómenos afectan al comportamiento de la ionosfera y a la estructura de esta. En cuanto al sondeo oblicuo, la gran parte de la literatura hace referencia a redes de ionosondas que emplean un único hop para realizar el estudio de la ionosfera, como es el caso del proyecto DAMSON, red de ionosondas oblicuas desplegadas a altas latitudes (Escandinavia) [7] o en [8]. El radio modem y/o ionosonda desarrollado por nuestro grupo de investigación está basado en el sistema software defined radio (SDR) propuesto en [9].

2.1 Sondeo del canal ionosférico

La técnica de sondeo de canal nos permite obtener la caracterización de éste y realizar un estudio estadístico de su comportamiento. Los datos obtenidos del resultado de estas pruebas nos permiten realizar una correcta parametrización de los esquemas de modulación. Estos esquemas de modulación se emplean en el diseño de la capa física para la transmisión de los datos de los sensores geomagnéticos instalados en la isa de Livingston. Por este motivo, desde el inicio del proyecto (2003), se han realizado dos tareas, el sondeo de canal ionosférico y el estudio de diferentes técnicas de transmisión entre base antártica Juan Carlos I (62.7°S, 299.6°E) y Cambrils, España, (41.0°N, 1.0°E) para definir la capa física del enlace de comunicación.

Actualmente los objetivos de sondeo de todo un ciclo solar y la definición de la capa física para este enlace de comunicaciones están llegando a su fase final. Por lo tanto, el grupo de investigación ha marcado unos nuevos objetivos como líneas de futuro aprovechando el *know how* obtenido con este proyecto. En esta segunda fase del proyecto, se pretende diseñar un sistema de comunicaciones HF NVIS capaz de obtener los datos de los distintos *dataloggers* instalados en la base Antártica, no solo los sensores geomagnéticos. Cada uno de los nodos conectados con cada *datalogger* obtendrá los datos de estos y los transmitirá verticalmente, aprovechando el rebote ionosférico, hasta un sistema concentrador que enviará los datos a su vez a Cambrils, ya sea mediante satélites geoestacionarios o mediante el enlace diseñado en este proyecto.

2.1.1 Sondeo oblicuo

El sistema de transmisión y sondeo, el cual se ha ido mejorando a lo largo del proyecto, ha sido desarrollado por el grupo de investigación GRECO. El sistema actual se implementó

en la campaña 2009-2010 [2]. Este sistema permite realizar tanto sondeos de banda ancha como sondeos de banda estrecha. De cara a mantener la serie histórica, cada campaña se analizan los resultados de los sondeos llevados a cabo las 24 horas del día en todo el margen de frecuencias de la banda de HF (2-30 MHz) con *steps* de 500 kHz. De estos sondeos se obtienen los parámetros de dispersión, tanto temporal como frecuencial, y un estudio de la disponibilidad del enlace. En el capítulo 6 y en [10] se detalla los métodos empleados para realizar el sondeo de canal ionosférico entre la Antártida y España, y los resultados obtenidos del sondeo de la campaña 2013-2014.

2.1.2 Estudio del canal NVIS

El sistema que realizará la comunicación vertical de última milla entre los sensores y el elemento concentrador emplea la plataforma IRIS [11] como dispositivo de procesamiento de señal. Este procesado se realiza en una FPGA Spartan-6 del fabricante Xilinx.

Se ha realizado un estudio del comportamiento del canal NVIS a latitudes medias en dos estaciones distintas, concretamente en octubre y marzo, mediante sondeo vertical, dicho sondeo se ha realizado aplicando las técnicas conocidas en el sondeo oblicuo. Pese a que el sistema deberá estar instalado en la Antártida y las condiciones del canal NVIS son distintas, este equipo debe ser exportable a otros escenarios, por ese motivo nos interesan los sondeos verticales a distintas latitudes, no solo las polares.

El sistema IRIS se encuentra en fase de prototipaje, por este motivo se ha empleado la Digisonde DPS-4D [12] desarrollada por la *University of Massachusetts Lowell's Center for Atmospheric Research* (UMLCAR) situada en Roquetas (Observatorio del Ebro). Pese a que la Digisonde DPS-4D es un equipo que nos permite obtener los parámetros que empleamos para caracterizar el sistema, esta no nos permite modificar el ancho de banda del sondeo, siendo este de 30 kHz, sin embargo, en el radio módem basado en la plataforma IRIS este es configurable.

En el anexo B y en [13] se detalla tanto el procesado realizado de los datos obtenidos de la Digisonde como los resultados obtenidos del sondeo. Actualmente se está trabajando en el modelado de este canal ionosférico vertical o NVIS.

2.2 Estudio de modulaciones

A lo largo del proyecto se han propuesto diversos esquemas de modulación tales como DS-SS [3], DS-SS *signaling* [14, 15], DS-SS *signaling quadriphase*, DS-SS *signaling quasi-quadriphase*, OFDM [15, 3], SC-FDE [4] y SC-FDMA [5] como candidatos para ser empleados en el diseño de la capa física del radio-módem. Dichos esquemas de modulación deben ser capaces de contrarrestar los efectos no deseados y las características del canal. Como se ha citado anteriormente, dicho canal es dispersivo en tiempo y frecuencia, con muy bajos niveles de SNR y altamente interferido.

Las esquemas de modulaciones probados para este enlace ionosférico han seguido la misma evolución que la telefonía móvil convencional, ya que ambas tecnologías poseen la problemática asociada a un canal dispersivo tanto en tiempo como en frecuencia.

2.2.1 Técnicas de espectro ensanchado

Direct Sequence Spread Spectrum (DS-SS) es un buen candidato como esquema de modulación, esta modulación se comporta bien en entornos con bajos niveles de SNR. Además, el ensanchamiento frecuencial que produce esta técnica presenta robustez al sistema frente a interferencias de banda estrecha, aportando diversidad frecuencial en canales selectivos en frecuencia y minimizando la interferencia con otros sistemas debido a la baja densidad espectral de potencia que presenta.

En un trabajo anterior [3] se probó esta técnica, para ello se realizaron pruebas con diferentes anchos de banda y longitudes de secuencia PN con el fin de obtener un buen compromiso entre BER y *throughput*. El *throughput* obtenido en dicho experimento es suficiente para transmitir un INTERMAGNET [10] (5040 bits por hora). Sin embargo, cabe destacar que este sistema es *simplex* y no se pueden aplicar técnicas de ARQ, por lo tanto cada INTERMAGNET se transmitirá repetidamente para aumentar la probabilidad de recepción. En este escenario, el *throughput* obtenido es insuficiente y se debe trabajar en la implementación de técnicas que maximicen la velocidad de transmisión de datos.

Para incrementar la eficiencia espectral existe la opción de reducir la longitud de las secuencias PN, sin embargo, esto reduciría la ganancia de proceso de la modulación y reduciría los niveles de SNR por símbolo en recepción. Por lo tanto, se ha propuesto una técnica llamada DS-SS *signaling* [14] para este canal HF. Esta técnica aumenta el número de bits sin aumentar el ancho de banda ni la longitud de la secuencia PN respecto a la técnica de DS-SS,

sin embargo, incrementa la complejidad del receptor. El DS-SS *signaling* consiste en mapear m bits en uno de los $M = 2^m$ *Spreading codes* de longitud 2^{m-1}. En este escenario, la familia de secuencias PN escogida debe poseer un nivel bajo de correlación cruzada para minimizar la probabilidad de error. Las secuencias PN empleadas son secuencias Golay debido al buen compromiso de sus propiedades de autocorrelación y correlación cruzada.

La complejidad de cálculo del receptor se incrementa respecto al DS-SS ya que el proceso de demodulación consiste en encontrar la máxima verosimilitud entre las M secuencias PN de la familia de códigos y la señal recibida. La decodificación de los bits se realiza de-mapeando aquella secuencia PN que ha obtenido el máximo valor de correlación.

Basándonos en DS-SS *signaling*, se han propuesto dos nuevos esquemas de modulación para aumentar el *throughput* de esta tecnología, DS-SS *signaling quadriphase* y DS-SS *signaling quasi-quadriphase*. La técnica de *quadriphase* consiste en transmitir dos DS-SS *signaling* en las componentes en fase y cuadratura (I y Q) de la señal. Por este motivo, el *throughput* se dobla respecto al DS-SS *signaling*, obteniendo una ganancia de *throughput* de $2m$ respecto a la técnica de DS-SS convencional. El hecho de emplear esta técnica requiere de ecualización de canal en recepción para compensar las rotaciones de fase producidas por este canal, que es dispersivo tanto en tiempo como en frecuencia.

Una técnica intermedia es la propuesta de *quasi-quadriphase*, dicha técnica separa las M secuencias PN en dos conjuntos, la primera mitad se emplea para mapear los bits que se enviarán en la componente I y la segunda mitad para los que se enviarán en la componente Q, con esta técnica la ganancia de *throughput* se reduce respecto a la técnica de *quadriphase* a $2(m-1)$. Sin embargo, la necesidad de ecualizar el canal para compensar las rotaciones de fase no es necesaria.

En el anexo A y en [6] se detallan estas técnicas, los test realizados y las conclusiones obtenidas de la comparación entre las tres modulaciones. Para ello se han realizado dos experimentos. El primero de ellos consistió en aplicar las mejores combinaciones de tiempo de símbolo, longitud de secuencias PN y ancho de banda obtenidas en [3], a las modulaciones de *quadriphase* y *quasi-quadriphase*.

El segundo de los experimentos consistió en mantener fijo el tiempo de símbolo a 120 ms, aplicando anchos de banda mayores a los probados en [3] (250, 500, 1000, 2000, 4000, 8330 y 16600 Hz), es decir, se ha modificado la longitud de la secuencia PN (número de chips

distintos), a los esquemas de modulación de *signaling* y *quadriphase*.

El autor ha participado en el diseño de las pruebas de *signalling*, *quadriphase* y *quasi-quadriphase* y en el análisis de los resultados de éstas.

2.2.2 OFDM

Para aumentar la eficiencia espectral se han probado esquemas multiportadora. En [15] se propuso emplear una modulación OFDM, y en [3] se presentó una comparativa entre la modulación DS-SS y la OFDM basada en datos reales transmitidos en este enlace HF.

La modulación OFDM presenta robustez frente a canales dipersivos temporalmente mediante el uso de un intervalo de guarda en cada símbolo OFDM, dicho intervalo se aprovecha para reducir la interferencia intersimbólica (ISI), las técnicas más extendidas son *Ciclix Prefix OFDM* (CP-OFDM) [16] y *Zero Padding OFDM* (ZP-OFDM) [16], es decir, añadiendo un prefijo cíclico o un intervalo de silencio, respectivamente.

Por otro lado, la OFDM aprovecha la diversidad frecuencial en canales selectivos en frecuencia, ya que divide el espectro útil en N sub-portadoras ortogonales de banda estrecha, es decir, su ancho de banda es menor que el ancho de banda de coherencia, las cuales modulan constelaciones PSK y QAM. El uso de portadoras ortogonales la convierten en una modulación con gran eficiencia espectral. Cada una de estas sub-portadoras debe ser ecualizada para compensar los efectos no deseados del canal, ya que se debe tener una referencia exacta de la fase (PSK y QPSK) y la amplitud (QPSK) para poder ser demoduladas correctamente.

Uno de los inconvenientes que presenta esta modulación es la sensibilidad al *Doppler shift*, ya que provoca la pérdida de ortogonalidad de las sub-portadoras, por lo tanto, en cada uno de los bins de la FFT, empleada en demodulación, se obtendrá energía tanto de la portadora deseada como de las adyacentes, *inter-carrier interference* (ICI), disminuyendo la potencia de la señal recibida y aumentando el nivel de ruido debido a la interferencia que provocan las portadoras adyacentes sobre esta. Este efecto es más acusado cuanto menor sea el ancho de banda de la sub-portadora. Por otro lado, el PAPR que presenta dicha modulación produce efectos no deseados en la señal, tales como la radiación fuera de la banda de la señal y la distorsión dentro de la banda. Estos efectos se producen debido a la ausencia de perfecta linealidad de los amplificadores de potencia de los dispositivos. Se han estudiado diversas técnicas para reducir los niveles de PAPR en los esquemas OFDM [17]. Las técnicas

más conocidas son: *i) clipping, ii) coding, iii) partial transmit sequence (PTS), iv) selected mapping (SLM), v) nonlinear companding transform, vi) tone reservation (TR)* y *vii) tone injection (TI)*.

El autor ha liderado el diseño de las pruebas realizadas respecto a la modulación OFDM y el estudio de las no linealidades producidos por el recorte de la forma de onda de la señal y el análisis de los resultados de éstas. Este trabajo es la continuación del trabajo realizado por Bergadà en [3].

2.2.3 SC-FDE

Debido a los inconvenientes de PAPR que presenta la OFDM se han propuestos otros esquemas de modulación basado en una única portadora (*single carrier*), como son la SC-FDE y la SC-FDMA.

La SC-FDE emplea el mismo concepto de intervalo de guarda que la OFDM, es decir, cada símbolo SC-FDE viene precedido de un prefijo cíclico. El uso del prefijo cíclico tiene dos objetivos, mitigar la interferencia entre bloques (IBI) y permitir tratar los datos en recepción como si fuesen fruto de la convolución circular entre los datos transmitidos y el canal. El hecho de obtener esta convolución circular permite ecualizar los datos mediante el producto de las transformadas de Fourier de los símbolos SC-FDE y de la estimación de canal. Los criterios de ecualización empleados son *Zero Forcing* (ZF) y *Minimum Mean Square Error* (MMSE).

Cada símbolo SC-FDE está formado por el prefijo cíclico y por k símbolos PSK o QAM, la longitud del símbolo SC-FDE viene determinada por la longitud de este prefijo cíclico, el cual debe ser mayor al *Multipath Delay Spread* máximo, y por kTs, donde Ts es el periodo de estos k símbolos. Se debe definir una estructura de trama que incluya una secuencia de estimación de canal y N símbolos SC-FDE, la longitud de esta trama debe ser inferior al tiempo de coherencia del canal para poder realizar la interpolación de la estimación de este, y así realizar una ecualización correcta.

El capítulo 4 y en [4] se define en profundidad el esquema de modulación de la SC-FDE, la ecualización en frecuencia MMSE empleada, las pruebas realizadas sobre datos reales en este enlace HF y el resultado de dichas pruebas. Los parámetros de configuración estudiados en este experimento se citan a continuación.

- Anchos de banda de 400, 800, 1250 y 2500 Hz.
- Tiempos de bloque de 10, 30, 50, 70 y 90 ms.
- Las constelaciones PSK y QPSK.

El autor ha liderado este trabajo, tanto en el diseño de las pruebas realizadas y como en el análisis de los resultados de éstas.

2.2.4 SC-FDMA

El estudio realizado respecto a la SC-FDMA se realiza en previsión de incorporar múltiples usuarios.

La SC-FDMA se presenta como sustituta de la OFDM como tecnología de capa física en el enlace HF utilizado. Esta modulación está basada en la OFDM, de hecho, emplea el mismo modulador/demodulador, pero en lugar de transmitir los símbolos en cada portadora, en esta se mapean (*subcarrier mapping*) los coeficientes obtenidos de una FFT previa realizada sobre los datos a transmitir. Este esquema, ya no presenta un espectro plano de N sub-portadoras, sino que se obtiene una única portadora del mismo ancho de banda que la OFDM. En el dominio temporal se observa que la señal no presenta las mismas fluctuaciones en la envolvente de la señal, es decir, los niveles de PAPR son menores que en OFDM. Por este motivo el 3GPP decidió emplear una OFDM en el canal de *downlink* y una SC-FDMA en el de *uplink*.

El trabajo realizado en el capítulo 5 y en [5] presenta un estudio de los niveles de PAPR tanto para la modulación OFDM como SC-FDMA en función del número de portadoras. El *subcarrier mapping* empleado en la SC-FDMA es el LFDMA, que presenta mayores niveles de PAPR, pero que por contra ocupa un ancho de banda menor.

A continuación se ha presentado un estudio del *Error Vector Magnitude* (EVM) producido por el hecho de aplicar la técnica de *clipping* y amplificación tanto a la señal de OFDM como SC-FDMA. Debido a que la medida de la distorsión dentro de la banda por el hecho de aplicar *clipping* es compleja, se emplea el EVM como figura de mérito. El EVM es una medida de la distancia Euclídea entre los puntos de la constelación de la señal demodulada y la señal transmitida. La técnica de *clipping* consiste en saturar la envolvente de la señal que supere un cierto umbral, generalmente se utiliza una constante sobre la potencia media de la señal, dicha constante se conoce con el nombre de *Input-Back-Off* (IBO). Los niveles de EVM aumentan cuanto menor es el IBO, es decir, cuando la saturación aplicada era mayor.

Tras aplicar el IBO correspondiente, la señal se amplifica para aumentar la potencia media de esta ya que los niveles de SNR observados en este canal son muy bajos, cuanto menor es el IBO mayor es la ganancia aplicada. El estudio de EVM se realizó mediante datos simulados para una constelación PSK y Q-PSK.

Se ha analizado el BER obtenido para ambos esquemas de modulación en simulación, tanto para un canal *Additive White Gaussian Noise* (AWGN) como para un modelo de canal Watterson [18], propuesto por la ITU-R para condiciones de canal bueno, moderado y pobre. Se han comparado estos resultados con los obtenidos sobre el análisis de datos reales. El test se ha realizado para diversas configuraciones de estas modulación:

- Número de sub-portadoras de 8, 16 y 32.
- Valores de IBO de 1, 4 y 7 dB.
- Las constelaciones PSK y QPSK.
- Tiempos de bloque de 10, 20 y 40 ms.

El autor ha liderado el diseño de las pruebas realizadas respecto a la modulación SC-FDMA y el estudio de las no linealidades producidos por el recorte de la forma de onda de la señal y el análisis de los resultados de éstas.

Las conclusiones obtenidas del análisis de los resultados de las pruebas con datos reales se encuentran en el capítulo 3 de este documento.

Referencias

[1] C. Vilella, D. Miralles, and J.L. Pijoan. An Antarctica-to-Spain HF ionospheric radio link: Sounding results. *Radio Science*, 43(4), 2008.

[2] A.G. Ads, P. Bergadà, C. Vilella, J.R. Regué, J.L. Pijoan, R. Bardají, and J. Mauricio. A comprehensive sounding of the ionospheric HF radio link from Antarctica to Spain. *Radio Science*, 48(1):1–12, 2013.

[3] P. Bergadà, R.M. Alsina-Pagès, J.L. Pijoan, M. Salvador, J.R. Regué, D. Badia, and S. Graells. Digital transmission techniques for a long haul HF link: DSSS versus OFDM. *Radio Science*, 49, 2014.

[4] M. Hervás, J.L. Pijoan, R.M. Alsina-Pagès, M. Salvador, and D. Badia. Single-carrier frequency domain equalisation proposal for very long haul HF radio links. *Electronics Letters*, 50(17):1252–1254, 2014.

[5] M. Hervás, R. M. Alsina-Pagès, J. L. Pijoan, M. Salvador, and D. Badia. Advanced modulation schemes for an Antarctic Long Haul HF Link. Performance comparison between SC-FDE, OFDMA and SC-FDMA in a hostile environment. *Telecommunication Systems*, 2015.

[6] R.M. Alsina-Pagès, M. Salvador, M. Hervás, P. Berguedà, J.L. Pijoan, and D. Badia. Spread spectrum high performance techniques for a long haul high frequency link. *IET Communications*, 9(8):1048–1053, 2015.

[7] P.S. Cannon, M.J. Angling, N.C. Davies, T. Wilink, V. Jodalen, B. Jacobson, B. Lundborg, and M. Broms. Damson hf channel characterisation-a review. In *MILCOM 2000. 21st Century Military Communications Conference Proceedings*, volume 1, pages 59–64. IEEE, 2000.

[8] M. Darnell, P.D.J. Clark, and S. Grob. Design and performance of a system for the derivation and analysis of hf channel state data. 2000.

[9] N.C. Davies, T.J. Willink, M.J. Angling, and P.S. Cannon. Initial Results from WHISPER; a Wideband HF Ionospheric Sounder for Propagation Environment Research. In *Proceedings Nordich HF conference*, Farö, 2001.

[10] M. Hervás, R.M. Alsina-Pagès, F. Orga, D. Altadill, J.L. Pijoan, and D. Badia. Narrowband and wideband channel sounding of an antarctica to spain ionospheric radio link. *Remote Sensing*, 7(9):11712–11730, 2015.

[11] M. Hervás, R.M. Alsina-Pagès, J.L. Pijoan, S. Martí, and D. Badia. IRIS: A software defined radio platform for educational purposes. Technical report, La Salle, URL, 2014.

[12] B.W. Reinisch, I.A. Galkin, G.M. Khmyrov, A.V. Kozlov, I.A. Lisysyan, K. Bibl, G. Cheney, D. Kitrosser, S. Stelmash, K. Roche, et al. Advancing digisonde technology: the dps-4d. In *Radio Sounding and Plasma Physics, AIP Conference Proceedings*, volume 974, pages 127–143, 2008.

[13] M. Hervás, J.L. Pijoan, R.M. Alsina-Pagès, M. Salvador, and D. Altadill. Channel sounding and polarization diversity for the NVIS channel. In *Proceedings Nordich HF conference*, Farö, 2013.

[14] M. Deumal, C. Vilella, J.C. Socoro, R.M. Alsina, and J.L. Pijoan. A DS-SS Signaling based System Proposal for Low SNR HF Digital Communications. In *10th IET International Conference on Ionospheric Radio Systems and Techniques*, London, 2006.

[15] P. Bergadà, M. Deumal, C. Vilella, J.R. Regué, D. Altadill, and S. Marsal. Remote sensing and skywave digital communication from antarctica. *Sensors*, 9(12):10136–10157, 2009.

[16] H.G. Myung, J. Lim, and D.J. Goodman. Single carrier FDMA for uplink wireless transmission. *IEEE Vehicular Technology Magazine*, 1(3):30–38, 2006.

[17] T. Jiang and Y. Wu. An overview: Peak-to-average power ratio reduction techniques for OFDM signals. *IEEE Transactions on Broadcasting*, 54(2):257–268, 2008.

[18] C. Watterson, J. Juroshek, and W. Bensema. Experimental Confirmation of an HF Channel Model. *IEEE Transactions on Communication Technology*, 18(6), 1970.

Capítulo 3

Resultados

En este capítulo se detallan los resultados obtenidos durante el periodo de investigación de la tesis doctoral del autor. Estos resultados se dividen en dos secciones, *i)* sondeo de canal OIS y VIS y *ii)* estudio de nuevos esquemas de modulación para la definición de la capa física.

3.1 Sondeo del canal ionosférico

A continuación se detallan los resultados obtenidos de las publicaciones del capítulo 6, sondeo oblicuo del canal HF de 12.760 km entre la Antártida y España, y del anexo A, sondeo vertical realizado en el observatorio del Ebro, (España).

3.1.1 Sondeo oblicuo

El sondeo oblicuo llevado a cabo en el proyecto antártico realiza un análisi de banda estrecha utilizando la definición de *Frequency of Largest Availability* (FLA), que es la frecuencia con mayor porcentaje de disponibilidad para cada una de las horas. Se han observado 4 zonas de operación: *i)* dia, *ii)* noche, *iii)* alba y *iv)* puesta del sol. El intervalo diurno abarca desde las 8 UTC hasta las 17 UTC, donde las frecuencias comprendidas entre 20 y 30 MHz, ofrecen las mejores prestaciones para la comunicación en términos de SNR. Durante la puesta del sol, aproximadamente a las 18 UTC, el rango de frecuencias usables cae linealmente hasta el intervalo de 10 a 20 MHz. Durante la noche, de 19 UTC a 6 UTC, el rango de frecuencias desde 6 a 15 MHz. Al alba, 7 UTC, el rango de mejores frecuencias de operación aumenta linealmente con el tiempo hasta situarse de 20 a 30 MHz. Por lo tanto, se puede concluir que durante la noche las mejores frecuencias de operación son las bajas, mientras que durante el día las altas y tanto el alba como la puesta del sol son dos regiones de conmutación entre estas. Cabe destacar, que hay un salto en la FLA tras el alba y la puesta del sol. La definición

de estas regiones se ha realizado a partir de los resultados obtenidos de dicho sondeo, ya que no se puede definir exactamente en base a la posición del sol porque la trayectoria que realiza la onda transmitida recorre diferentes husos horarios.

El rango de frecuencias que proporciona la mayor disponibilidad para el establecimiento del enlace está claramente relacionado con las características de la ionización de las distintas capas de la ionosfera. Como se ha citado anteriormente en el capítulo 1, la densidad de electrones libre en la capa D de la ionosfera cae rápidamente durante la puesta del sol, debido a que esta capa es absorbente a frecuencias bajas, la ausencia de ionización permite que las frecuencias bajas se propaguen hacia las capas superiores, esto no ocurre durante las horas de sol. La ionización de la capa F persiste durante la noche, aunque la densidad de electrones se reduce, y el rango de frecuencias que se reflejan en esta capa se reduce también debido a esta menor densidad de electrones libres.

Del análisis del sondeo de banda ancha se han obtenido los parámetros de *i) Multipath Delay Spread* y *ii) Doppler Spread*. Al igual que el análisis de banda estrecha, se han definido las mismas 4 regiones de operación. Durante las horas diurnas, en el rango de 20 a 30 MHz se han observados los mayores valores de *Multipath Delay Spread* y *Doppler Spread*, este hecho es debido a la ionización producida por el sol, ya que el número de electrones libres en las distintas capas aumenta durante el día respecto a la noche, produciendo que la señal se refleje en mas puntos (*Multipath Delay Spread*) y que este mayor número de capas se muevan en altura (*Doppler Spread*). Este aumento del *Multipath Delay Spread* se debe tener en cuenta en el diseño del esquema de modulación ya que produce interferencia inter-simbólica. Durante las horas nocturnas, 19 UTC a 6 UTC, se observan las mejores medidas tanto en términos de disponibilidad como de *Multipath Delay Spread* y *Doppler Spread*. Las frecuencias que mejores prestaciones pueden ofrecer están alrededor de los 10 MHz, pese a que el rango disponible llega a 20 MHz. La media de *Multipath Delay Spread* es de 2 a 3 ms, con poca desviación, mientras que el máximo *Doppler Spread* esta alrededor de 0.7 Hz. Se puede observar como el *Multipath Delay Spread* para cualquier hora concreta decrece a medida que la frecuencia aumenta (véase Fig. 6.17), la observación de esta tendencia se afirmo en la tesis de Vilella (véase Figura 4.32 de esta). No obstante, pese a observarse esta tendencia, que apunta que el mayor *Multipath Delay Spread* se encuentra a bajas frecuencias, el análisis de los datos revela que durante las horas diurnas a altas frecuencias hay valores de picos elevados (entre las 10 y las 17 UTC), a demás, si observamos la desviación estándar, es mas elevada a estas frecuencias que durante el resto del día. Esta observación no se hizo antes en los estudios realizados por Vilella, ya que la máxima frecuencia de estudio fueron

16.5 MHz. En los estudios que realizó Ahmed [1], puede verse en al Fig. 4.35 de esta tesis como a las 13, 14, 19 i 21 UTC también existen estos picos. La diferencia horaria entre este rango y el observado en esta tesis es debida a la diferencia entre las fechas de una campaña y la otra. Los resultados que presenta Ahmed corresponden a la campaña 2009/10, durante 01/01/2010 y 02/02/2010, mientras que el análisis de la campaña 2013/14 se llevó a cabo entre el 25/01/2014 y el 18/02/2014. Respecto al *Doppler Spread*, la diferencia no se puede apreciar con suficiente claridad, no obstante a altas frecuencias durante las horas diurnas es ligeramente superior, la desviación típica también es mas grande en este rango de frecuencias.

El análisis tando de banda estrecha como de banda ancha proporcionan resultados similares en términos de disponibilidad. Las horas nocturnas son las que presentan mejores prestaciones para la recepción, en banda estrecha presentan los mayores valores de SNR y en banda ancha los menores valores de *Multipath Delay Spread* y *Doppler Spread*. Estos resultados nos permiten diseñar dos esquemas de modulación para dos modos de operaciones distintos, *High Throughput Mode* (HTM) y *Robust Mode* (RM). El modo de operación HTM se emplearía durante la noche mientras que el RM durante el día, el alba y la puesta del sol, cuando las condiciones en recepción son menos favorables.

El hecho de realizar las campañas de sondeos y test de nuevos esquemas de modulación durante un breve espacio de tiempo del verano austral provoca que el volumen de muestras obtenidas del estado de la ionosfera no sea muy elevado, por lo tanto, se puede dar el caso de que los resultados obtenidos en alguna de las campañas no sea significativo respecto a todo el ciclo solar. Nuestro grupo de investigación ha realizado un estudio que compara los resultados obtenidos del sondeo oblicuo de banda estrecha entre la Antártida y España y los resultados obtenidos de 5 observatorios que realizan sondeos verticales en puntos intermedios de la trayectoria de propagación que sigue la señal entre ambos puntos, obteniendo relaciones entre los resultados de unas y otras [2]. Actualmente dicho estudio se está ampliando a todo el ciclo solar, teniendo en cuenta información de eventos atmosféricos y geomagnéticos a este estudio para obtener nuevas correlaciones entres los resultados de los sondeos oblicuos y dichos eventos. De esta manera se pretende obtener nuevas correlaciones entre el comportamiento de la ionosfera y dichos eventos atmosféricos y geomagnéticos así como obtener una estimación de la bondad o grado de confianza de dichos sondeos con respecto al análisis de los resultados tanto de dichos eventos como de los sondeos verticales.

3.1.2 Sondeo vertical

Se presentan los resultados del sondeo vertical realizado durante dos días completos en dos estaciones distintas del año, también se presenta la capacidad de mejora de la recepción al aplicar diversidad de polarización. El estudio de diversidad se ha realizado gracias a que el dispositivo de medida (Digisonde DPS-4D [3]) es capaz de separar la onda ordinaria y la onda extraordinaria, las cuales se reflejan a alturas diferentes, realizando recorridos distintos.

A partir de los resultados obtenidos, se observa que la onda extraordinaria posee un *Multipath Delay Spread* medio ligeramente mayor que la ordinaria, ya que generalmente la onda extraordinaria se refleja a mayor altitud que la ordinaria. En cuanto a *Doppler Spread*, es la onda ordinaria la que presenta valores algo mayores a la extraordinaria en todos los casos.

Debido a que la capa D es absorbente durante las horas del día a bajas frecuencias, cuando está ionizada, y esta absorción es mayor para la onda extraordinaria que para la ordinaria. Se observa que la onda ordinaria presenta mayor SNR a bajas frecuencias (2.5 MHz a 4.5 MHz) durante las horas diurnas. También se ha observado que la onda extraordinaria posee una mayor frecuencia de operación máxima que la onda ordinaria.

El hecho de aplicar diversidad de polarización, simplemente sumando en fase ambas señales, onda ordinaria y onda extraordinaria, ha provocado una mejora sustancial en el BER. A partir de estos resultados de BER, se pueden definir dos rangos de trabajo, de 2 a 8.5 MHz durante las horas diurnas y de 2 a 3.5 MHz durante las nocturas. Cabe destacar que este estudio se realizó con señales de 30 kHz de ancho de banda, que es 10 veces mayor que un canal estándar HF de 3 kHz, por lo que la SNR es baja. El rango de frecuencias propuesto se ampliaría empleando un ancho de banda menor.

3.2 Técnicas de transmisión para la definición de la capa física

3.2.1 Esquemas de modulación basados en DS-SS

El test de transmisión de *signaling*, *quadriphase* y *quasi-quadriphase* realizado durante la campaña 2012-2013, nos ha permitido comparar los resultados obtenidos en recepción del BER. Cabe destacar que se pretende obtener el mejor compromiso entre BER y *bit rate*.

Los mejores resultados de BER se obtuvieron con aquellos esquemas con periodo de símbolo mas grande, es decir, con mayor factor de sobremuestreo. Comparando las tres técnicas, *signaling* es la mas robusta, ofreciendo un nivel de BER y *bit rate* en contraposición mas bajo. *quasi-quadriphase* presenta un BER mas moderado pero incrementa el *bit rate* respecto a la técnica de *signaling*. Sin embargo, la que presenta un nivel de *bit rate* mas elevado es *quadriphase*, aunque el BER observado es el mayor de las tres.

Por lo tanto, aunque *signaling* sea la mas robusta de las tres, su *throughput* es demasiado bajo para nuestra aplicación, mientras que la que presenta un mejor compromiso entre BER [4] y *bit rate* es *quasi-quadriphase* [5]. Por último, el estudio de ancho de banda manteniendo el factor de sobremuestreo constante, demuestra que las modulaciones con mayores anchos de banda presentan el mejor BER. Esto es debido al mayor *process gain*.

3.2.2 SC-FDE

El estudio realizado de la modulación SC-FDE en el capítulo 4, demuestra que la constelación PSK con anchos de banda de 400, 800 y 1250 Hz con tiempos de bloques cortos, puede ser una buena candidata como esquema de modulación en radio enlaces HF de gran alcance con valores de SNR pequeños.

Los tests realizados demuestran que el BER observado es menor que el comparado en estudios previos basados en OFDM, ya que debido a la PAPR la potencia media de la OFDM es menor que la SC-FDE, por la tanto la SNR también lo es. Además, SC-FDE presenta una eficiencia espectral mayor que los sistemas basados en DS-SS.

Por lo tanto, este esquema de modulación se postula como el idóneo para ser usado como capa física del HTM.

3.2.3 Esquemas de modulación basados en *multicarrier* o *single carrier*

El test realizado aplicando *clipping* y amplificación de la OFDM y SC-FDMA, incrementa la potencia media de la señal, por lo tanto la SNR en recepción, demuestra que pese al aumento del EVM, el BER decrece en recepción si se compara con las versiones sin *clipping* ni amplificación. Cuando la constelación es densa, 16-QAM y 64-QAM, no se puede aplicar un IBO de 0 dB, ya que el EVM producido por este *clipping* abrupto produce una distorsión demasiado grande dentro de la banda, y el BER irreducible es demasiado grande.

La *Cummulative Density Function* de la SNR ($CDF(SNR)$) del análisis de los datos reales nos permite observar que el comportamiento de la SC-FDMA es mejor que el de la OFDM, sin embargo esta modulación tiene un coste computacional mayor, ya que emplea una FFT/iFFT adicional en el transmisor/receptor.

De la comparación de estas tres técnicas con datos reales y simulados, en el caso de un canal pobre con muy bajo nivel de SNR, obtenemos que los esquemas basados en SC-FDE y la versión recortada de la SC-FDMA con IBOs de 1 dB presentan resultados similares. Sin embargo, los resultados del caso concreto de SC-FDE con bloques de 30 ms son mejores que la SC-FDMA, por lo tanto es el mejor esquema de modulación.

Referencias

[1] A.G. Ads et al. *Soundings of the ionospheric HF radio link between Antarctica and Spain*. PhD thesis, Ph. D. dissertation, Univ. Ramon Llull, Barcelona, Spain, 2013.

[2] A.G. Ads, P. Bergadà, J.R. Regué, R.M. Alsina-Pagès, J.L. Pijoan, D. Altadill, D. Badia, and S. Graells. Vertical and oblique ionospheric soundings over the long haul hf link between antarctica and spain. *Radio Science*, 50(9):916–930, 2015.

[3] B.W. Reinisch, I.A. Galkin, G.M. Khmyrov, A.V. Kozlov, I.A. Lisysyan, K. Bibl, G. Cheney, D. Kitrosser, S. Stelmash, K. Roche, et al. Advancing digisonde technology: the dps-4d. In *Radio Sounding and Plasma Physics, AIP Conference Proceedings*, volume 974, pages 127–143, 2008.

[4] J.G. Proakis and D.G. Manolakis. *Digital communications*, volume 3. McGraw-Hill, 1995.

[5] R.M. Alsina-Pagès, M. Salvador, M. Hervás, P. Berguedà, J.L. Pijoan, and D. Badia. Spread spectrum high performance techniques for a long haul high frequency link. *IET Communications*, 9(8):1048–1053, 2015.

Parte II

Contribuciones

Capítulo 4

Single Carrier Frequency Domain Equalization Proposal for Very Long Haul HF Radio Links

M. Hervás, J.L.Pijoan, R.M. Alsina-Pagès, M. Salvador and D. Badia

Abstract. A single carrier frequency domain equalisation (SC-FDE) modulation scheme which represents a step forward in the investigation since it obtains higher bit rates than previous proposals with spread spectrum techniques is presented. The focus of this reported work is the data transmission from remote sensors using very low-power HF ionospheric communications. In particular, the authors´ research group has been studying the ionospheric channel parameters and data transmission techniques from Antarctica since 2003. Both, the spread spectrum and multicarrier modulations have been tested previously in order to obtain a good trade-off between bit error rate and bit rate. A proof of principle of the single carrier technique with promising results is presented.

Source: Electronics Letters, Volume 50, Issue 17, 14 August 2014, p. 1252-1254
DOI: 10.1049/el.2014.1184 , Print ISSN 0013-5194, Online ISSN 1350-911X

4.1 Introduction

Communications from remote sensors can be done via satellite or skywave ionospheric communications. Concerning polar communications, the geostationary satellites are not always visible and skywave ionospheric HF links are of special interest either as a low bit rate alternative or as a backup system. During the last decades, the data rates in the HF band have increased significantly from 75 to 4800 bps through a 3 kHz channel in robust mode or up to 12800 bps for uncoded operation at 64-QAM when the conditions are extraordinarily good [1].

During the last 10 years our research group is involved in a project dealing with a long haul radio link (12.700 Km) between the Spanish Antarctic Station (SAS) in Livingston Island (62.6S, 60.4W) and Cambrils (41.0N, 1.0E), Spain. The main objectives of the project are the ionospheric channel sounding and characterization, and the data transmission from remote sensors. A historical series of channel availability, SNR, Doppler spread and multipath delay spread is being recorded every year during the austral summer along a complete solar cycle in order to design the best modulation scheme at any time. The HF modem has been designed to work under very strict power restrictions. Moreover, the antenna has to be a single monopole with low environmental impact. The effective radiated power at the transmitter side is low, so that, the SNR at the receiver is low. Therefore, modulation schemes with bandwidths out of standard lower than 3 kHz have to be tested.

The HF channel is a time-variant and time-dispersive communication channel. So the latest improvements in efficient modulations for the wireless multipath channel can be adapted to our case.

First, a Direct Sequence Spread Spectrum (DS-SS) scheme was tested in [2, 3]. It was a modified version of the traditional DS-SS in order to optimize the spectral efficiency. This modification consists on mapping m data bits into one of the $M = (2^m)$ spreading codes. At the receiver, the transmitted bits are obtained by correlating the received time-frequency synchronized signal with the M spreading codes. Maximum correlation value determines the most probable transmitted spreading code, i.e. the most probable transmitted group of m bits. Although it was a robust proposal, the final bit rate was too low for certain remote sensing applications. In order to increase the bit rate, an OFDM proposal was tested in [4–6, 3]. Due to power constraints and the Peak to Average Power Ratio (PAPR), the number of subcarriers was below 32 and the achieved bit rate for a reasonable bit error rate (BER) was around 100 bps.

The new wireless communication standard Long Term Evolution (LTE) uses OFDMA and SC-FDMA modulation schemes, for the downlink and uplink channel, respectively [7]. The SC-FDMA modulation overcomes the problem of the PAPR for a limited power

capability at the user equipment. SC-FDMA is a near constant envelope version of OFDMA that allows us to benefit from the maximum power of the amplifier.

4.2 Proposal

Our proposal is to use a Single Carrier Frequency Domain Equalization (SC-FDE) which is the specific type of a SC-FDMA for a single user. Fig.4.1a shows the block diagram of a SC-FDE receiver and for comparison, Fig.4.1b an OFDM receiver. We can see that both systems use the same communication component blocks and the only difference between the two diagrams is the location of the Inverse Discrete Fourier Transform (IDFT) block [7].

The modulator divides the information into blocks and adds a Cyclic Prefix (CP) at the beginning of each block to avoid Inter Symbolic Interference (ISI) between adjacent blocks. CP is a replica of the last part of a data block, and has to be longer than the maximum multipath delay spread of the channel. It also ensures that the convolution of the channel impulse response with the modulated symbols has the form of a circular convolution as shown in equation (4.1).

$$Y[k] = X[k]H[k] = DFT\{x[n] \otimes h[n]\} \tag{4.1}$$

where $y[n]$ is the received signal, $x[n]$ is the transmitted signal and $h[n]$ the channel impulse response. Then, the equalization of the signal is done directly in frequency domain as we can see in equation (4.2), where $X[k]$, $Y[k]$ and $H[k]$ are the DFT of the transmitted and received signals and the channel impulse response, respectively.

$$X[k] = \frac{Y[k]}{H[k]} = Y[k]\frac{H^*[k]}{H[k]H^*[k]} = Y[k]\frac{H^*[k]}{|H[k]|^2} \tag{4.2}$$

This equalization method is known as Zero-Forcing (ZF) and presents some problems when the system is noisy. A better approach is the Minimum Mean Square Error (MMSE) method, which takes into account the noise power as stated in equation (5.8). ZF and MMSE behave the same way when the noise power tends to zero.

$$X[k] = Y[k]\frac{H^*[k]}{|H[k]|^2 + \varphi} \tag{4.3}$$

Fig. 4.2 shows our frame proposal for the SC-FDE test. The CP time (Tcp) is equal to 3 ms, because previous studies in [8, 9] concluded that the multipath delay spread is lower

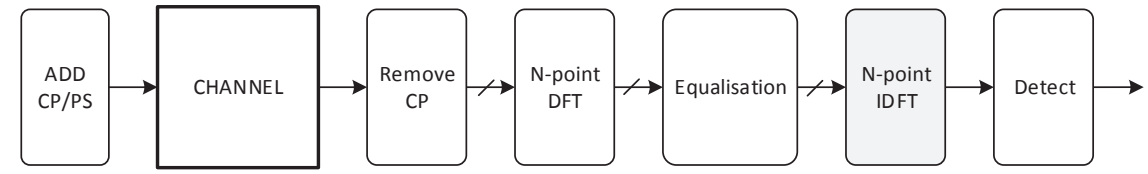

(a) SC-FDE

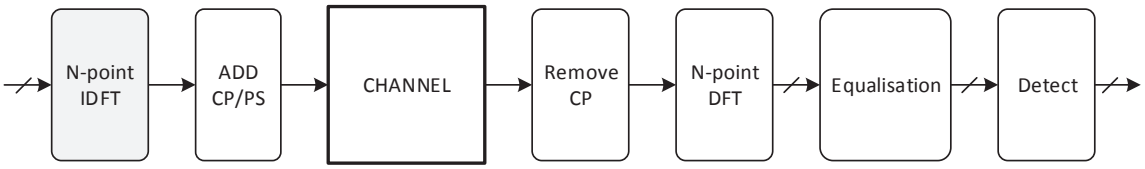

(b) OFDM

Fig. 4.1 Block diagrams of SC-FDE and OFDM

than 2.5 ms. The equalization sequence is inserted every 200 ms (Teq) which is comparable to the coherence time of the channel (Tc).

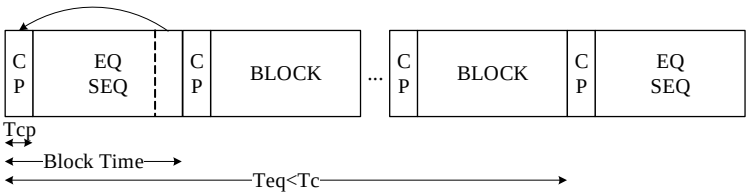

Fig. 4.2 Frame proposal for the SC modulation scheme

4.3 Validation

In order to obtain the optimum parameters for the physical layer we have tested several values of block time, bandwidth and constellation diagram enumerated below. These values have been chosen taking into account the low SNR observed in previous studies. Therefore, bandwidths lower than 3 kHz and the most simple in phase modulations were tested.

- Bandwidths of 400, 800, 1250 and 2500 Hz.
- Block times of 10, 30, 50, 70 and 90 ms.
- PSK and QPSK constellations.

We have developed the tests under the Software Defined Radio (SDR) platform described in [10]. The system is designed for sounding the channel with both narrowband and wideband signals throughout 40 minutes per hour, transmit sensor's data and testing new modulation schemes during 10 minutes every hour.

The following results have been obtained from real data transmitted during the campaign 2012-13 on February 22nd. Although we have not a statistically representative database the obtained preliminary results validate the proof of principle.

Fig. 4.3 shows the mean variation of BER with SNR throughout all the transmitted blocks from the Spanish Antarctic Station. The SNR fluctuations depend on the HF channel conditions and the signal bandwidth. The mean value of BER has been integrated in steps of 2 dB of SNR for all the demodulated results. If we compare the real and the simulated PSK and QPSK curves we observe an increment of about 12 dB of the required SNR to obtain a similar BER. This is caused by the multipath delay spread, the Doppler effect, impulsional noise, interference and imperfect channel equalization.

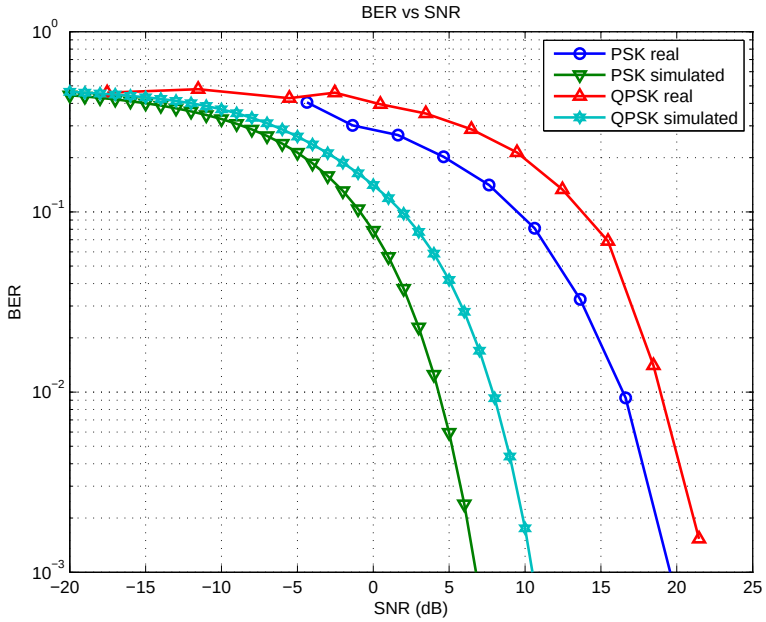

Fig. 4.3 Real and simulated measures of BER vs SNR for PSK and QPSK

As we may expect a SNR higher than 5 in 90% of cases, depending on the bandwidth and the ionospheric conditions, the resulting BER is lower than 0,18 for PSK. These values of BER are often found in long and hostile radio links with low transmission power and very simple antennas.

In order to study the performance of the modulation scheme, there are some figures of merit such as the error vector magnitude (EVM), SNR and BER. We have estimated the Cumulative Density Function (CDF) of EVM and BER over a long time to compare the

performance in terms of block time, bandwidth and constellation diagram. In Fig. 4.4, for a block time of 30 ms, the minimum value of SNR in 90% of cases (which corresponds to $P(SNR > K) = 100 \cdot (1 - CDF(K))$) ranges from 4 dB for a bandwidth of 2500 Hz to 7 dB for a bandwidth of 400 Hz. Obviously, there is a trade-off between the bandwidth and SNR or, in other words, between bit rate and BER.

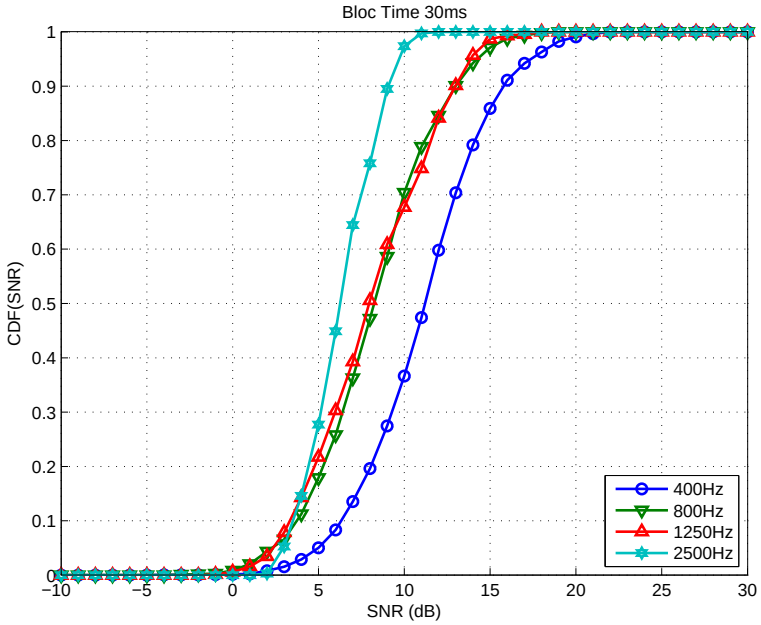

Fig. 4.4 CDF of BER for a block time of 30 ms as a function of bandwidth

In table 1 you can see the achieved bit rate and the CDF for a BER lower than 0.05 as a function of bandwidth and block time. We assume a CDF higher than 0.5 as a minimum threshold for operation, since it means that the BER is lower than 0.05 the 50 percent of cases. We can distinguish 3 different modes of operation looking at the trade-off between bit rate and BER. The robust mode, with a bit rate around 300 bps for a bandwidth of 400 Hz and block time of 10 ms. The high bit rate mode, with a bit rate around 600 bps for a bandwidth of 800 Hz and block time of 10 ms. Finally, there is third mode with a good trade-off around 380 bps for a bandwidth of 400 Hz and block time of 70 ms.

4.4 Conclusion

The proposed SC-FDE modulation scheme based on the LTE uplink has been tested. The frequency domain equalization has a much lower implementation cost than the time domain equalization. The modulator scheme of figure 4.1 uses the Fast Fourier Transform (FFT) to equalize the channel, so it makes SC-FDE very attractive to SDR implementations.

BW (Hz)	Tb (ms)	BR (bps)	$CDF(BER)$ (>0.05)
400	10	307.7	0.79
400	30	363.6	0.63
400	50	377.4	0.63
400	70	383.6	0.64
400	90	387.1	0.39
800	10	615.4	0.52
800	30	727.3	0.49
800	50	754.7	0.48
800	70	767.1	0.47
800	90	774.2	0.33
1250	10	961.5	0.44
1250	30	1136.4	0.35
1250	50	1179.2	0.18
1250	70	1198.6	0.32
1250	90	1209.7	0.24
2500	-	-	<0.32

Tabla 4.1 *Test results for PSK constellation*

From table 1, we can conclude that uncoded PSK with bandwidth of 400, 800 and 1250 Hz for lower block times is a good candidate to be used as a modulation scheme for a long haul ionospheric radio links.

The results present higher bit rates with lower BER compared with previous studies in [5, 3]. More specifically, SC-FDE outperforms OFDM due to the near constant envelope that increases the mean power of the transmitted signal. Moreover, SC-FDE presents a much higher spectral efficiency than DS-SS, and this is an important issue in the HF band.

These previous conclusions encourage us to test SC-FDE more intensively in order to define a complete physical layer for low-power, remote sensing applications.

Acknowledgment

This work has been funded by the Spanish Government under the projects CTM2010-21312-C03-03.

M. Hervás, J.L.Pijoan, R.M. Alsina-Pagès, M. Salvador and D. Badia(*GR-SETAD - La Salle, Universitat Ramon Llull, Spain*)

E-mail: mhervas@salleurl.edu

Referencias

[1] MIL-STD-188-110B, 'Military Standard - Interoperability and Performance Standards for Data Modems', US DoD, 2000.

[2] Deumal, M.; Vilella, C.; Socoro, J.C. et al.: 'A DS-SS Signaling Based System Proposal for Low SNR HF Digital Communications', *Ionospheric Radio Systems and Techniques*, 2006, pp. 128-132.

[3] Bergadà, P.; Alsina-Pagés, R.M.; Pijoan, J.L. et al.: 'Digital Transmission Techniques for a Long Haul HF Link: DS-SS vs. OFDM', *Radio Science*, to appear.

[4] Zhang, Z.; Zeng F.; Ge, L. et al.: 'Design and Implementation of Novel HF OFDM Communication Systems ', *IEEE International Conference on Communication Technology (ICCT)*, 2012, pp.1088-1092.

[5] Bergadà, P.; Alsina-Pagés, R.M. and Pijoan, J.L.: 'Time Interleaving Study for an OFDM Long-Haul HF Radio Link', *Ionospheric Radio Systems and Techniques*, 2009, pp.1-4.

[6] Bergadà, P.; Deumal, M.; Vilella, C. et al.: 'Multicarrier Modulation Proposal for Long Distance HF Data Links', *Ionospheric Effect Symposium*, 2008.

[7] Myung, H. G and Goodman, D.J.: 'Single Carrier FDMA. A New Air Interface for Long Term Evolution', *Wiley Series on Wireless Communications and Mobile Computing*, 2008.

[8] Vilella, C.; Miralles, D. and Pijoan, J.L.: 'An Antarctica-to-Spain HF ionospheric radio link: Sounding results', *Radio Science*, 2008, **43**.

[9] Vilella, C.; Socoro, J.C.; Pijoan, J.L. et al.:'An Antarctica to Spain HF Link. Oblique Sounding Results', *Ionospheric Radio Systems and Techniques*, 2006, pp. 91-94.

[10] Ads, A.G.; Bergadà, P.; Vilella, C. et al.: 'A comprehensive sounding of the ionospheric HF radio link from Antarctica to Spain', *Radio Science*, 2013, **48**, pp.1-12.

Capítulo 5

Advanced modulation schemes for an Antarctic Long Haul HF Link

M. Hervás · R.M. Alsina-Pagès · J.L. Pijoan · M. Salvador · D. Badia

Abstract. This paper presents the comparison of the BER performance between SC-FDE, OFDMA and SC-FDMA in a long haul HF data link with low SNR. The goal of the comparison is to define two operation modes for two QoS; a robust mode and a high throughput mode, in order to transmit data from remote sensors in Antarctica through a 12760 km ionospheric link with a power amplifier of only 200 W. Clipping and amplification of the waveforms have been applied to SC-FDMA and OFDMA in order to compensate the PAPR and therefore maximize the SNR. The Antarctic HF link has been studied for 11 years, and we have described the link in terms of availability, SNR, delay and Doppler profile, and also spread spectrum techniques have been tested for data transmission. Based on those previous studies results we have developed a test bed to compare these transmission techniques, providing promising results in our low power ionospheric link from Antarctica.

keywords. SC-FDE · OFDMA · SC-FDMA · PAPR · HF · Ionosphere

Source: Telecommunication System, DOI: 10.1007/s11235-015-0110-x

5.1 Introduction

This paper presents an approach to adapt the Long Term Evolution (LTE) physical layer modulation schemes, for a HF long haul unidirectional radio link between the Spanish Antarctic Station (SAS) on Livingston Island (62.6° S, 60.4° W) and Cambrils (41.0° N, 1.0° E), in Spain (see Fig. 5.1). The project has two main goals: the sounding of the oblique HF ionospheric channel and the transmission of the remote sensors data (located around the SAS), both performed during the austral summer. The radio link is 12760 km long and has 4-5 hops [1] between the ionosphere and the Earth.

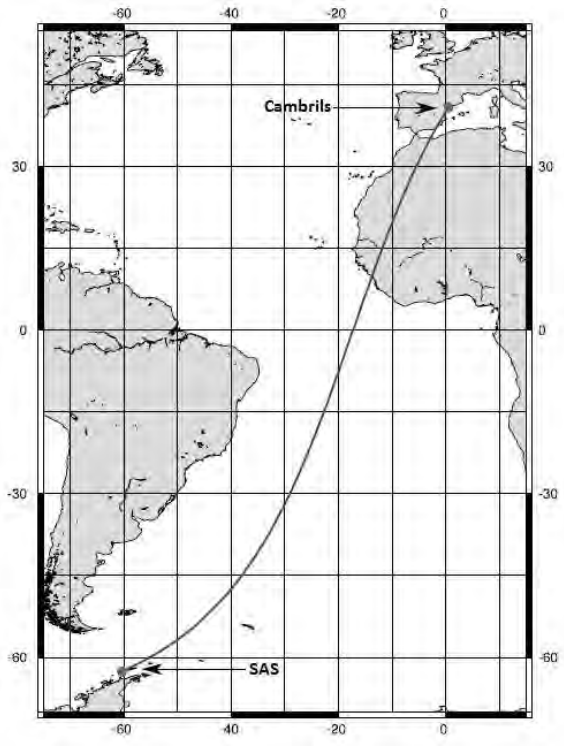

Fig. 5.1 Geographical link characteristics

The power amplifier in the transmitter is limited to 200 W, and the antennas used are very simple due to strict environmental restrictions in Antarctica. These factors and the long haul link lead to a very low SNR at the receiver. Our research group (GR-SETAD) has been involved in this project for a whole solar cycle [2]. The channel soundings [3–5] have allowed us to have historical series of channel availability, SNR, Doppler Spread and Multipath Delay Spread during a complete solar cycle, and several modulation schemes have been tested to transmit the data of the remote sensors with maximum bitrate (BR) and minimum bit error rate (BER) [6–8].

Data rates in the HF band for 3 kHz channels have a range from 75 to 4800 bps in robust mode [9]. This is not applicable in our system because these standards require higher SNR than the available in this link, although the proposed BR would be enough for our throughput requirements.

The modulation schemes tested previously in this channel were based on direct sequence spread spectrum (DS-SS) [8, 10] for very low SNR and low throughput, which can be called robust mode, and single-carrier or orthogonal frequency division multiplexing (OFDMA) schemes [7, 8, 11–13] for moderate SNR and higher throughput using bandwidths lower than 3 kHz. The results in our previous works about modulation did not reach the needed throughput, and we have to design a new modulation proposal.

The aim of this work is to compare the performance of an OFDMA with a single-carrier frequency division multiplexing access (SC-FDMA) in terms of BR and BER, to find a trade-off between BER and BR for 2 qualities of service (QoS), robust mode and high throughput mode. Both modulation proposals will be tested using clipping to reduce the PAPR, and amplifying the resulting signal to minimize the back off of the amplifier. That attempts to increase the SNR at the receiver, which is one of the main drawbacks of this link. Therefore, a study of the trade-off between the distortion and the increase of the mean power due to the clipping is done. The tests presented in this work have been done for both simulated and real data transmitted from the SAS. This comparison will be done to obtain the better clipped modulation scheme in terms of BER for a small number of sub-carriers.
In Sect. (5.2), a description about the systems is done; the modulation schemes proposed are described in Sect. (5.3); the results from simulation are shown in Sect. (5.4) and results in real data are presented in Sect. (5.5) and Sect. (5.6), and finally, in Sect. (5.7) the conclusions about the tests are commented.

5.2 System description

The main goal of this project is to establish a continuous HF transmission link between the SAS and Cambrils. A sounding is needed to choose the best frequencies in terms of performance. Our system is prepared to cope with all the project requirements: *i)* sounding of the channel, *ii)* transmission of the remote sensors data, and in this case *iii)* testing new modulation schemes. The transmitter (see Fig. 5.2) consists of a rugged monopole antenna of 7.5 m, a power amplifier of 200 W and a proprietary radio-modem which is deeply described in [2, 5]. The receiver (see Fig. 5.3) consists of 3 antennas, a monopole of 7.5 m, an inverted

V (which is a 28 m folded dipole to cover the entire HF band [14]) and a Yagi tuned at 14.5 MHz, and 2 proprietary radio-modem that can be attached to 2 receiver antennas each. Both receiver and transmitter contain a GPS for time synchronization, which is done with a pulse per second (PPS) with an accuracy of 1 μs [2, 5]. Both systems contain an oven-controlled crystal oscillator (OCXO), which are adjusted every campaign to minimize the Doppler shift effect caused by the clock differences between the transmitter and the receiver. Further details can be found in [2].

The use of a directive antenna and a higher power amplifier in the transmitter side would obviously improve the value of the received SNR in Cambrils. However, the restrictions of natural impact of these elements and the very strict power availability in the SAS limit us to simpler antennas and reduced transmitted power.

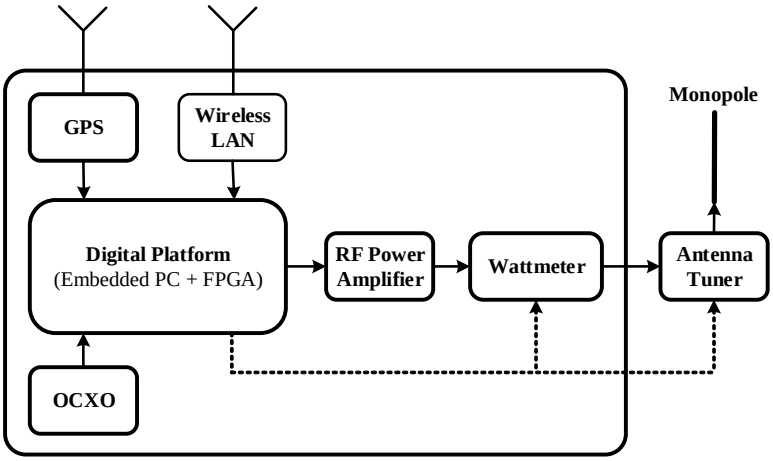

Fig. 5.2 Block Diagram of the Transmitter

5.3 Overview of the Modulation Schemes

The two modulation schemes studied in this work use frequency domain equalization (FDE) based on pilot sequences. Both schemes have the same data frame (see Fig. 5.4), consisting on the insertion of an equalization sequence, which is a sequence applied for CIR estimation, periodically. This time (T_{eq}) is lower than the coherence time (T_{COH}), which is considered 300 ms, where the channel can be considered static. The cyclic prefix (CP) is an extension of the last samples of each data block at the beginning of the block. The CP duration should be larger than the multipath delay spread, to completely remove the inter-block interference (IBI) and allow us to equalize the channel in the frequency domain.

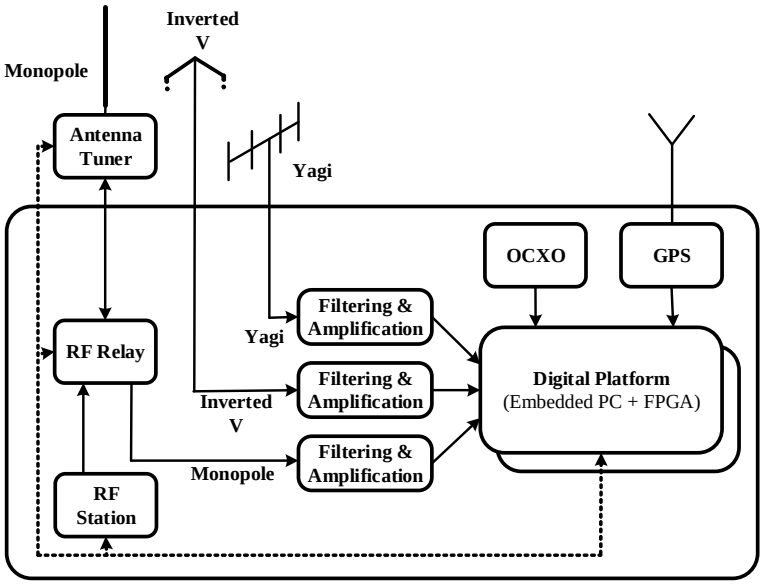

Fig. 5.3 Block Diagram of the Receiver

A brief description of the clipped versions of OFDMA and SC-FDMA is done to detail the modulation proposal.

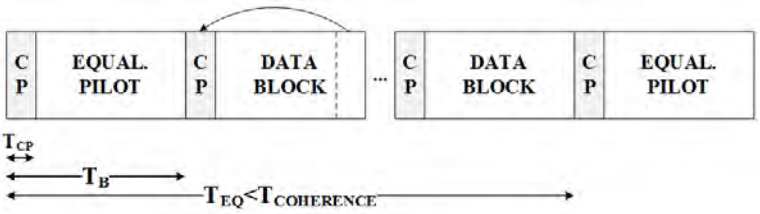

Fig. 5.4 Data Frame structure

5.3.1 OFDMA

The adoption of the OFDMA modulation scheme for downlink radio channel by the 3GPP for LTE is a consequence of the successful implementation in other applications such as Digital Video Broadcasting (DVB), Asynchronous Digital Subscriber Line (ADSL), IEEE 802.11 a/g or Wimax [15]. This technique was adopted because of its high spectral efficiency and its low complexity to reduce frequency-selective fading channels. For these reasons, we are testing this modulation scheme in our HF radio channel.

The OFDMA is a multi-carrier modulation [16] which transmits N_{car} complex values $S_n, n = 0, 1, ..., N_{car} - 1$, in parallel using N_{car} orthogonal sub-carriers. The OFDMA wave-

form is defined as (5.1), where n is the number of carriers, v is the number of samples and N_{car} the total number of available carriers or the total number of samples in time domain [8].

$$x[v] = \frac{1}{N_{car}} \sum_{n=0}^{N_{car}-1} S_n e^{j2\pi nv/N_{car}} \quad v = 0, 1, ..., N_{car} - 1 \tag{5.1}$$

A block diagram of the OFDMA structure is shown in Fig. 5.5.

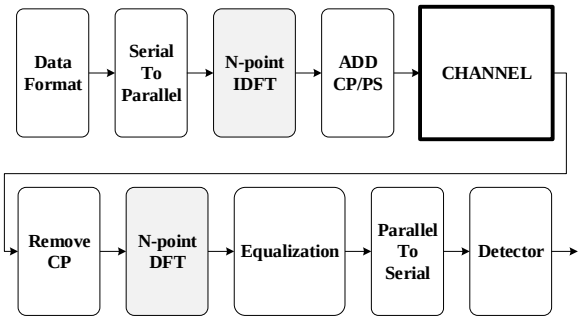

Fig. 5.5 Diagram of the OFDMA modulation

One of the main drawbacks of OFDMA is its non-constant envelope, usually measured with the PAPRm which is defined in equation (5.2), which is the ratio between the maximum peak power of each symbol and the mean power of the signal.

$$PAPR(x(t)) = \frac{max(|x(t)|^2)}{E[|x(t)|^2]} \tag{5.2}$$

The PAPR depends on the number of sub-carriers of the OFDMA, the larger the number of sub-carriers the higher the PAPR value. Therefore, a small number of sub-carriers have higher mean power than a large one. This dependence can be seen with the complementary cumulative distribution function (CCDF), which evaluates when $P(PAPR > PAPR_0)$, for different number of N_{car} and different symbol constellations (PSK, Q-PSK, 8-PSK and 16QAM). In Fig. 5.6, the dependency between the N_{car} and the PAPR for a Q-PSK constellation is shown. The CCDFs of PAPR remain constant independently of the constellation (PSK, Q-PSK, 8-PSK and 16-QAM), the CCDF of the PAPR only depends on the number of sub-carriers [17], because the CCDF can be approximated by $P(PAPR > PAPR_0) \approx 1 - (1 - e^{PAPR_0})^{N_{car}}$, for this reason only Q-PSK is shown.

There are several techniques to reduce the PAPR in OFDMA schemes [18]. The most known techniques are: *i)* clipping, *ii)* coding, *iii)* partial transmit sequence (PTS), *iv)* selected mapping (SLM), *v)* nonlinear companding transform, *vi)* tone reservation (TR) and *vii)* tone

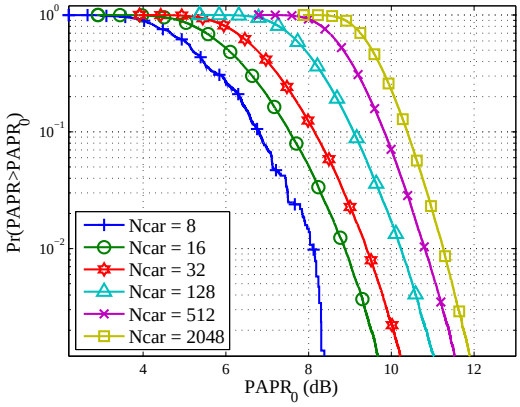

Fig. 5.6 CCDF of PAPR for Q-PSK OFDMA

injection (TI). Clipping is the easiest way to reduce the PAPR and has the lowest computational cost, for this reason this paper is focused on this technique. It consists on clipping the amplitude of the input signal to a predetermined value, as indicated on equation (5.3), where W is the threshold value, $x[n]$ the input signal, $y[n]$ the output signal of the clipper and $\phi(x[n])$ the phase of the input signal.

$$y[n] = \begin{cases} x[n], & \text{if } |x[n]| \leq W \\ We^{i\phi(x[n])}, & \text{otherwise} \end{cases} \tag{5.3}$$

Input back-off (IBO) is defined as the difference between the squared clipped parameter W^2 and the signal mean power. This clipping generates a non-linear distortion. This distortion rotates the constellation and produces noise both in-band and out-band [17]. To measure the in-band noise and the rotation of the constellation the error vector magnitude (EVM) is usually used, defined in (5.4), where P_{ideal} and P_{real} are the ideal and the demodulated position in-phase and quadrature of the constellation, respectively.

$$EVM = \sqrt{\frac{P_{real}}{P_{ideal}}} \tag{5.4}$$

The lower the IBO, the higher the EVM, as shown comparing the sub-carriers Q-PSK OFDMA with different IBO values in Fig. 5.7 with the PAPR observed for the same N_{car} of Fig. 5.6. Therefore, for more complex constellations, which can only achieve low EVM values, the use of low level of clipping cannot be used.

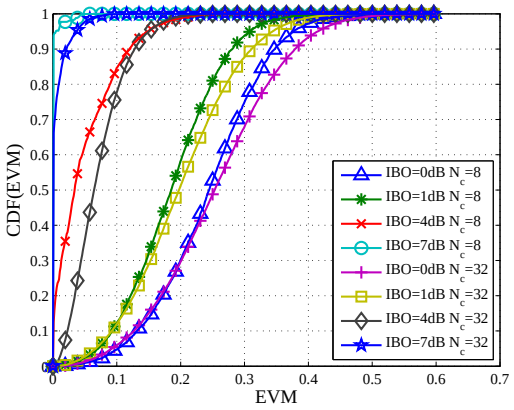

Fig. 5.7 CDF of EVM for Q-PSK sub-carriers

5.3.2 SC-FDE

SC-FDE is a modified version of the common single carrier transmission which performs the equalization in frequency domain. This technique is able to mitigate the effects of frequency-selective channels, and has a similar complexity to OFDMA as we can see comparing the block diagram of OFDMA and SC-FDE in Fig. 5.5 and Fig. 5.8, respectively.

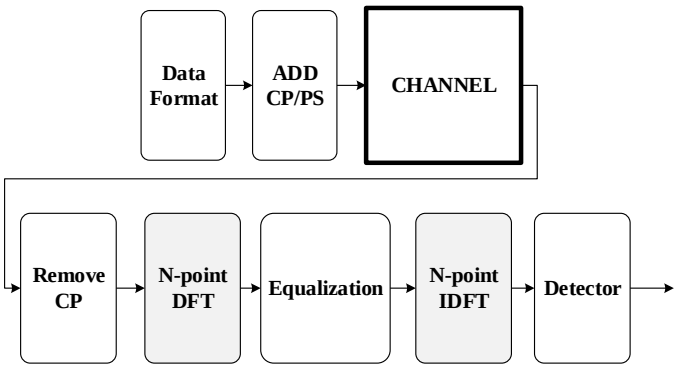

Fig. 5.8 Diagram of the SC-FDE modulation

The frequency domain equalization is computationally more efficient than time domain equalization and this is important for real time data processing. In fact, for channels with high multipath delay spread, the time domain equalization becomes impracticable due to the large number of taps required. SC-FDE presents some advantages compared to multi-carrier schemes such as OFDMA. Mainly, SC-FDE is less sensitive to non-linearities because the PAPR is lower, and is more robust to Doppler shift effect that produces inter-carrier interference (ICI) in OFDMA because of the low frequency spacing between sub-carriers. For these

reasons, we chose this technique to be tested over our HF channel.

The linear distortion introduced by a multipath propagation channel, producing inter-symbolic interference (ISI), can be compensated with equalization methods. Frequency domain equalization is a point-wise multiplication as we can see in (5.5) and (5.6), where $Y(f)$, $H(f)$, $X(f)$ and $C(f)$, are the Fourier transform of the received signal, the channel impulse response (CIR), the transmitted signal and the coefficients of the equalizer in frequency domain, respectively.

$$Y(f) = H(f) \cdot X(f) \tag{5.5}$$

$$X(f) = C(f) \cdot Y(f) \tag{5.6}$$

For channel equalization with linear filtering technique, the most commonly used criterion are zero-forcing (ZF) (5.7) and minimum mean square error (MMSE) (5.8) which mitigate the effect of the low SNR. The noise estimation N_0 is evaluated measuring in several different bandwidth intervals out of the channel bandwidth and H_{est} is the estimation of the CIR.

$$C(f) = \frac{1}{H_{est}(f)} \tag{5.7}$$

$$C(f) = \frac{H^*_{est}(f)}{|H_{est}(f)| + N_0} \tag{5.8}$$

The removal of the CP from the data block in the receiver side prevents the IBI, and ensures that the convolution of the channel impulse response (CIR) with the transmitted signal follows the structure of a circular convolution. Therefore, a FDE can be applied because the circular convolution in the time domain is equivalent to the point-wise multiplication in the DFT domain [19].

The clipping to reduce the PAPR is not necessary for the designed SC-FDE modulation, because the envelope has always a constant value. Then, the PAPR is 0 dB for a band base square waveform. A preliminary study with SC-FDE over the long haul of our interest can be found in [7].

5.3.3 SC-FDMA

SC-FDMA is a technique for high throughput which uses a single carrier with frequency domain equalization. It can be considered as a modified version of SC-FDE with frequency division multiplexing access. This novel technique keeps the PAPR lower than in OFDMA

because of its single carrier structure. SC-FDMA has similar throughput performance and essentially similar computational complexity than OFDMA [15].

In SC-FDMA, the data is modulated into N_{car} complex symbols, typically Q-PSK, 16-QAM and 64-QAM for LTE standard. Afterwards, the block of N_{car} data symbols is applied to a N_{car} size DFT, known as DFT-precoding operation (5.9).

$$A_n = \frac{1}{\sqrt{N_{car}}} \sum_{i=0}^{N_{car}-1} S_i e^{-j2\pi in/N_{car}} \tag{5.9}$$

Next step is to shift the baseband N_{car} DFT carriers to a desired part of the total spectrum with a total of M carriers, which is known as sub-carrier mapping. There are mainly 3 ways to do the sub-carrier mapping: *i)* localized FDMA (LFDMA), *ii)* interleaved FDMA (IFDMA) and *iii)* distributed FDMA (DFDMA). Fig. 5.9 illustrates the whole process from the DFT-precoding to the sub-carrier mapping.

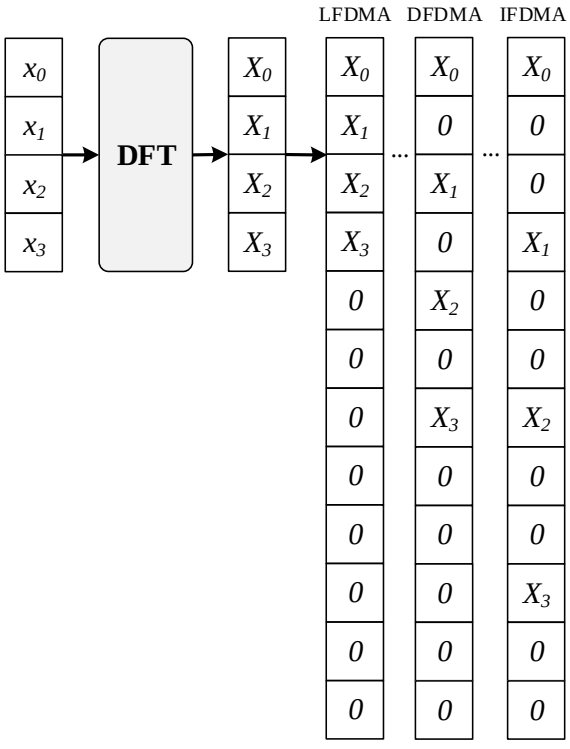

Fig. 5.9 Sub-carrier mapping of SC-FDMA

The block diagram of the SC-FDMA is shown in Fig. 5.10.

Several studies show that IFDMA has lower PAPR than LFDMA [20–22]. This paper is focused on LFDMA, which uses the lowest bandwidth. LFDMA can be seen as an inter-

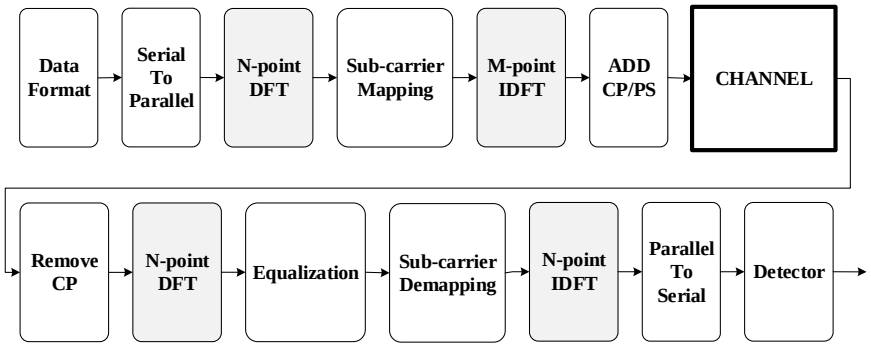

Fig. 5.10 Diagram of the SC-FDMA structure

polator filter of the input complex data symbols where these data symbols are placed every $L = M/N_{car}$ samples, which is the oversampling factor. The rest of samples are the transition between the symbols, and those increase the PAPR.

While the PAPR only depends on the N_{car} in OFDMA, in SC-FDMA depends on the N_{car} and the constellation modulated on the carriers (see Fig. 5.11a and Fig. 5.11b). However, the PAPR is lower for SC-FDMA than OFDMA.

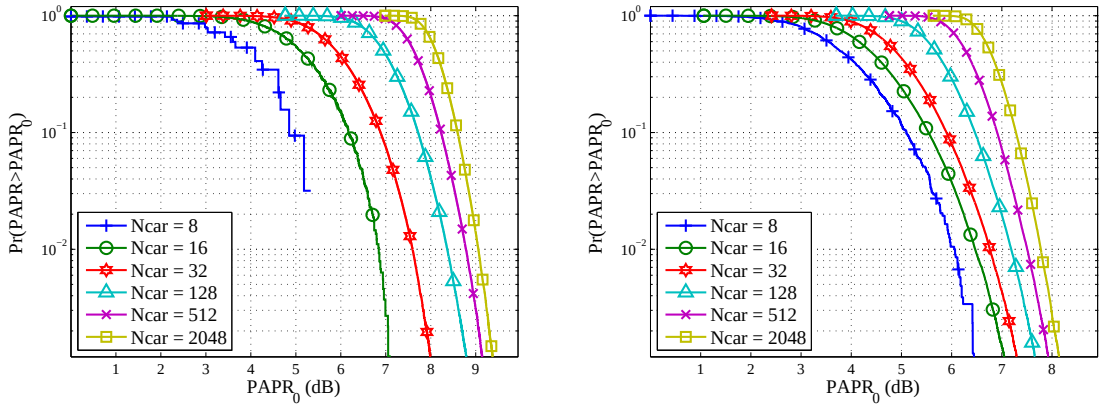

(a) PSK (b) Q-PSK

Fig. 5.11 CCDF of PAPR for SC-FDMA scheme

Measuring the EVM after clipping the signal for different IBOs we can observe that SC-FDMA presents lower EVM values than OFDMA (see Fig. 5.7 and Fig. 5.12). For instance, for OFDMA and SC-FDMA with $N_{car} = 8$ and IBO=1 dB the $CDF(0.1)$ are 0.43 and 0.047, respectively. Mainly, because SC-FDMA has lower PAPR than OFDMA, and the proportion of clipped signal is lower as well. Hence, the BER should be lower for SC-FDMA than OFDMA. In Fig. 5.12, different N_{car} for the same level of IBO produce exactly the

same EVM. Therefore, the N_{car} does not impact in the EVM despite the PAPR depends on it. In [23], the number of sub-carriers does not have any impact for SC-FDMA in terms of BER for an additive white Gaussian noise (AWGN) channel.

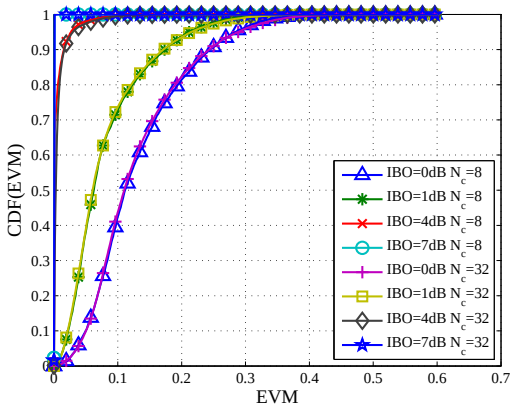

Fig. 5.12 CDF of EVM for Q-PSK sub-carriers

5.4 Simulation Results

The modulation schemes tested in this paper have been simulated through a ionospheric HF channel with Matlab using the ITU-R F.1487 [24], which specifies three HF conditions for good, moderate and poor channels in terms of multipath delay spread and Doppler spread (see Table 5.1).

Tabla 5.1 HF channel recommendations parameters by ITU-R F.1487

Channel	*Multipath Delay Spread* (ms)	*Doppler Spread* (Hz)
Good	0.5	0.1
Moderate	1	0.5
Poor	2	1

The Doppler spectrum of a HF channel is based on a Watterson model described in [25]. The reason for having large multipath delay spread compared to other wireless channels is that the signal can bounce several times between the E and F layers of the ionosphere. However, the Doppler spread is small because the layers are moving slowly [26].

The aim of this work is to compare a SC-FDE with a clipped version of OFDMA and SC-FDMA to be used in ionospheric HF communications, mostly in those channels where the SNR is very low [2].

The signal generated in base band is filtered with a Watterson channel for good, moderate and poor channel conditions. Finally, a desirable white noise power is added without taking into account the power of the input signal which has been clipped and filtered because we want to evaluate the improvement in the performance obtained due to the signal amplification. In the receiver, the signal is demodulated and the results are given in terms of BER. To remove the IBI, a CP of 3.5 ms is used, which is larger than the 2 ms proposed for testing poor HF channels [24]. A linear filtering equalization with MMSE criterion has been applied with the perfect knowledge of the CIR which has been used to simulate the channel.

5.4.1 SC-FDE

The simulation is based on a testbench in which different duration of block, BW and constellation have been tested. This parameters are listed below:

- Bandwidths of 400, 800 and 1250 Hz.
- Duration of block of 10, 30, 50 and 70 ms.
- PSK, Q-PSK and 8-PSK constellations.

The simulations have been carried out for good, moderate and poor channel conditions. For good channel conditions, the BER only depends on the SNR and it is independent of the duration of the block due to a long coherence time. The coherence time, which is proportional to the inverse of the Doppler spread (0.1 Hz), is greater than the longest block (70 ms). However, for poor channel conditions, in which the Doppler spread is 1 Hz, the longer the block the worse the BER, as could be predicted (see Fig. 5.13 for 400 and 800 Hz), due to the variability of the channel during the transmission of a block.

As a conclusion, the shorter the block the lower the BER. However, the spectral efficiency of the transmission is higher for longer block because the total amount of CP added is smaller. A trade-off between spectral efficiency and BER should be obtained. In Table 5.2, we can observe that the spectral efficiency for PSK transmission is 0.70 for 10 ms and 0.90, 0.93 and 0.95 for 30, 50 and 70 ms, respectively. Therefore, 10 and 70 ms are discarded because of the spectral efficiency and the BER, respectively, and both 30 and 50 ms are good candidates.

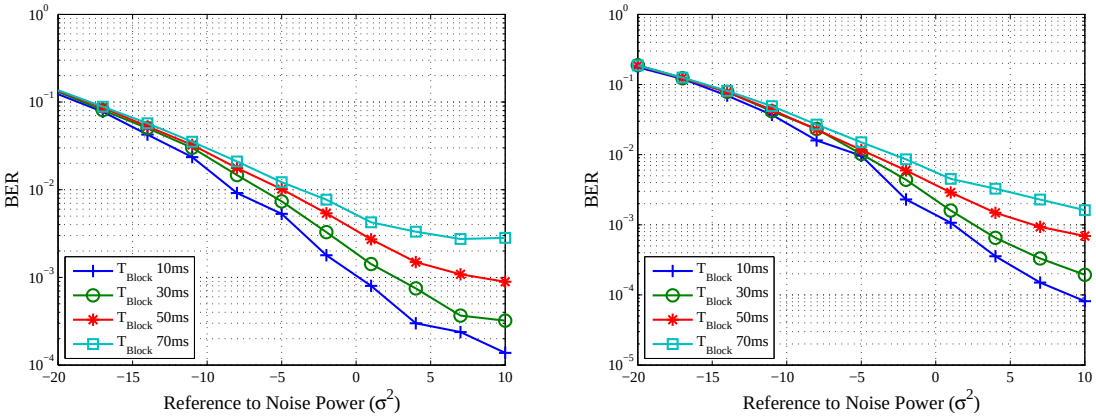

(a) 400 Hz Q-PSK (b) 800 Hz Q-PSK

Fig. 5.13 BER for SC-FDE with poor channel conditions

Tabla 5.2 Spectral efficiency for the SC-FDE tested

Constel.	*Tb* (*ms*)	*Spec.Eff.* (*bps*/*Hz*)
PSK	10	0.74
PSK	30	0.90
PSK	50	0.93
PSK	70	0.95
Q-PSK	10	1.48
Q-PSK	30	1.79
Q-PSK	50	1.87
Q-PSK	70	1.90

5.4.2 OFDMA and SC-FDMA

A comparison between OFDMA and SC-FDMA is done because of the previous successful results obtained with OFDMA and the promising better outcomes of SC-FDMA, which pre-sents lower PAPR. The simulation clips the generated OFDMA and SC-FDMA signals for different IBOs, and amplifies the signal to keep the maximum amplitude in time domain to 0 dBW. This amplification improves the SNR at the receiver. The test has been done for OFDMA symbol duration of 10, 20 and 40 ms, IBOs of 1, 4 and 7 dB and using 8, 16 and 32 carriers. In Table 5.3 we summarize the parameters of the different schemes tested for both OFDMA and SC-FDMA.

Tabla 5.3 Detail of the modulation parameters

T_B (ms)	N_{car}	BW (Hz)	Bitrate (bps)		Spc. Eff. (bps/Hz)	
			BPSK	Q-PSK	BPSK	Q-PSK
10	8	781,3	582,2	1164,4	0,75	1,49
10	16	1562,5	1164,5	2329	0,75	1,49
10	32	3125	2329	4658	0,75	1,49
20	8	390,6	333,6	667,2	0,85	1,71
20	16	781,3	667,2	1334,4	0,85	1,71
20	32	1562,5	1334,4	2668,8	0,85	1,71
40	8	195,3	179,9	359,8	0,92	1,84
40	16	390,6	359,9	719,8	0,92	1,84
40	32	781,3	719,7	1439,4	0,92	1,84

In the simulation through an AWGN channel we can observe that the lower the IBO, the lower the BER, as could be predicted. For instance, in Fig. 5.14a for OFDMA, the BER for IBO=1 and IBO=4 dB are $3.5 \cdot 10^{-3}$ and $8.5 \cdot 10^{-3}$, respectively, with -9 dB of ratio between the maximum signal peak and the noise power. Moreover, SC-FDMA outperforms OFDMA for the same level of IBO for both PSK and Q-PSK. However, OFDMA and SC-FDMA for 16-QAM with 32 carriers in Fig. 5.14b presents an irreducible residual BER. This irreducible BER is higher as lower the IBO. This is observed on clipped signals with amplitude and phase modulation because 16-QAM and 64-QAM are more sensible to the EVM than PSK and Q-PSK.

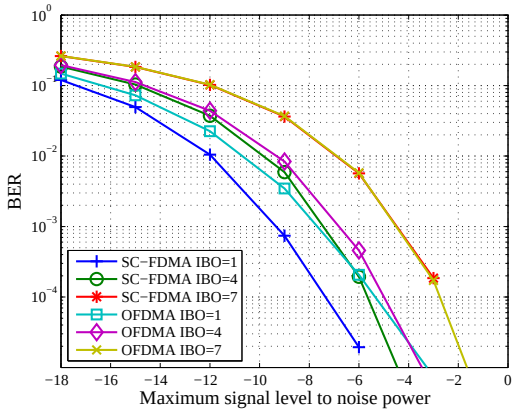

(a) BER vs SNR for 16 sub-carriers Q-PSK

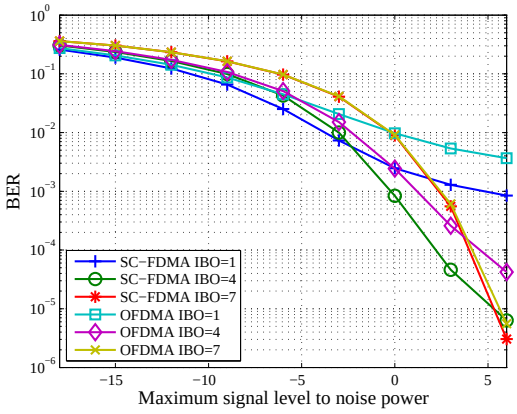

(b) BER vs SNR for 32 sub-carriers 16-QAM

Fig. 5.14 BER vs SNR with an AWGN channel

From the simulation through a HF Watterson channel we can observe that the lower the IBO, the lower the BER. In this case, irreducible BER is presented for both PSK and Q-PSK modulation (see Fig. 5.15f, for Q-PSK where the peak to noise power is higher than 10 dB). It is produced by the EVM of clipping the signal, the noise enhancement of applying channel equalization to remove the ISI, and the Doppler shift that produces ICI. This effect is observed in both OFDMA and SC-FDMA. However, SC-FDMA outperforms OFDMA with lower irreducible BER.

5.4.3 Comparison between modulations

From the previous simulations, we can conclude that the results of the clipped version of SC-FDMA outperforms OFDMA with the same configuration parameters such as symbol duration and number of sub-carriers because of its lower inherent PAPR and its most robustness to ICI. This is observed for all values of IBO tested over all channel conditions.

Good channel conditions

In Fig. 5.16, a comparison between the best results of each modulation scheme is carried out for good channel conditions. This comparison is done for bandwidths of 800 Hz and the Q-PSK constellation. SC-FDE uses blocks of 10 ms and OFDMA and SC-FDMA use clipping values of 1 dB because these configurations present the best results in terms of BER .

SC-FDE present better performance compared with OFDMA and SC-FDMA. SC-FDMA with 32 sub-carriers presents better performance than the rest of SC-FDMA and OFDMA. We can observe that both SC-FDE and SC-FDMA have better performance than OFDMA.

Poor channel conditions

In Fig. 5.17, the comparison between the best results of each modulation scheme is carried out for poor channel conditions.
SC-FDE present better results than the other modulation schemes. In this case, the modulation scheme of SC-FDMA with 16 sub-carriers outperforms SC-FDMA with 32 sub-carrier for positives values of SNR due to the irreducible residual BER of SC-FDMA with 32 sub-carriers. We can observe that both SC-FDE and SC-FDMA have also better performance than OFDMA.

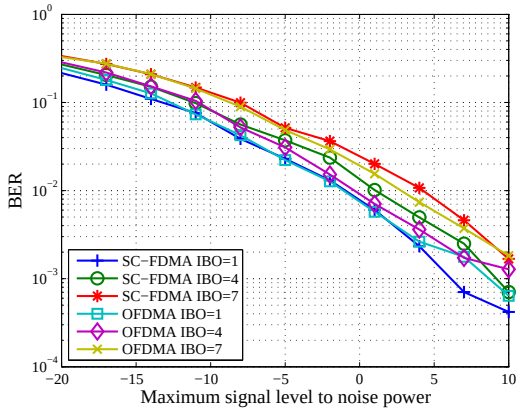

(a) $N_{car} = 8$ Good

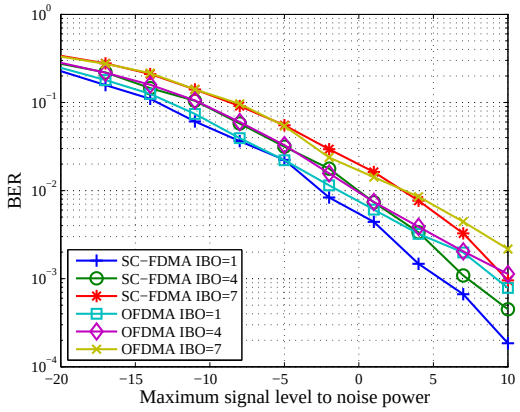

(b) $N_{car} = 16$ Good

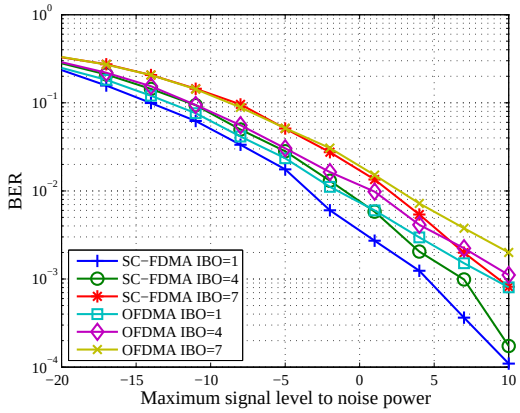

(c) $N_{car} = 32$ Good

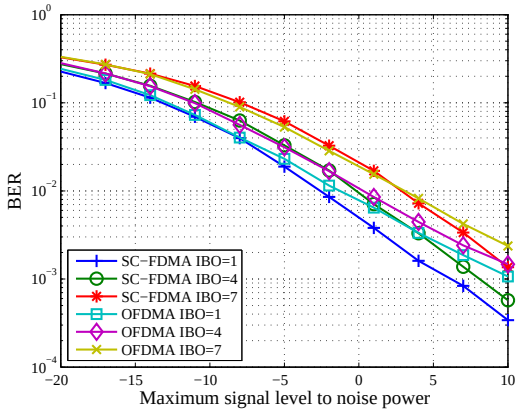

(d) $N_{car} = 8$ Poor

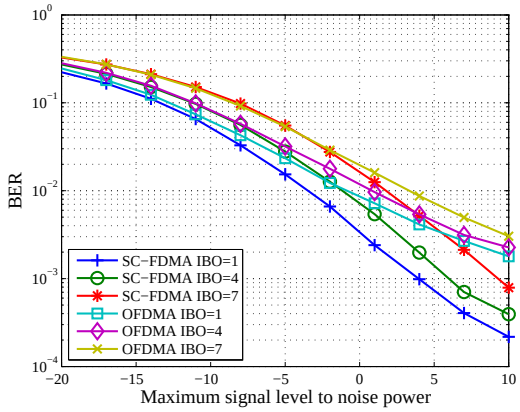

(e) $N_{car} = 16$ Poor

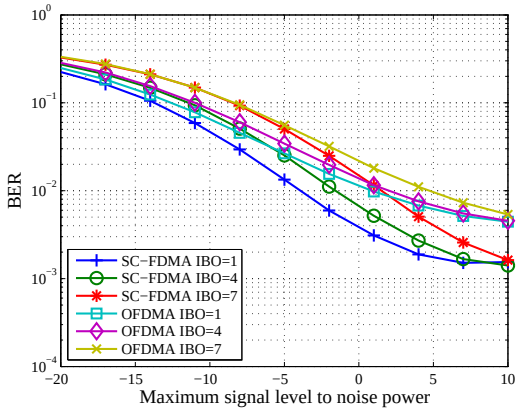

(f) $N_{car} = 32$ Poor

Fig. 5.15 BER for Q-PSK for good and poor channel conditions with different number of sub-carriers and a bandwidth of 800 Hz

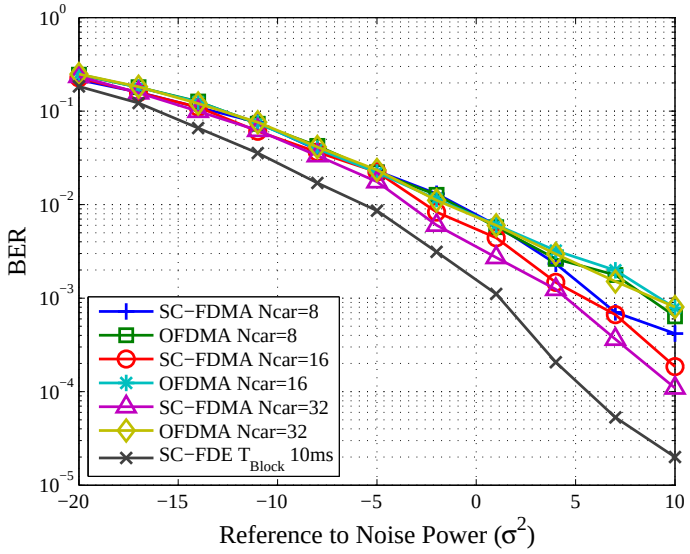

Fig. 5.16 Best results for each modulation scheme for good channel condition

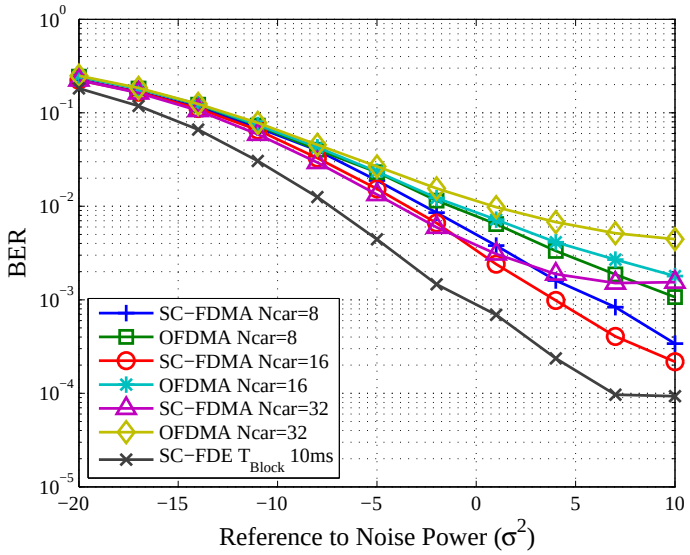

Fig. 5.17 Best results for each modulation scheme for poor channel condition

5.5 Test Design

The tests over the 12760 km ionospheric channel are transmitted during 10 min, which is the reserved time to test modulation schemes. The modulation test are transmitted at the best frequency for each hour, obtained by sounding the previous days, as we can see in Table 5.4 where the frequency carrier of each time slot tested for February 6th of 2014 are detailed. In the receiver side, the data in the three antennas is saved simultaneously [3, 4]. To evaluate

the proposed frequency domain equalization schemes, the structure of the frame of Fig. 5.4 was used, T_{CP} is 3.5 ms. The equalization sequence is a Zadoff-Chu sequence [15], which has constant envelope and constant spectrum module. For hardware simplicity, the length of the Zadoff-Chu sequence is the same as the symbol duration, it means that longer data blocks have more samples for channel equalization. A training set of PN m-sequences [27] is sent at the beginning of each modulation test which guarantees a correct acquisition and synchronization. These training sequences consist of 3 m-sequences of 2047 chips each and an oversampling factor of 10. Those received data blocks with ratios between the maximum and the mean of the correlation of less than 12 dB are discarded because of its low SNR level, assuming bad channel conditions.

The test parameters of each modulation scheme are described below.

Tabla 5.4 Detail of frequency carrier setup of each hour for February 6th of 2014.

Time (Hour)	*Freq.* (MHz)	*Time* (Hour)	*Freq.* (MHz)	*Time* (Hour)	*Freq.* (MHz)
0	13.0	8	12.5	16	25.0
1	12.5	9	13.0	17	23.0
2	13.0	10	19.0	18	24.0
3	12.5	11	24.0	19	13.0
4	13.0	12	24.0	20	13.5
5	8.5	13	24.0	21	13.0
6	5.0	14	24.0	22	13.5
7	13.5	15	24.0	23	13.0

5.5.1 SC-FDE

The SC-FDE test characteristics are:

- Bandwidths of 400, 800, 1250 and 2500 Hz.
- Block times of 10, 30, 50 and 70 ms.
- PSK, Q-PSK and 8-PSK constellations.

5.5.2 OFDMA and SC-FDMA

The parameters of the OFDMA and SC-FDMA modulation schemes tested are listed below and also shown in Table 5.3.

- N_{car} of 8, 16 and 32 carriers.
- Block times of 10, 20 and 40 ms.
- PSK and Q-PSK constellations.

The duration of blocks is different from the ones in SC-FDE. In fact, 10, 20 and 40 ms are 10.24, 20.48 and 40.96 ms, which correspond to power of 2 samples at a frequency sampling of 100 ksps to apply the FFT algorithm. The time synchronization has been modified and improved from previous OFDMA studies [8], for this reason, the results presented in this paper outperform the previous ones due to the fact that OFDMA and SC-FDMA are very susceptible to synchronisation errors.

5.6 Test results

The data transmission was conducted during the austral summer of the campaign 2013-14. SC-FDE, OFDMA and SC-FDMA results are analyzed and the BER results are presented. These results were obtained after transmitting the different tests designed, through the long haul link of 12760 km from Antartica to Spain. The results of these tests are extremely important in our system because this channel is really challenging and the SNR expected in the receiver side is very low.

5.6.1 SC-FDE

SC-FDE analyzed was transmitted during the following days: *i)* January 28th, *ii)* February 8th, *iii)* February 9th and *iv)* January 15th. The CDF of the BER is used to compare the performance of the modulation scheme because it is clearer to analyse the results. The best results in terms of BER are summarized in Table 5.5. The tests with $CDF(0.05) < 0.3$ have been discarded in this paper, so only those with the best performance are shown. We have the most robust mode with a BW of 400 Hz, PSK and blocks of 50 ms and a throughput of 373.8 bps. We can also have a higher throughput with a bandwidth of 400 Hz, Q-PSK and blocks of 50 ms with a throughput of 747.7 bps. The performance of 10, 30 and 50 ms for a bandwidth of 400 Hz has similar results. The scheme chosen is 50 ms because it has the higher spectral efficiency due to the lower number of CPs and the $CDF(BER)$ is better up to 0.04, which is the comparison between the Q-PSK with a BW of 400 Hz and 10 ms and the Q-PSK with a BW of 400 Hz and 50 ms. We can define these as 2 operation modes.

Tabla 5.5 Test results for SC-FDE

$Constel.$	BW (Hz)	Tb (ms)	$Bitrate$ (bps)	$Spec.Eff.$ (bps/Hz)	CDF (BER) (> 0.05)
PSK	400	10	296.3	0.74	0.54
PSK	400	30	358.2	0.90	0.56
PSK	400	50	373.8	0.93	0.57
PSK	400	70	381.0	0.95	0.39
PSK	800	10	592.6	0.74	0.40
PSK	800	30	716.4	0.90	0.32
Q-PSK	400	10	592.6	1.48	0.41
Q-PSK	400	30	716.4	1.79	0.42
Q-PSK	400	50	747.7	1.87	0.45
Q-PSK	400	70	761.9	1.90	0.37

5.6.2 OFDMA and SC-FDMA

OFDMA and SC-FDMA analyzed were transmitted during the following days: *i)* January 31st, *ii)* February 1st, *iii)* February 11th and *iv)* February 15th. OFDMA test results are summarized in Table 5.6 and SC-FDMA in Table 5.7. The same criterion of SC-FDE has been used, only $CDF(0.05) > 0.3$ are shown.

Tabla 5.6 Test results for OFDMA

$Constel.$	Tb (ms)	N_{car}	BW (Hz)	IBO dB	$Bitrate$ (bps)	CDF (BER) (> 0.05)
PSK	10	8	781,3	1	582	0,38
PSK	20	8	390,6	1	334	0,72
PSK	20	8	390,6	4	334	0,34
PSK	20	16	781,3	1	667	0,39
PSK	40	8	195,3	1	180	0,50
PSK	40	8	195,3	4	180	0,50
PSK	40	8	195,3	7	180	0,53
PSK	40	16	390,6	1	360	0,53
Q-PSK	20	8	390,6	1	667	0,34
Q-PSK	20	8	390,6	4	667	0,39
Q-PSK	40	8	195,3	1	360	0,47
Q-PSK	40	8	195,3	7	360	0,31

Tabla 5.7 Test results for SC-FDMA

$Constel.$	Tb (ms)	N_{car}	BW (Hz)	IBO dB	$Bitrate$ (bps)	CDF (BER) (> 0.05)
PSK	10	8	781,3	1	582	0,38
PSK	10	8	781,3	4	582	0,50
PSK	20	8	390,6	1	334	0,50
PSK	20	8	390,6	4	334	0,47
PSK	20	8	390,6	7	334	0,31
PSK	40	8	195,3	1	180	0,53
PSK	40	8	195,3	4	180	0,66
PSK	40	8	195,3	7	180	0,53
PSK	40	16	390,6	1	360	0,39
PSK	40	16	390,6	4	360	0,52
PSK	40	32	781,3	1	720	0,35
Q-PSK	20	8	390,6	1	667	0,30
Q-PSK	20	8	390,6	4	667	0,30
Q-PSK	40	8	195,3	1	360	0,44
Q-PSK	40	8	195,3	4	360	0,55

We can define two operation modes for both OFDMA and SC-FDMA. For OFDMA, we define a robust mode with 8 sub-carriers and BW of 390.6 Hz, PSK and blocks of 20 ms with a throughput of 334 bps. We can also have a higher throughput with 8 sub-carriers a bandwidth of 390.6 Hz, Q-PSK and blocks of 20 ms with a throughput of 667 bps. For SC-FDMA, we define a robust mode with 8 sub-carriers and BW of 195.3 Hz, PSK and blocks of 40 ms with a throughput of 180 bps. We can also have a higher throughput with 32 sub-carriers a bandwidth of 781.3 Hz, PSK and blocks of 40 ms with a throughput of 720 bps.

In Fig. 5.18, we can observe, using the same bandwidth of 800 Hz, that 8 carriers have lower BER than 32 carriers for OFDMA and SC-FDMA due to the lower frequency spacing, which is 100 and 25 Hz, respectively. Therefore, when the number of carriers increases maintaining the bandwidth, the BER decreases, due to the ICI effect. The fact of having more carriers over the same bandwidth means that the frequency spacing is lower. The ICI produced by the Doppler effect is higher for lower frequency spacing, because the percentage of overlapped carrier is also higher. Moreover, the best performance is obtained with IBO of 1 dB rather than IBO of 4 or 7 dB because of the improvement of SNR. The SNR is improved

with higher power amplification and there is a trade-off between that improvement and the increment of the EVM, that gives us better performance in terms of BER.

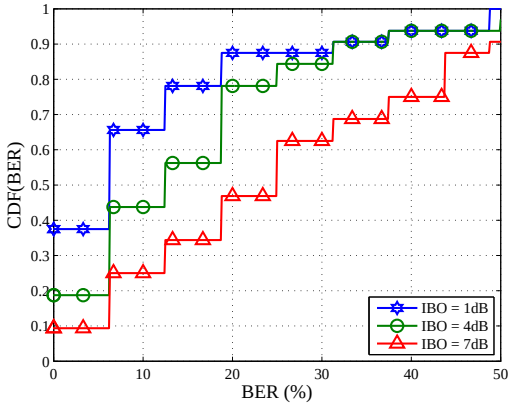

(a) $T_s = 10ms$ and $N_{car} = 8$ for OFDMA

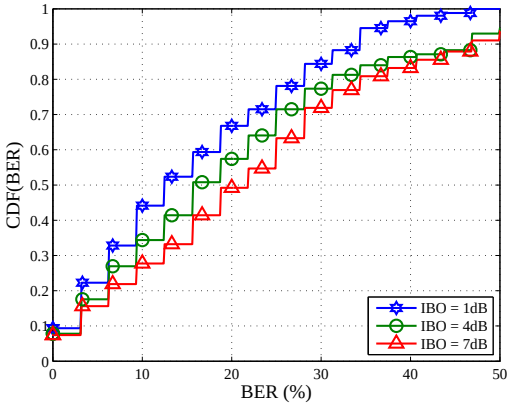

(b) $T_s = 40ms$ and $N_{car} = 32$ for OFDMA

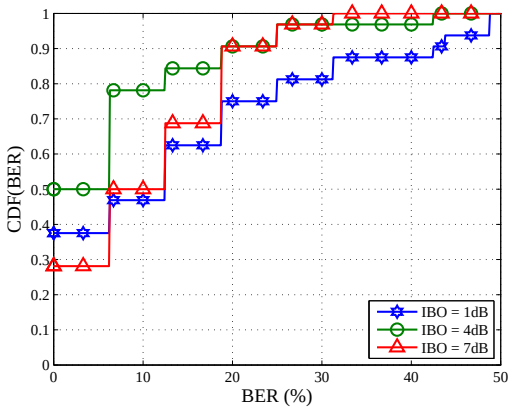

(c) $T_s = 10ms$ and $N_{car} = 8$ for SC-FDMA

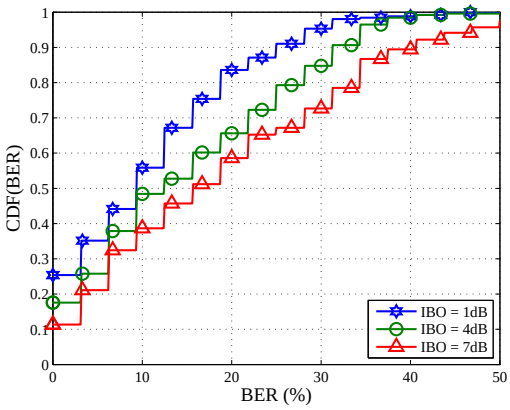

(d) $T_s = 40ms$ and $N_{car} = 32$ for SC-FDMA

Fig. 5.18 OFDMA and SC-FDMA results for a bandwidth of 800 Hz and PSK modulation

The results of CDF(BER) for 1 dB IBO outperforms the other IBOs. However, in Fig. 5.18c, we can observe that the CDF(BER) for the IBO of 4 dB is better than 1 dB, but is only because for 4 dB test experienced better SNR than for 1 dB (see Fig. 5.19). This punctual changes of slope in the figures are due the variations that real data performance, and the fact that we have only 5 days of data. The figures of CDF(BER) show lack of resolution in the x-axis because the measure of BER has been calculated over the average of blocks of 16 and 32 bits. As a conclusion, for both OFDMA and SC-FDMA, decreasing the number of sub-carriers and maintaining the bandwidth of the modulation produces lower BER due to the ICI. Moreover, as we can expect, the lower the bandwidth the better the BER because the SNR observed at the receiver side is higher. It is desirable to obtain a trade-off between

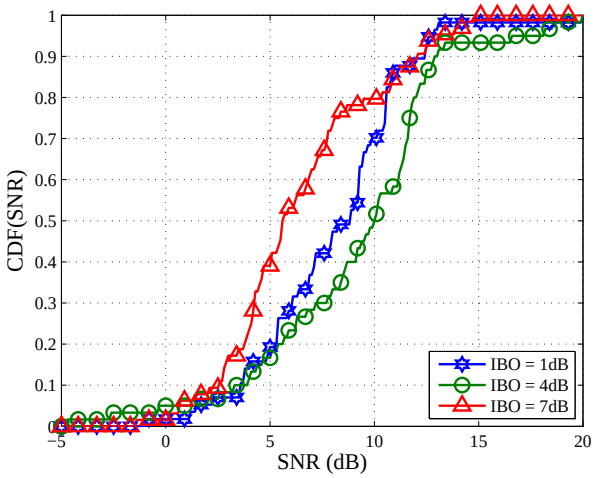

Fig. 5.19 CDF of SNR for $T_s = 10\ ms$ and $N_{car} = 8$ PSK SC-FDMA

the sub-carrier spacing and the total bandwidth to avoid ICI, and also to obtain high level of SNR in the receiver side.

5.7 Conclusions

In this paper we have presented a performance comparison between SC-FDE, OFDMA and SC-FDMA in a 12760 km long haul Antarctic link. This study has been done simulating an AWGN and the HF Watterson channel [25] model proposed by the ITU-R for good, moderate and poor ionospheric conditions.

From simulated results of SC-FDMA and OFDMA, we can conclude for PSK and Q-PSK that the use of a higher limit to clip the envelope of the signal, reducing the PAPR and increasing the mean transmitted power, has demonstrated an increase of SNR for both SC-FDMA and OFDMA. Therefore, it obtains a lower BER in the receiver even though the EVM has increased. For 16-QAM and 64-QAM this technique cannot be applied with a limiter of an IBO of 1 dB because the EVM obtained is too large and has a high irreducible BER. Moreover, SC-FDMA is less sensitive to Doppler effect.

Experimental results in a real channel were performed during the 2013/2014 campaign at the SAS, through the HF link from Antarctica to Spain of 12760 km with a transmission power of 200 W and very basic antennas, and these results are presented. This long-haul HF link is time and frequency dispersive and has very low level of SNR because of the distance

between the transmitter and the receiver. In real data, SC-FDMA presents better outcomes of CDF(BER) than OFDMA. However, this modulation scheme has higher computational cost than OFDMA.

The comparison among the three techniques with the real and simulated data, for the case of this very poor channel with very low SNR, SC-FDE and the clipped version of SC-FDMA with IBOs of 1 dB have similar outcomes. However, SC-FDE results with a blocks of 30 ms outperforms SC-FDMA, and it is the best modulation scheme presented in this paper.
In future works, the frequency spacing will be increased to improve robustness to Doppler spread for OFDMA and SC-FDMA, the use of different frequency mapping to reduce the PAPR in SC-FDMA will be tested, and different root-raised cosine (RRC) filters for SC-FDE to reduce the bandwidth increasing the SNR will be used to lower the BER at the receiver.

Acknowledgements

This work has been funded by the Spanish Government under the project CTM2010-21312-C03-03.

Referencias

[1] Perkiomaki, J. (2013).HF Propagation Prediction and Ionospheric Communications Analysis. URL www.voacap.com.

[2] Pijoan, J.L., Altadill, D., Torta, J.M., Alsina-Pagès, R.M., Marsal, S., Badia, D. (2014). Remote Geophysical Observatory in Antarctica with HF Data Transmission: A Review. *Remote Sensing* **6**(8), 7233–7259. DOI 10.3390/rs6087233. URL http://www.mdpi.com/2072-4292/6/8/7233/.

[3] Vilella, C., Miralles, D., Pijoan, J.L. (2008). An Antarctica-to-Spain HF ionospheric radio link: Sounding results. *Radio Science* **43**(4).

[4] Vilella, C., Miralles, D., Altadill, D., Acosta, F., Solé, J.G., Torta, J.M., Pijoan, J.L. (2009). Vertical and oblique ionospheric soundings over a very long multihop HF radio link from polar to midlatitudes: Results and relationships. *Radio Science* **44**(2).

[5] Ads, A., Bergadà, P., Vilella, C., Regué, J.R., Pijoan, J.L., Bardají, R., Mauricio, J. (2013). A comprehensive sounding of the ionospheric HF radio link from Antarctica to Spain. *Radio Science* **48**(1), 1–12. DOI 10.1029/2012RS005074. URL http://doi.wiley.com/10.1029/2012RS005074.

[6] Alsina-Pagès, R.M., Salvador, M., Hervás, M., Bergadà, P., Pijoan, J.L., Badia, D. (2015). Spread Spectrum High Performance Techniques for a Long Haul HF Link. *IET Communications*-To appear.

[7] Hervás, M., Pijoan, J.L., Alsina-Pagès, R.M., Salvador, M., Badia, D. (2014). Single-carrier frequency domain equalisation proposal for very long haul HF radio links. *Electronics Letters* **50**(17), 1252–1254. DOI 10.1049/el.2014.1184. URL http://digital-library.theiet.org/content/journals/10.1049/el.2014.1184.

[8] Bergadà, P., Alsina-Pagès, R.M., Pijoan, J.L., Salvador, M., Regué, J.R., Badia, D., Graells, S. (2014). Digital transmission techniques for a long haul HF link: DSSS

versus OFDMA. *Radio Science* **49**(7), 518–530. DOI 10.1002/2013RS005203. URL http://doi.wiley.com/10.1002/2013RS005203.

[9] MIL-STD-188-110B. (2000). Military Standard - Interoperability and Performance Standards for Data Modems. US DoD.

[10] Deumal, M., Vilella, C., Socoró, J., Alsina, R.M., Pijoan, J.L. (2006). A DS-SS signaling based system proposal for low SNR HF digital communications. In *Proceedings of IET 10th International Conference on Ionospheric Radio Systems and Techniques (IRST 2006)*, pp. 128–132. IET.

[11] Zhang, Z., Zeng, F., Ge, L., Chen, S., Yang, B., Xuan, G. (2012). Design and implementation of novel HF OFDMA communication systems. In *Proceedings of IEEE 14th International Conference on Communication Technology (ICCT)*, pp. 1088–1092. IEEE.

[12] Bergadà, P., Deumal, M., Alsina, R.M., Pijoan, J.L. (2009). Time interleaving study for an OFDMA long-haul HF radio link. In *Proceedings of IET 11th International Conference on Ionospheric Radio Systems and Techniques (IRST 2009)*, pp. 1–4. IET.

[13] Bergadà, P., Deumal, M., Vilella, C., Pijoan, J.L. (2008). Multicarrier Modulation Proposal for Long Distance HF Data Links. In *Proceedings of Ionospheric Effects Symposium (IES'08)*.

[14] Barker, Williamson. (2014). Broadband Frequency Agile HF Folded Dipole Antenna. URL https://www.bwantennas.com/instr/fdipole.pdf

[15] Sesia, S., Toufik, I., Baker, M. (2009). LTE: The UMTS Long Term Evolution. *John Wiley & Sons, Ltd*.

[16] Fazel, K., Kaiser, S. (2003). Multi-Carrier and Spread Spectrum Systems. *John Wiley & Sons, Ltd*.

[17] Deumal, M. (2008). Multicarrier communication systems with low sensitivity to nonlinear amplification. Ph.D. thesis, Enginyeria i Arquitectura La Salle, Universitat Ramon Llull, Barcelona.

[18] Jiang, T., Wu, Y. (2008) An overview: peak-to-average power ratio reduction techniques for OFDMA signals. *IEEE Transactions on Broadcasting* **54**(2), 257–268.

[19] Myung, H.G., Goodman, D.J. (2008). Single Carrier FDMA: A New Air Interface for Long Term Evolution. *John Wiley & Sons, Ltd*.

[20] Myung, H.G., Lim, J., Goodman, D. (2006). Single Carrier FDMA for uplink wireless transmission. *IEEE Vehicular Technology Magazine* **1**(3), 30–38. DOI 10.1109/MVT.2006.307304.

[21] Stemick, M., Rohling, H. (2007). OFDMA-FDMA scheme for the Uplink of a Mobile Communication System. *Wireless Personal Communications* **40**(2), 157–170. DOI 10.1007/s11277-006-9106-x. URL http://link.springer.com/10.1007/s11277-006-9106-x.

[22] Frank, T., Klein, A., Costa, E., Schulz, E. (2005). IFDMA-a promising multiple access scheme for future mobile radio systems. In *Proceedings of IEEE 16th International Symposium on Personal, Indoor and Mobile Radio Communications (PIMRC)*, vol. 2, pp. 1214–1218. DOI 10.1109/PIMRC.2005.1651634.

[23] Gazda, J., Drotár, P., Galajda, P., Kocur, D. (2010). Comparative evaluation of OFDMA and SC-FDMA based transmission systems. In *Proceedings of IEEE 8th International Symposium on Applied Machine Intelligence and Informatics (SAMI)*, pp. 177–181. IEEE

[24] Recommendation ITU-R F.1487. (2000). Testing of HF modems with bandwidths of up to about 12 kHz using ionospheric channel simulators. In: ITU-R.

[25] Watterson, C., Juroshek, J., Bensema, W.D. (1970). Experimental confirmation of an HF channel model. *IEEE Transactions on Communication Technology* **18**(6), 792–803. DOI 10.1109/TCOM.1970.1090438

[26] Davies, K. (1990). Ionospheric radio. 31. *Peter Peregrinus, Ltd.*

[27] Gold, R. (1968). Maximal recursive sequences with 3-valued recursive cross-correlation functions (corresp.). Information Theory, IEEE Transactions on **14**(1), 154–156.

Marcos Hervás received the BSc degree in Telecomunications engineering from Universidad de Alicante (UA), Alicante, Spain, the MSc in Telecomunications engineering from Enginyeria La Salle, Universitat Ramon Llull (URL), Barcelona, Spain, in 2008 and 2011, respectively. Currently is a PhD candidate in the Electronic and Communications (ECO) area at the Engineering Department from URL. His current research interest include the areas of wireless communications and the corresponding digital signal processing

and its electronics, especially for OFDMA, SC-FDMA, HF ionospheric communication and the implementation of software defined radio communication systems in FPGA devices.

Rosa Ma Alsina-Pagès received her BSc and MSc in Electronics and Telecommunications in La Salle, Universitat Ramon Llull (URL) in 1999, 2001 and 2004 respectively. She obtained her PhD in Telecommunication Engineering with Cum Laude in 2012, also in La Salle (URL). She has several papers in communications and signal processing journals. Her current research interests include digital signal processing, physical layer modulation and code design and ionospheric HF communications.

Joan Lluís Pijoan received his MsC degree in Telecommunications from the Polytechnical University of Catalonia (UPC) in 1994 and the PhD degree from Ramon Llull University in 2000. Joan Lluís Pijoan has been the leader of several research projects concerning low power advanced HF communications with Antarctica and multicarrier modulations applied to low voltage and high voltage systems, with a strong cooperation in European Actions COST 262 "Spread Spectrum Systems and Techniques in Wireless and Wired Communications" and COST 289 "Spectrum and Power Efficient Broadband Communications".

Martí Salvador received his BSc and MSc in Telecommunications from Universitat Ramon Llull (URL) in 2013 and 2014 respectively. He has been working in the Electronic and Communications area of the URL where he has received a research internship for three years. His study fields are mainly Mobile Communications, HF and Ionospheric Communications.

David Badia received the BSc degree in Telecommunications engineering from EUETT La Salle, associate to Universitat Politècnica de Catalunya, the MSc degree in electrical engineering, and the PhD degree from Enginyeria La Salle, Universitat Ramon Llull (URL), Barcelona, Spain, in 1990, 1995 and 2012, respectively. He is a lecturer of the Communications and Signal Theory Department since 1987, and member of the new research group in electronic systems, telecommunications and data analysis GR SETAD.

Capítulo 6

Narrowband and Wideband Channel Sounding of an Antarctica to Spain Ionospheric Radio Link

M. Hervás, R.M. Alsina-Pagès, F. Orga, D. Altadill, J.L. Pijoan and D. Badia

Abstract. La Salle and Ebro Observatory have been involved in several joint projects about remote sensing in Antarctica for the last 11 years (approximately one solar cycle). The Ebro Observatory has been monitoring and analyzing the geomagnetic and the ionospheric activity in the Antarctic Spanish station Juan Carlos I, ASJI, (62.7°S, 299.6°E) for more than eighteen and ten years respectively. La Salle has two main goals in the project. The first one is the data transmission and reception from Antarctica to Spain to obtain a historical series of measurements of channel sounding of this 12760 km ionospheric HF radio link. The second one is the establishment of a stable data low power communication system between the ASJI and Cambrils, Spain, (41.0°N, 1.0°E) to transmit the data from the remote sensors located in the island. In this paper, both narrowband and wideband soundings have been carried out to figure out channel availability performed using a frequency range from 2 to 30 MHz with 0.5 MHz step during the 24 hours of the day, encompassing wider channel measurements than previously done, in terms of hours and frequency. This paper presents the results obtained for the austral summer in 2014, using a monopole antenna at the transmitter and an inverted V on the receiver side.

keywords. geomagnetism; remote sensors; HF; ionosphere; channel sounding; Antarctica

Source: Remote Sensing, Volume 9, Issue 8, 21 May 2015, p. 1048–1053

6.1 Introduction

Analyzing the ionosphere and the magnetic field in the Antarctica is an important contribution to understand of Earth's phenomenons concerning the geophysical science. Knowledge acquired on the characteristics of the channel does not only improve the performance of high frequency (HF) radio-communication systems, but also contributes to ionospheric science. Vertical and oblique sounding techniques are frequently used to obtain the characteristics of the ionospheric communications channel for a given radio-link. The geomagnetic observatories have been collecting for years the magnetic field variations in fixed locations having a wide range of time scales, from seconds to centuries, to make possible the understanding of the behavior of the magnetic field of the Earth. The Antarctic Spanish station Juan Carlos I (ASJI) is located in the Livingston Island, a place of great interest because it monitors the sub-auroral zone [1]. The ASJI has a geomagnetic observatory with the International Association of Geomagnetism and Aeronomy code LIV. LIV is remotely managed by the Ebro Observatory Institute (EO) in Spain and it is aimed to monitor the magnetic field variations of that region. ASJI is only attended by scientist and technicians during the austral summer, typically from December to February. As ionospheric exploration by vertical soundings is one of the most commonly used to observe the vertical structure of the ionosphere, a VIS (Vertical Incidence Sounder) was installed at the ASJI during the summer expedition of 2004-2005 by OE. In 2003, an OIS (Oblique Incidence Sounder) was also installed in the ASJI by La Salle with a double objective: *i)* to measure the characteristics of the ionospheric channel from ASJI to Spain, taking into account days, annual and solar cycle variations and *ii)* to settle a robust hardware and software platform for an HF radio-communication system from ASJI to Spain. The later system should be able to operate under hard environmental conditions, with the best digital modulations designed for a low power and high interference communications system. The OIS covers a long haul ionospheric link (see Figure 6.1), of around 12760 km, from the ASJI (62.7°S, 299.6°E) to Cambrils (41.0°N, 1.0°E). In previous works, both narrowband and wideband soundings had been analyzed [2], but both carrier frequencies and the time of transmission were limited. Since 2008, an enhanced transmitter and receiver were installed [3], and the oblique sounding observations can be widely recorded. The results presented in this paper give light to the knowledge of this long haul link, but also help us to design the physical layer characteristics remaining from the previous studies [4–6], where less carrier frequencies were used and the tests were not performed during the entire day.

This paper is organized as follows. Section 2 describes all the measured parameters. Section 3 gives details of the communications hardware equipment between the Remote Geophysical Observatory and Spain. Section 4 explains the test design for narrowband

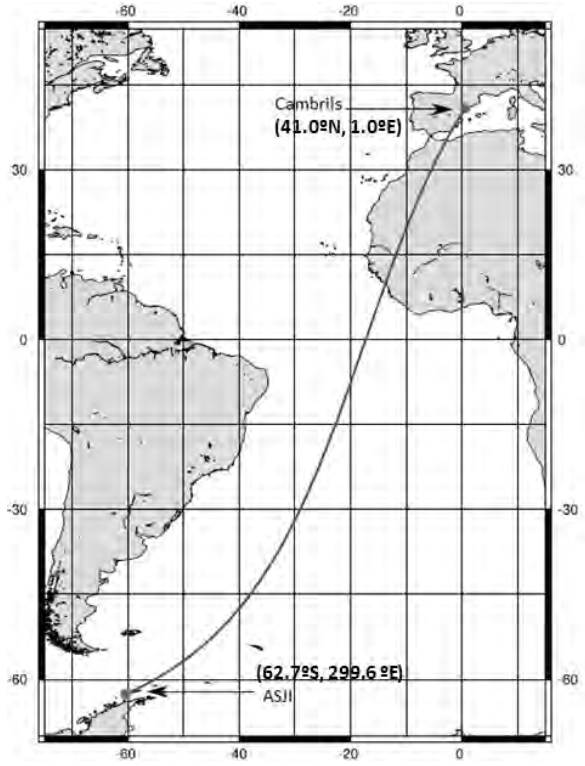

Fig. 6.1 Geographical link characteristics. The transmitter is located in the ASJI, in Livingston Island (62.7°S, 299.6°E) and the receiver is placed in Cambrils (41.0°N, 1.0°E).

and wideband sounding measurements through a long-distance HF link in 2014 campaign. Section 5 presents the results of the sounding measurements. Finally, section 6 contains the conclusions and the future work.

6.2 Measured Parameters

This section describes the main sensors located at the ASJI and its measurements.

6.2.1 Measurements of Geomagnetic Parameters

Measuring geomagnetic parameters is a complex task due to the fact that the physical magnitude to be measured is a vector. This requires an accurate determination of the magnitudes with respect to a fixed reference frame and skilled staff from both technical and scientific point of view.

The geomagnetic vector can be given in either three of coordinate systems based on a geographic reference: *i)* Cartesian: where X, Y, Z are the geographic north, east and

altitude projections respectively. *ii)* Cylindrical: where H and Z are the horizontal and altitude projections and D is the declination angle between the geographic north and the magnetic field, establishing that the positive is towards east. *iii)* Spherical: where F is the total vector magnitude, D is the declination and I is the inclination angle between the horizontal projection and the magnetic vector itself, establishing positive downwards.

As far as the geomagnetic sensors are concerned, a D/I fluxgate theodolite (see Figure 6.2) is mounted in the first hut of the ASJI. This sensor permits a manual measurement of the Declination and Inclination angles of the vector magnetic field in absolute terms, which permits to discuss about the uncertainties of this instrument [7]. It consists of a fluxgate magnetometer bar mounted on the telescope of a non-magnetic theodolite.

Fig. 6.2 The manual D/I fluxgate theodolite being manipulated by a specialist.

A variometer type δD/δI vector magnetometer (see Figure 6.3) is mounted in the second hut to measure automatically the variations of the magnetic field vector once per minute. It consists of two perpendicular pairs of Helmholtz coils the polarization of which allows measuring the Declination and Inclination variations with a Proton magnetometer located at their center [8]. The Proton magnetometer measures the total magnetic field intensity, F, when the coils are not polarized.

Fig. 6.3 δD/δI vector magnetometer deployed at the ASJI with the two perpendicular pairs of Helmoltz coils and the Proton magnetometer allowing to measure the variations of D/I.

The last of these three huts houses the electronic system controlling this automatic instrument. A new three-axis fluxgate magnetometer (see Figure 6.4) was added during the 2008 expedition. It is able to measure automatically the magnetic field variations from an analogue output sampling at both 1 and 0.1 Hz by the corresponding Analog to Digital Converter, ADC.

Fig. 6.4 The three-axis automatic fluxgate magnetometer was added in 2008.

Once the raw data is processed, the definitive data set is sent to the World Data Centers becoming accessible to the scientific community. Nowadays, a real-time access to the data is

provided through a satellite link thanks to the International Real-time Magnetic observatory (INTERMAGNET). Nevertheless, a reliable skywave link designed by La Salle and the Ebro Observatory is active as a backup. A future project is motivated to separate our sensor data from the INTERMAGNET link and transmit only through the autonomous skywave link which, besides, is becoming another interesting sensor of the ionosphere due to the capability of measuring the ionosphere performance.

6.2.2 Vertical incidence soundings of the ionosphere

A Vertical Incidence ionospheric Sounder (VIS) was installed at the ASJI (Figure 6.5) during the 2004-2005 survey to provide information of the ionospheric characteristics in this region. Data provided by the VIS is used to characterize the climatology of the ionosphere and to investigate the ionospheric effects caused under geomagnetically disturbed periods.

Fig. 6.5 The VIS installed at the ASJI is the Advanced Ionospheric Sounder (AIS) developed by the Instituto Nazionale di Geofisica e Vulcanologia (INGV) of Rome, Italy. For more details about the ionosonde see [9].

The VIS located at the ASJI records a vertical incidence ionogram every 10 minutes. A ionogram is a graph that represents the time-of-flight for every radio frequency transmitted

vertically and received after its reflection in the ionosphere. Figure 6.6 shows an example of a ionogram recorded by the VIS at the ASJI where the particular layers of the ionosphere can be seen clearly. For more details about the VIS soundings see [10].

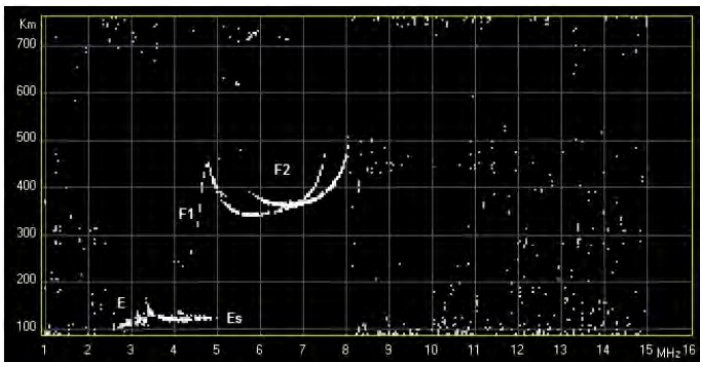

Fig. 6.6 An example of a ionogram recorded by the VIS at the ASJI where one can see clearly the particular layers of the ionosphere.

Oblique incindence soundings of the ionosphere

The oblique ionosonde is developed by La Salle to analyze and characterize the ionospheric channel between Antarctica and Spain [2]. It is used to obtain useful and key parameters for modeling the HF radio link; i.e, link availability, power delay profile of the channel and frequency dispersion. The soundings are carried out during the austral summer, when the ASJI is operative, the transmitter antenna is located at the ASJI (see Figure 6.7), and the receiver is located in Cambrils, Spain. More details of the HF data transmission are given in the section 4.

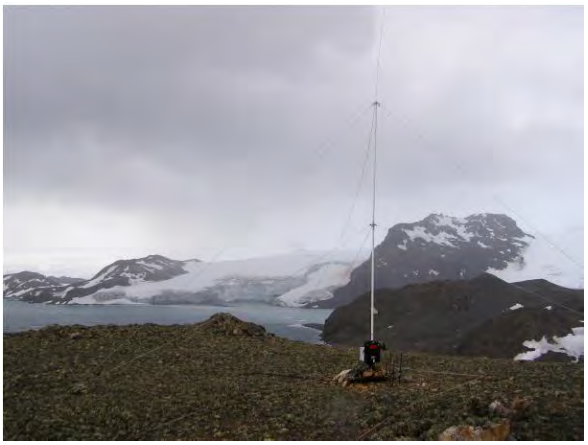

Fig. 6.7 The antenna of the oblique ionosonde transmitter in the ASJI.

6.3 System Descrip

The hardware of the ionosphe
data transmission system has b
and to get the best frequency a
has been entirely redesigned fr
It was upgraded with faster and more reliable equipment during the 2009-2010 expedition. As a result of the last improvement, the system is able to operate at a higher bandwidth up to 40 kHz and to sample at 100 ksps. Also the system was redesigned to be more flexible concerning the frequency and bandwidth selection for the soundings.

The main features of the transmitter and receiver hardware are described below.

6.3.1 Hardware of the Transmitter

The core is composed by an embedded PC with a Digital Signal
inside which performs the tasks of controlling and configuring the s
main DSP unit is the XTremeDSP-IV from Nallatech and it incl
described below: *i)* a Virtex-II is responsible for clock configuration,
the interface between the PCI bus and *iii)* a Virtex-4 which perfo
procedures. In order to perform these software radio operations, the Virtex-4 is equipped with two 14-bit ADC, two 14-bit DAC and all the arithmetic and peripheral drivers. Figure 6.8 shows a block diagram of the transmitter.

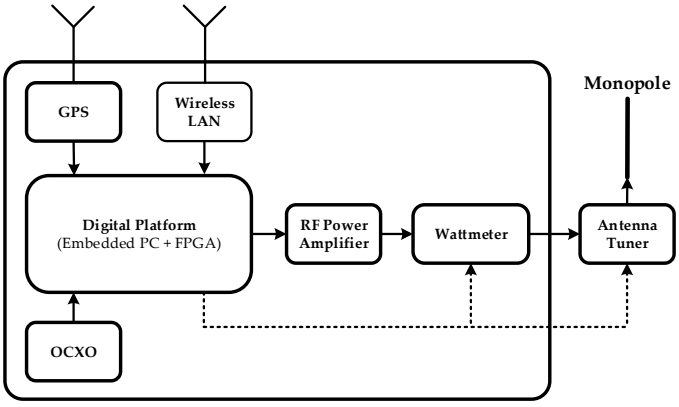

Fig. 6.8 Scheme of the transmitter that consists of an embedded digital platform and different peripherals used to control the system and to improve the synchronization.

Moreover, a GPS unit is placed to make possible the time synchronization using the Pulse Per Second (PPS) signal, which makes possible to measure the propagation time of the wave

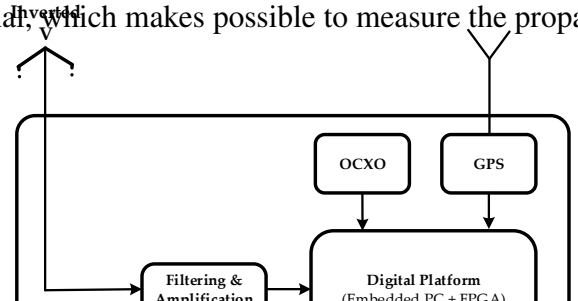

with an accuracy of 1 μs. Also, a 100 MHz Oven Controlled Crystal Osc installed in both transmitter and receiver in order to increase the frequenc accuracy. The Wattmeter measures the forward and reverse transmitted notice severe impedance mismatch. And the FPGA is capable, thanks to its peripheral drivers, to switch off the amplifier in case of malfunctioning. The Antenna Tuner is used to semi-automatically tune the monopole antenna, which transmits the signal.

As far as the deployment is concerned, all the transmitter hardware is close to the antenna at the top of a hill near to the ASJI. All the electronics is sealed inside a watertight box which protects against severe weather conditions and provides electromagnetic shielding. The system is remotely accessed through a Wireless Local Area Network (WLAN) from the laboratory in the ASJI.

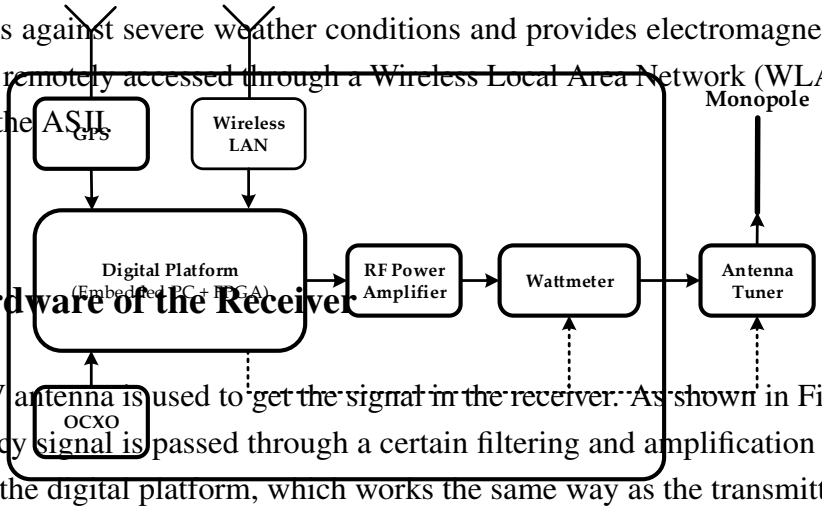

6.3.2 Hardware of the Receiver

An inverted-V antenna is used to get the signal in the receiver. As shown in Figure 6.9, the radio frequency signal is passed through a certain filtering and amplification process, and given next to the digital platform, which works the same way as the transmitter described above.

Moreover, the receiver also has an OCXO and a GPS to improve both frequency and time synchronization. A block diagram of the receiver is shown in Figure 6.9.

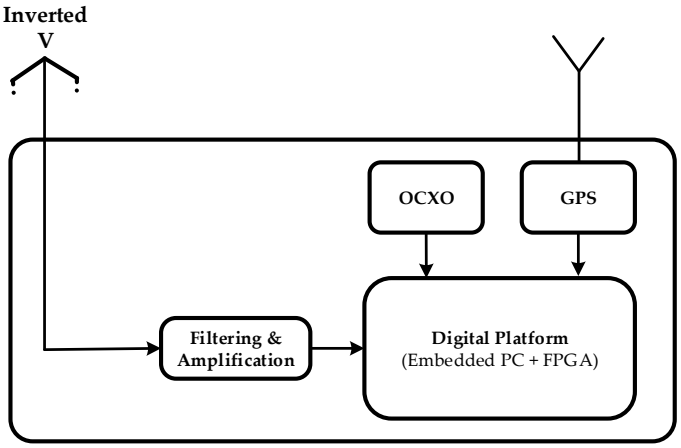

Fig. 6.9 Scheme of the receiver that consists of several filtering stages and a digital platform with peripherals to improve synchronization.

6.4 Data analysis

This section presents a detailed explanation of the test description and the analysis algorithms for narrowband and wideband oblique sounding.

6.4.1 Tests Description

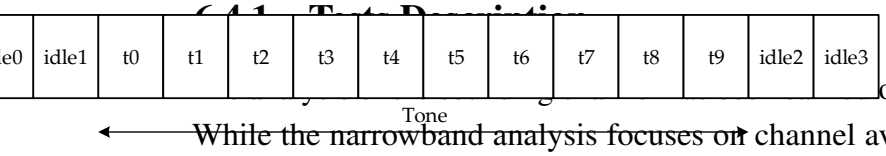

out in both narrowband and wideband. While the narrowband analysis focuses on channel availability and Signal to Noise Ratio (SNR), the wideband calculates the scattering function from the estimated channel impulse response, and then evaluates the multipath delay spread and Doppler spread.

The soundings are carried out during 24 hours a day (sessions) for a frequency carrier ranging from 2 to 30 MHz with steps of 500 Hz which corresponds to 57 sub-sessions. Every sub-session is divided into a frame to subdivide the time into two experiments, using 40 s for both of them. Finally, every session has a time slot of 22 minutes (called 'others' in the figure) to transmit the data from the sensors, and to test also new modulations schemes. The structure of the periodic experiment conducted during the 2013-2014 campaign is described in Figure 6.10. These soundings were carried out for 25 days, between January 25th and February 18th.

The idle intervals are included in all frames to ensure the system synchronization. The antenna tuning of 20W is required because the transmitter antenna is a monopole. The channel sounding is carried out in the processes called 'tone' and 'PseudoNoise (PN) sequence' during 10 s each.

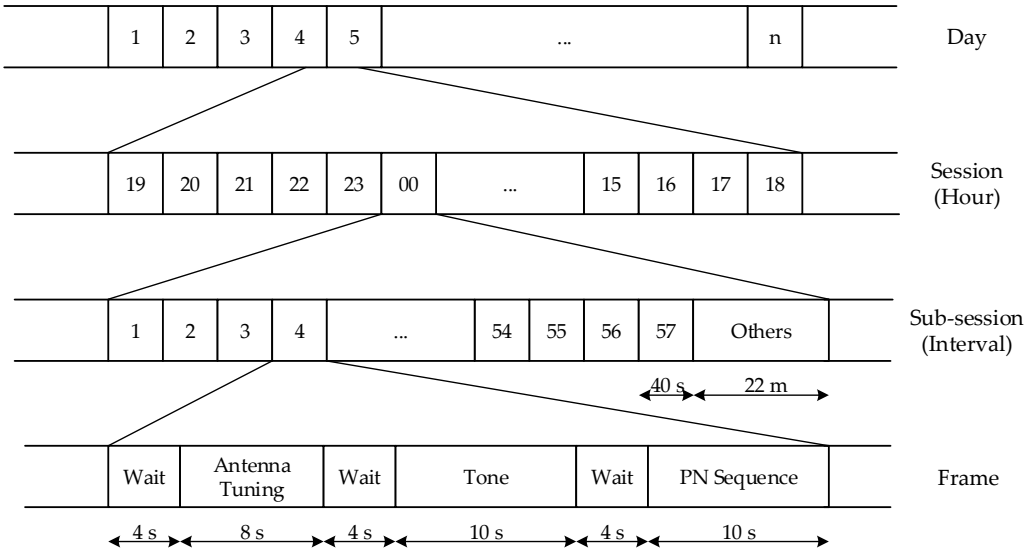

Fig. 6.10 Frame structure of the channel sounding.

The narrowband analysis is necessary to characterize the channel in terms of SNR and availability, using a sine wave as the transmitted signal. This tone is transmitted during 10 s. The configuration parameters are detailed in Table 6.1.

Tabla 6.1 Configuration parameters and setup for the narrowband sounding in 2013-2014 survey.

Parameter	**Value**
Signal	Sine wave
Duration	10 s
Silence	4 s

The wideband analysis is necessary to characterize time and frequency dispersion in the channel. The transmitted signal for the wideband analysis is a PN sequence [11] with the configuration parameters detailed in Table 6.2.

Tabla 6.2 Configuration parameters and setup for the wideband sounding in 2013-2014 survey.

Parameter	**Value**
Sampling frequency	100 kHz
PN sequence length	127
Family of sequences	m-sequence
Chip frequency	5 kHz
Number of sequences per test	300

6.4.2 Narrowband Analysis

The narrowband analysis focuses on SNR and channel availability computation. The channel availability is defined as the probability of a link to reach a minimum SNR value and therefore achieving a certain quality of service (see [12] for more details). A minimum SNR value of 6 dB was specified to estimate the channel availability in a bandwidth of 10 Hz [2]. In order to improve the reliability of the detection system, due to the probability of high noise and interference, several techniques were developed in [3]. SNR is computed with the comparison between the received power measured during the tone intervals and the noise power measured during the idle periods.

The first step is to filter the signal to obtain a usable power profile, conducted in frequency domain with the Fast Fourier Transform (FFT). Afterwards, a windowing is applied to *i)*

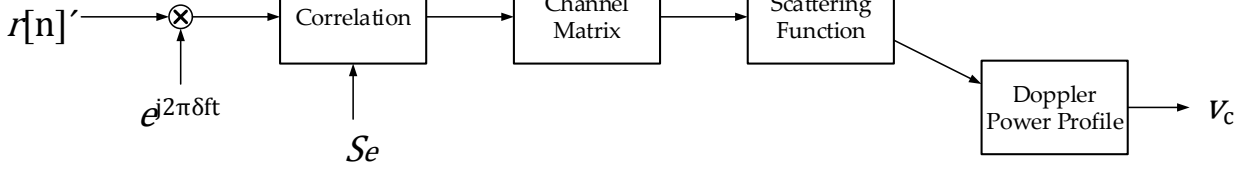

remove the non-desirable signals out of the reception frequency and *ii)* avoid creating transients from the impulsive interferences falling far away from the reception frequency when an ideal filter is used. Previous tests showed that the Kaiser window presents a better smooth response [3].

The measurements of SNR can be distorted easily because of high level of interferences. To overcome this problem a time framing technique is used, consisting on dividing the tone interval in 10 smallest sub-intervals of 1 s each, and observing the evolution of the SNR along the whole interval (see in Figure 6.11).

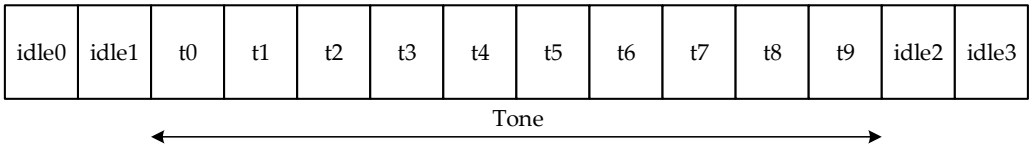

Fig. 6.11 Diagram of time framing technique for narrowband sounding.

According to previous experiments, two SNR threshold values are defined, $Th_{Low} = 3dB$ and $Th_{High} = 6dB$. Only those measurements that fulfill $SNR \geq Th_{Low}$ over 70% of the segments or $SNR \geq Th_{High}$ over 60% of the segments are taken into account to estimate the SNR and channel availability. An estimation of the SNR result of 17th February is shown in Figure 6.12.

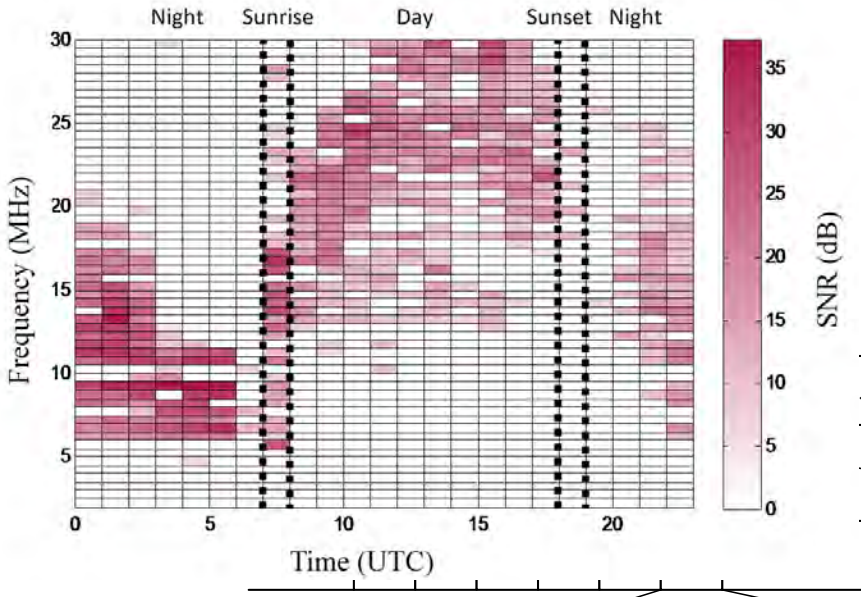

Fig. 6.12 SNR of February 17th (in dB) over a bandwidth of 10 Hz, in which the regions of day, night, sunrise and sunset can be appreciated.

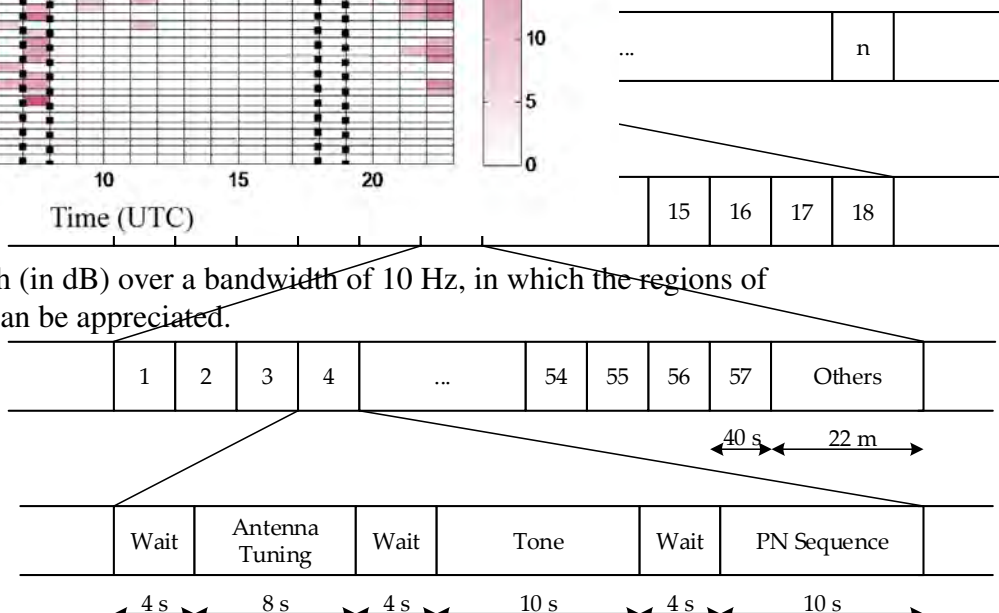

Wideband Analysis

The wideband analysis is performed sending PN waveforms with good cyclic cross-correlation characteristics, therefore using M-sequences [13]. The computation process for the wideband sounding is detailed in Figure 6.13.

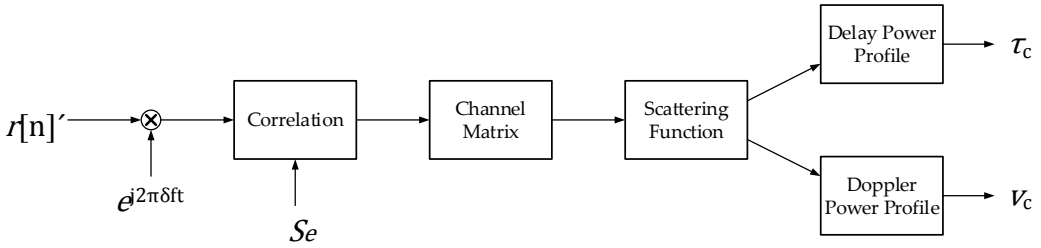

Fig. 6.13 Diagram of the computation process for wideband channel sounding.

The wideband analysis is crucial to characterize time and frequency dispersion in the channel. First, the received signal r[n] (with the characteristics described in 4.1) is correlated with the original PN sequence Se. The correlation function is calculated as

$$\phi_{r,S_e}[n] = \sum_{k=0}^{N_e-1} r[n+k]S_e[k] \tag{6.1}$$

where N_e is the length of the PN sequence. Hence, the channel impulse response $h[n,\tau]$ can be written as:

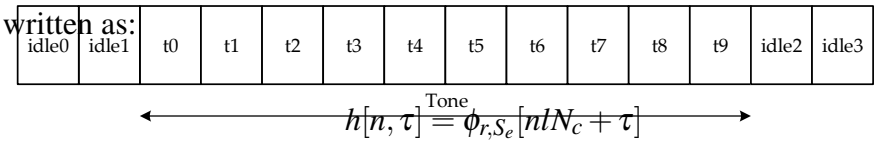

$$h[n,\tau] = \phi_{r,S_e}[nlN_c + \tau] \tag{6.2}$$

where τ is the delay variable, l is the number of chips and N_c is the number of samples per chip. From equation 2, the following parameters are calculated: scattering function, composite multipath spread and composite Doppler spread. The scattering function $R_s[\tau, v]$ is calculated as the FFT of the channel impulse response [13].

$$R_h[\xi,\tau] = \sum_{\xi} h^*[n,\tau]h[n+\xi,\tau] \tag{6.3}$$

$$R_s[\tau,v] = \sum_{\xi} R_h[\xi,\tau]e^{-j2\pi\xi v} \tag{6.4}$$

Both the composite multipath spread and the composite Doppler spread are calculated from the data obtained in the scattering function $R_s[\tau,v]$]. Let $[\tau_1,\tau_2]$ be the multipath observation window, and $[v_1,v_2]$ the Doppler spread observation window. Consequently, both

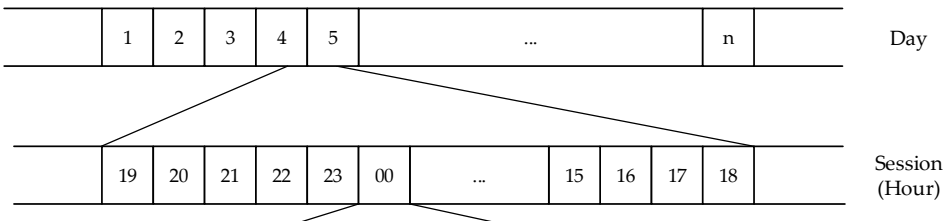

multipath power profile is defined as

$$\phi[\tau] = \sum_{v=v_1}^{v_2} R_s[\tau, v] \tag{6.5}$$

And the Doppler power profile is defined as

$$\phi[v] = \sum_{\tau=\tau_1}^{\tau_2} R_s[\tau, v] \tag{6.6}$$

In this work, the window have been set to [-3.5,3.5] (ms) and [-2.5,2.5] (Hz) respectively, due to maximum delay and Doppler spread values obtained in previous tests [2]. Next, the spread parameters are calculated. The multipath spread is measured from the multipath power profile as the 80% of the power spread [2]. This parameter is named composite multipath spread (t_{eff}) and was defined in [14]. The same way, the Doppler spread is measured from the Doppler power profile as the 80% power spread. It is named composite Doppler spread (u_{eff}), and it was defined in [15]. In Figure 6.14 we can observe the performance of the wideband sounding of the February 1st 2014, at 00 UTC for 13 MHz of carrier frequency. In Figure 6.14a the channel response $h[n, \tau]$ is plot, and the channel variations along time can be observed. In Figure 6.14b, the scattering function has been calculated using $h[n, \tau]$, and $R_s[\tau, v]$ is obtained after performing the FFT. In Figure 6.14c, the multipath power profile is observed for the previously defined time window, and finally, in Figure 6.14e, the Doppler power profile is plotted for the previously defined frequency window.

Finally, the last of the wideband analysis is the number of paths, which is defined as follows. The number of paths is measured comparing the number of paths found at two energy levels in terms of percentage of the maximum; the final number chosen is the higher value measured. The two thresholds are settled in the 70% and the 45% of the maximum value corresponding to the strongest path. With this method the system evaluates the maximum number of paths, taking into account both the strongest ones and the weakest ones. The two thresholds were settled testing the results over the data, measuring which levels of energy determined the more realistic result depending on the channel response. In figure 6.15 both thresholds are settled, and two different measures are obtained: the 70% one detects one path, and the 45% threshold detects two paths. None of the two detects the third small path inbetween, but the lower value could not be settled in a smaller value because it led to confusion in the case of a noisy enviroment.

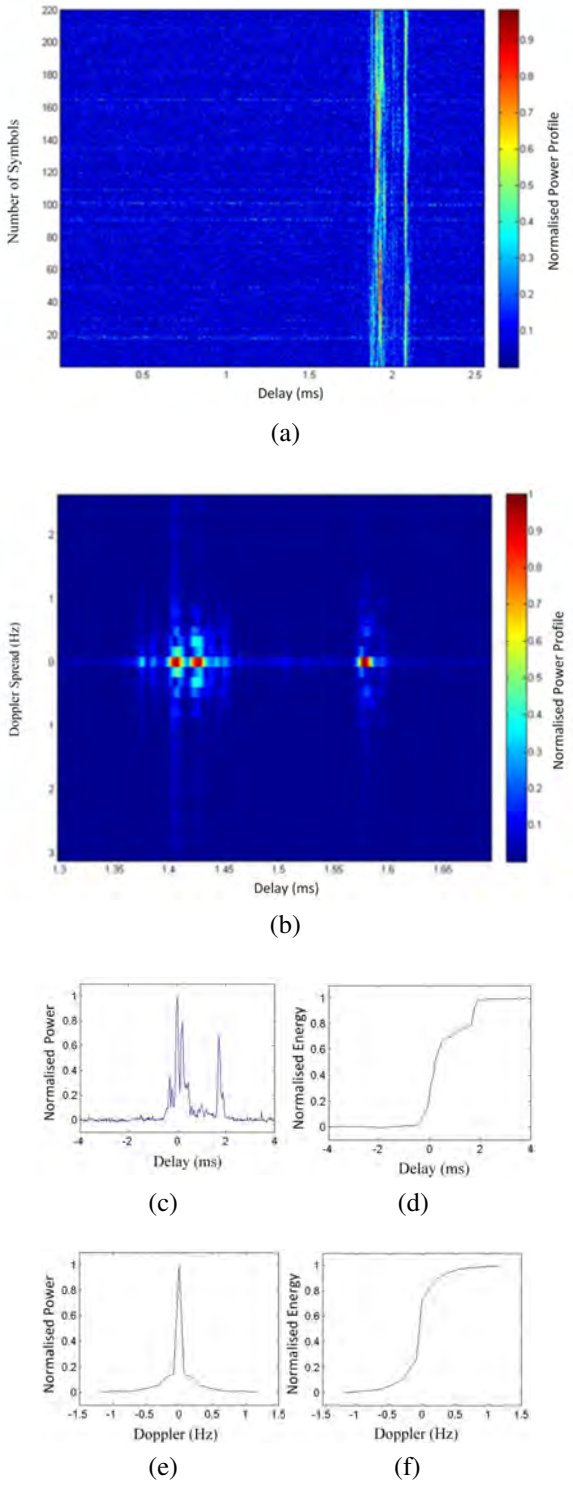

Fig. 6.14 Wideband channel response and measures for February 01st 2014 at 07 UTC with 13 MHz of carrier frequency: **(a)** normalized channel response $h[n,\tau]$, **(b)** normalized scattering function $R_s[\tau,v]$, **(c)** multipath power profile (in ms), **(d)** the integral of the multipath power profile to calculate delay spread (in ms), **(e)** Doppler power profile (in Hz), and **(f)** the integral of the Doppler power profile to calculate Doppler spread (in Hz).

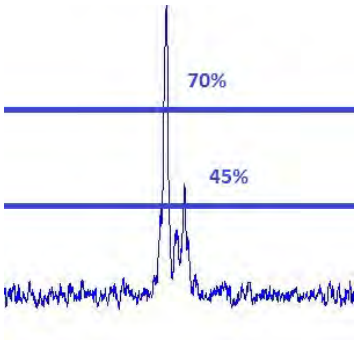

Fig. 6.15 Example of channel response, and the measure of the number of paths on the 70% and on the 45%. The first one only detects one path, and the second one detects two paths. None of them detects the third small path.

6.5 Results

6.5.1 Narrowband Results

The results of narrowband analysis shown in Figure 6.16 represent the average plot of the channel availability for the survey. Figure 6.16 depicts the channel availability for frequencies ranging from 2 to 30 MHz as function of time. The Frequency of Largest Availability (FLA) for a particular time is shown as a dashed line. Four different zones can be distinguished: day, night, sunrise and sunset. During the day interval, from 08 UTC to 17 UTC, the frequencies ranging from 20 to 30 MHz present the better performance in terms of SNR. For the sunset period, around 18 UTC, the interval of frequencies that performs best falls linearly with the time between 20 and 30 MHz to 10 and 20 MHz. The night period is defined from 19 UTC to 06 UTC and the frequencies ranging from 6 to 15 MHz show the best results. Finally, for the sunrise, which is the period defined around 07 UTC, its best operation frequencies increase linearly with the time from frequencies between 6 and 15 MHz to frequencies ranging from 20 to 30 MHz. In consequence, we can conclude the best reflective frequencies during the daytime are the highest frequency range, the nighttime the lowest one, and sunrise and sunset are regions of switching between these periods of time performing in an unstable condition for all frequencies. It is worth noticing a drop in the FLA after sunrise (9-10 UT) and a post sunset jump (20-21 UT) of the FLA. These effects deviate from the expected smooth transition of the FLA from nighttime to daytime conditions and vice versa.

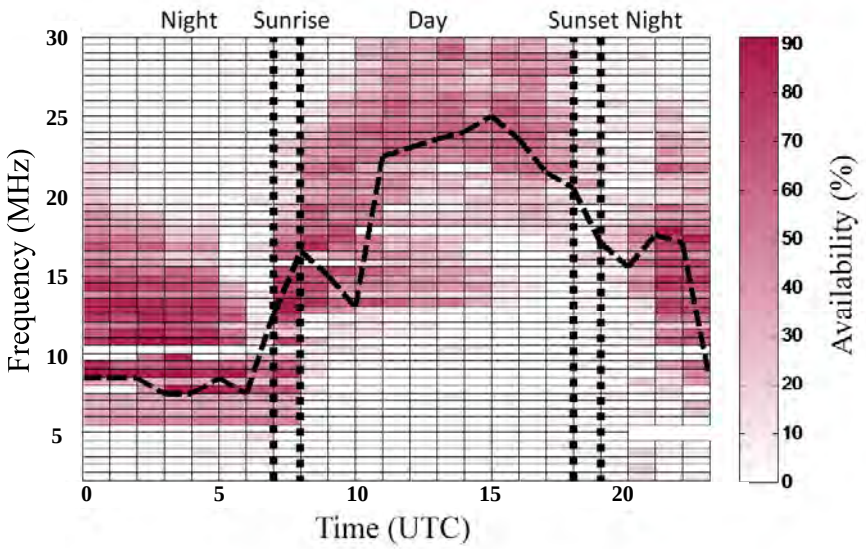

Fig. 6.16 Channel availability of the campaign 2014 measured during the austral summer, from January 25th to February 18th.

6.5.2 Wideband Results

The results of wideband analysis are shown in Figure 6.17, containing delay spread, Doppler spread and number of paths.

Figure 6.17a and Figure 6.17c, present the mean delay spread and the mean Doppler spread, from which one can distinguish four different performance zones also: day, night, sunrise and sunset [14]. Figure 6.17b and Figure 6.17d show the standard deviation for the delay spread and the Doppler spread respectively. During day interval, from 08 UTC to 17 UTC, high frequencies ranging from 20 MHz to 30 MHz show the higher delay spread and Doppler spread for all measures. This means that the channel is available for a wide range of frequencies but its channel response is varying and unstable, and the intersymbol interference caused by a long channel response is an important parameter for the modulation design. Sunset time, around 18 UTC, presents an irregular performance when comparing high frequencies and low ones, but low frequencies start performing better while high frequencies decrease its availability. Also sunrise, around 07 UTC shows unstable performance in terms of wideband availability. Nighttime, shown both on the right and on the left of Figures 6.17, ranging from 19 UTC to 06 UTC, presents the best measurements in terms of channel availability and parameters. Best frequencies are around 10 MHz, despite channel is available until 20 MHz. Delay spread mean values are around 2 or 3 ms, with low deviation, and maximum Doppler spread values are around 0.7 Hz. All these information is compared to figure 6.17e and 6.17f, which show the number of paths calculated in the channel response.

The number of paths is a difficult parameter to evaluate, depending on the energy level threshold to consider a new path. The number of paths in this study is calculated evaluating the number of countable paths in both the 70% of the maximum and in the 45% of the maximum, and saving the highest value. During the day hours, from 08 UTC to 17 UTC, the lower number of paths is shown. Both in sunrise and in sunset, it shows unstable performance in terms of number of paths. And finally, the number of paths during the night reaches its highest levels, showing good propagation through several different channel lengths.

6.5.3 Discussion

Narrowband and wideband analysis conducted show similar results in terms of availability depending on the hour of the day. Nighttime is the best reception time, using frequencies from 8 MHz to 20 MHz. Narrowband presents its best SNR results while wideband shows its smaller delay spread and Doppler spread measurements. These results allow us to conclude that for the best hours and frequencies, high throughput modulations like OFDM should be used, in order to increase the bit rate of the communication. Delay spread and Doppler spread won't worsen the results in a severe way, according to the measured values. Despite of that, the OFDM modulation should be designed taking into account coherence time and coherence bandwidth calculated using the measured parameters of Doppler spread and delay spread. Finally, at sunrise, sunset and daytime, a more robust modulation should be used. Direct-Sequence Spread Spectrum could be a good option assuming lower throughput, but ensuring a more robust communication against channel variations or fadings.

6.6 Conclusions

This paper presents the main results of the oblique sounding measurement recorded during the campaign of 2014 with a transmitter placed in the Remote Geophysical Observatory of the ASJI and the receiver located in Cambrils (Spain). The sounding has been carried out for both narrowband and wideband to characterize the channel in terms of SNR, availability, multipath delay spread, Doppler spread and number of paths. These measurements of the long haul link improve the knowledge of the performance of the ionospheric channel 12760 km long, and allow us to fully define the physical layer to send the data of the remote sensors deployed among the island from the Antarctica to Spain. The values measured of narrowband and wideband confirm that both soundings show similar results in terms of availability depending on the hour of the day and of the frequency used. Furthermore, the wideband analysis present results of the period of the day that is more suitable for data

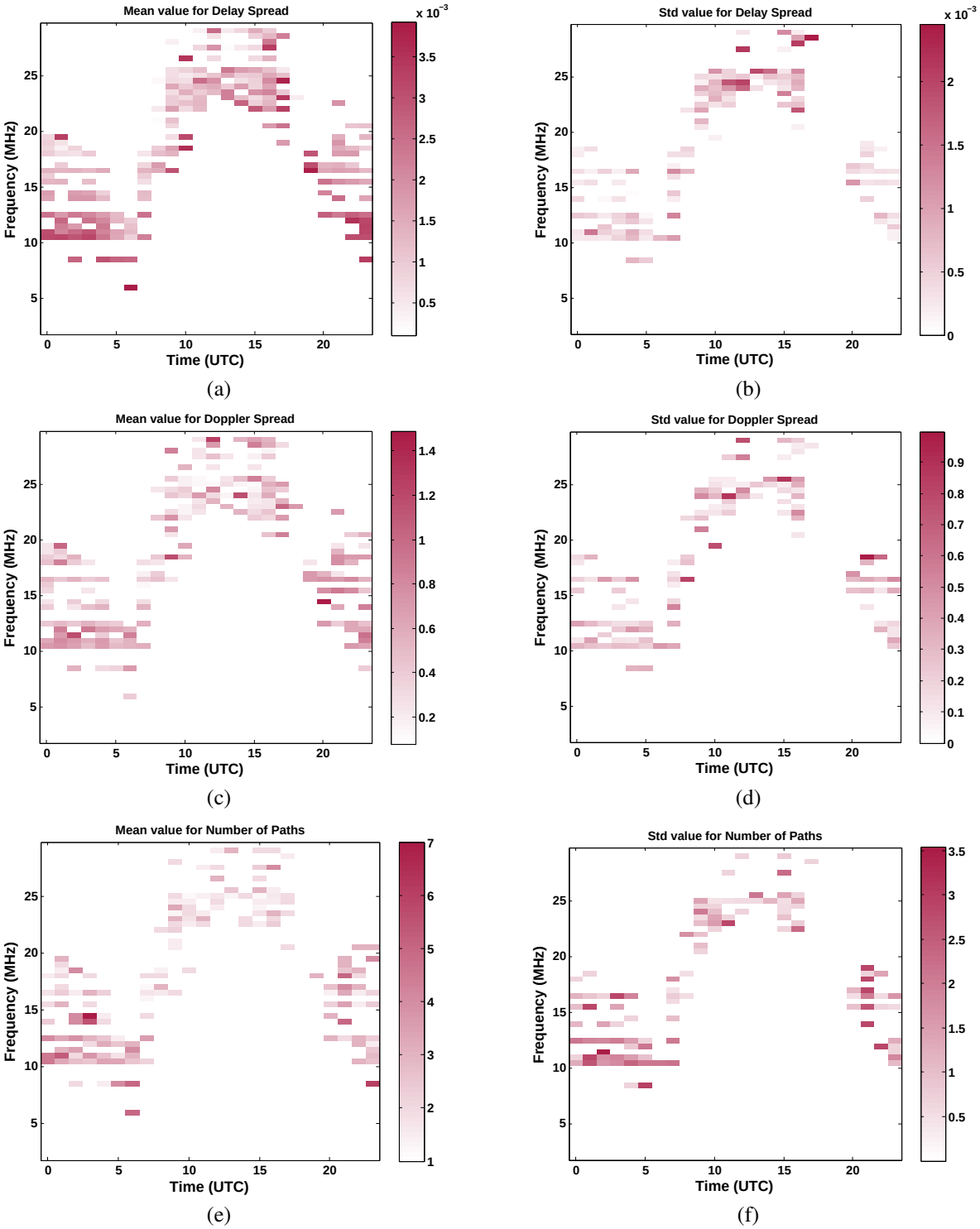

Fig. 6.17 Wideband channel measurements during the campaign 2014: **(a)** mean of delay spread (in ms), **(b)** standard deviation of delay spread (in ms), **(c)** mean of Doppler spread (in Hz), **(d)** standard deviation of Doppler spread (in Hz), **(e)** mean of number of paths, and **(f)** standard deviation of number of paths.

transmission, because the channel shows a good performance (with low Doppler spread and low delay spread). It also describes the hours of the day when the channel measurements, despite showing some availability, present worst results. This leads us to design a proper robust modulation for those hours, while the best transmission hours and frequencies use high throughput modulation techniques.

The future work is focused on two main goals. The first one is the study of the historical series of Doppler spread, delay spread, number of paths and SNR for the entire solar cycle (around 11 years), using part of the data we have already measured. The second goal is to end the design of the HF modem; the channel characteristics shown in this paper are crucial for a proper design of the modulation, coding and interleaving of the physical layer of the modem.

Acknowledgment

This research has been supported by the Spanish Government under projects CTM2010-21312-C03-03 and ˘C03-01. In addition to the authors of this paper, the following people have been part of the research groups of these projects: Ahmed Ads, Raúl Bardají, Estefania Blanch, Oscar Cid, Juan José Curto, Simó Graells, Miguel Ibáñez, Joan Mauricio, Santiago Marsal, Joan Ramon Regué, Xavier Rosell, Martí Salvador, Antoni Segarra, José Germán Solé and Joan Miquel Torta.

Author Contributions

Marcos Hervás analyzed and wrote the part of the paper related with the narrowband soundings. Dr Rosa Ma Alsina-Pagès had the idea to write this paper, and analyzed and wrote the wideband sounding study in this paper. Ferran Orga wrote the introductory part, the measured parameters and the system description of this paper. Dr David Altadill has been the principal investigator of project -C03-01 and coordinator of both projects and he has reviewed the paper. Dr Joan Lluis Pijoan has been the principal investigator of project -C03-03, he has been involved in the part of channel sounding and testing of advanced modulations and reviewed the paper. Dr David Badia installed the transmission system in Antarctica, installed the receiver system in Spain and reviewed the paper.

Conflicts of Interest

The authors declare no conflict of interest.

Referencias

1. Torta, J.M.; Gaya-Piqué, L.R.; Riddick, J.C.; Turbitt, C.W. A Partly manned geomagnetic observatory in Antarctica provides a reliable data set. *Contrib. Geophys. Geodesy Geophys. Inst. Slov. Acad. Sci.* **2001**, *31*, 225-230.

2. Vilella, C.; Miralles, D.; Pijoan, J.L. An Antarctica-to-Spain HF ionospheric radio link: Sounding results. *Radio Sci.* **2008**, doi:10.1029/2007RS003812.

3. Ads, A.G.; Bergadà, P.; Vilella, C.; Regué, J.R.; Pijoan, J.L.; Bardají, R.; Mauricio, J. A comprehensive sounding of the ionospheric HF radio link from Antarctica to Spain. *Radio Sci.* **2012**, doi:10.1029/2012RS005074.

4. Hervás, M.; Pijoan, J.L.; Alsina-Pagès, R.M.; Salvador, M.; Badia, D. Single-carrier frequency domain equalization proposal for very long haul HF radio links. *Electron. Lett.* **2014**, *17*, 1252-1254, doi: 10.1049/el.2014.1184.

5. Bergadà, P.; Alsina-Pagès, R.M.; Pijoan J.L.; Salvador, M.; Regué, J.R.; Badia D.; Graells, S. Digital transmission techniques for a long haul HF link: DS-SS vs. OFDM. *Radio Sci.* **2014**, doi:10.1002/2013RS005203.

6. Alsina-Pagès, R.M.; Salvador, M.; Hervás, M.; Bergadà, P.; Pijoan, J.L.; Badia, D. Spread spectrum high performance techniques for a long haul high frequency link. *IET Com.* **2015**, *9*, 8, 1048-1053, doi:10.1049/iet-com.2014.0807.

7. Marsal, S.; Torta, J.M. An evaluation of the uncertainty associated with the measurement of the geomagnetic field with a D/I fluxgate theodolite. *Measur. Sci. Technol.* **2007**, *18*, doi:10.1088/0957-0233/18/7/046.

8. Marsal, S.; Torta, J.M.; Riddick, J.C. An assessment of the BGS δDδI vector magnetometer. *Publs. Inst. Geophys. Pol. Acad. Sci.* **2007**, *99*, 158-165.

9. Zuccheretti, E.; Bianchi, C.; Sciacca, U.; Tutone, G.; Arokiasamy, J. The new AIS-INGV digital ionosonde. *Ann. Geophys.* **2003**, *46*, 647-659.

10. Bergadà, P.; Deumal, M.; Vilella, C.; Regué, J.R.; Altadill, D.; Marsal, S. Remote sensing and skywave digital communication from Antarctica. *Sensors* **2009**, doi:10.3390/s91210136.

11. Golomb, S. Shift Register Sequences; Holden-Day: San Francisco, USA, **1967**.

12. Goodman, J.; Ballard, J.; Sharp, E. A long-term investigation of the HF communication channel over middle- and high-latitudes paths. *Radio Sci.* **1997**, *32*, 1705-1715, doi:10.1029/97RS01194.

13. Proakis, J. Digital Communications, 4th ed.; McGraw Hill: Boston, MA, USA, **2000**.

14. Angling, M.J.; Davies, N.C. An assessment of a new ionospheric channel model driven by measurements of multipath and Doppler spread. *In Proceedings of the 1999 IEEE Colloquium on Frequency Selection and Management Techniques for HF Communications* **1999**, London, UK.

15. Warrington, E.M.; Stocker, A.J. Measurements of the Doppler and multipath spread of the HF signals received over a path oriented along the midlatitude trough. *Radio Sci.* **2003**, *38*, doi:10.1029/2002RS002815.

Parte III

Conclusiones

Capítulo 7

Conclusiones

Tras 11 de años de proyecto se puede afirmar que el establecimiento de un radio enlace mediante rebote ionosférico entre la Antártida y España llega a su diseño mas fiable. Dicho enlace emplea baja potencia (200 W) y antenas muy simples debido a las restricciones medioambientales, y de logística que impone el desplazarse a la Antártida, por lo tanto, el *bit rate* obtenido también lo es. Este *throughput* depende de la condiciones ionosféricas en cada momento. Dichas condiciones producen variaciones de la disponibilidad de frecuencia de utilización diariamente, así como el nivel de SNR y de interferencias en recepción, y la dispersión frecuencial y temporal de la respuesta impulsional del canal.

En el diseño de la capa física se debe tener en cuenta que pretendemos establecer un canal *simplex*, es decir, no se posee *feedback* de las condiciones del canal. Por lo tanto, no se pueden aplicar técnicas para que en transmisión se tenga el conocimiento de cual es la frecuencia que proporciona el mejor nivel de SNR, ni que frecuencias se deben evitar para no tener *fadings*, como lo hacen otros protocolos de la capa de enlace. En consecuencia, se debe configurar el sistema (tanto en transmisión como en recepción) con una frecuencia portadora fija, basándonos en la recopilación de datos históricos, para obtener los mejores niveles de SNR y condiciones del canal de comunicaciones. Para ello, se están realizando sondeos oblicuos del canal, tanto de banda estrecha como de banda ancha, desde los inicios del proyecto. Tanto el *hardware* como el procesado del análisis de los datos se ha mejorado con la evolución del proyecto. Actualmente, se realiza el sondeo en toda la banda de HF (2-30 MHz) durante las 24 horas del día.

Para estudiar las variaciones del canal se emplean los sondeos de banda estrecha y de banda ancha. El sondeo de banda estrecha nos permite obtener el nivel de SNR y la disponibilidad del canal, y así realizar el estudio estadístico de la evolución temporal de éste a lo

largo de los días. El sondeo de banda ancha se emplea para obtener la respuesta impulsional del canal, para ello se realiza la correlación de la señal recibida con las secuencias PN transmitidas. A partir de la matriz de canal, se obtiene la función de *scattering*, y sobre esta se calculan los parámetros de *composite multipath* y *Doppler Spread*.

Los resultados obtenidos de ambos sondeos difieren entre la noche y el día. Ambos tipos de sondeo ofrecen resultados similares en términos de disponibilidad. De estos sondeos se concluye que las horas nocturnas ofrecen las mejores prestaciones para la recepción, ya que los niveles de SNR y disponibilidad son mas elevados durante estas y los valores de *Multipath Delay Spread* y *Doppler Spread* son menores respecto a las horas diurnas. El *Multipath Delay Spread* medio está entre 2 y 3 ms y el *Doppler Spread* alrededor de 0.7 Hz. En base a estos resultados, se decide diseñar dos modos de operación, uno para cada franja horaria. Durante la noche se utilizaría el HTM, este modo empleará una modulación basada en SC-FDE o SC-FDMA. Durante el día, la puesta de sol y el alba se empleará el RM, utilizando un esquema de modulación basado DS-SS.

En este trabajo se han estudiado diversos esquemas de modulación basados en modificaciones sobre la modulación DS-SS: *signaling*, *quasi-quadriphase* y *quadriphase*. *Signaling* es el esquema que mayor robustez presenta, sin embargo el *bit rate* obtenido es demasiado bajo para ser empleado en la transmisión de los datos de los sensores que se desea enviar, ya que esta transmisión debe hacerse enviando dichos datos con repetición, esto es debido a que no se puede implantar un sistema basado en ARQ ya que el canal es *simplex*. El esquema de modulación *quadriphase* dobla el *bit rate* respecto el *signaling* ya que emplea las componentes de fase y cuadratura para transmitir un *signaling* en cada una de ellas, sin embargo, la robustez del sistema se ve afectada por dos motivos: *i)* este esquema necesita de ecualización en recepción para evitar la interferencia entre ellas debido al desfase introducido por el canal y *ii)* el hecho de emplear dos señales independientes, mantenidendo la potencia de la señal del amplificador, disminuye en 3 dB la SNR de cada componente respecto al *signaling*. La solución que se presenta con *quadriphase* presenta un *bit rate* intermedio entre ambos esquemas, ya que la mejora que presenta *signaling* respecto a DS-SS es un factor m, *quadriphase* $2m$ y *quasi-quadriphase* $2(m-1)$, ya que mapea la mitad del diccionario de bits en cada una de las componentes. Este mapeo permite evitar el uso de ecualización de canal, ya que la interferencia entre componentes desaparece. El hecho de obtener un valor menor de SNR de 3 dB, implica que la robustez será menor que en *signaling*. Por último, se considera que la solución propuesta con *signaling* es la mejor candidata para ser empleada en RM ya que presenta la mejor robustez, pese a que no cumpla con los requerimientos de

transmisión de un INTERMAGNET.

La configuración escogida en el RM consiste en la transmisión de 10 secuencias PN. Estas secuencias son de tipo m y poseen una longitud de 2047 chips con un upfactor de 6 muestras por chip, ocupando un ancho de banda de 16.6 kHz. Cada símbolo contiene 11 bits de información, por lo tanto, el *frame* de 10 secuencias 110 bits con una duración de 1.26 s, proporcionando un *Bitrate* de 90 bps, 71.4 bps si se tiene en cuenta la sincronización temporal.

La propuesta realizada empleando SC-FDE como esquema de modulación presentó mejores resultados que los obtenidos previamente con modulaciones multiportadora. Ya que obtenía BER menores para valores de *bit rates* mayores. Esto es debido a que los niveles de SNR son mayores para una modulación basada en *single carrier* que para una multiportadora cuando la máxima potencia de pico es la misma para ambos esquemas, ya que las modulaciones multiportadora tienen un valor mas elevado de PAPR, es decir, la diferencia entre la potencia máxima y la potencia media es mayor. Por lo tanto, la potencia media de la señal también lo es. Además, si el *subcarrier spacing* de la OFDM no es suficientemente grande, ésta sufre de ICI debido a *offsets* de frecuencia, empeorando el BER, y en nuestra aplicación no puede ser, ya que el ancho de banda esta muy limitado debido al bajo nivel de SNR observado en recepción.

En base a los resultados obtenidos en el test de SC-FDE, se decidió ampliar este experimento para poder ser comparado con una SC-FDMA, que es la versión multiusuario de la SC-FDE, y a su vez con una OFDM durante la misma campaña. Debido a que estos esquemas poseen mayores valores de PAPR que la SC-FDE, por lo tanto la potencia media de la señal es menor. Se ha aplicado un *soft limiter* con distintos valores de IBO y amplificado la señal resultante, de esta manera se incrementó la potencia media de la señal. Pese a que el *clipping* aplicado con el IBO de menor valor producía distorsión dentro de la banda, incrementando el EVM en recepción, el aumento de potencia de la señal produjo mejor resultado que para IBOs de valores grandes, en los casos en que las constelaciones son simples PSK y QPSK. De este estudio se ha concluido que la SC-FDMA obtuvo resultados mejores de BER que la OFDM, debido al ICI que presentaba esta. Además, los resultados de BER de SC-FDMA y SC-FDE eran muy similares. Por lo tanto, el esquema de modulación propuesto para el HTM será SC-FDE, debido a que presentó buenas prestaciones y tiene un coste computacional mas bajo que SC-FDMA y OFDM.

La configuración escogida en el HTM consiste en la transmisión de 4 bloques de datos de 50 ms cada uno de ellos y 20 símbolos PSK, empleando un ancho de banda de 400 Hz. Para realizar la ecualización en frecuencia se inserta una secuencia CAZAC cada 4 bloques. Estos 5 bloques poseen un CP de 3 ms, por lo tanto, la trama tiene una duración total de 265 ms.

Capítulo 8

Líneas de Futuro

Actualmente se está trabajando en la definición total de la capa física del radio módem para dar por concluido uno de los objetivos del proyecto. Para poder definir esta correctamente, se ampliará el estudio realizado con los esquemas de modulación recopilados en esta tesis, para las mejores configuraciones observadas, de forma que se analicen diversos códigos de canal y profundidades de *interleaving*. A raíz de los resultados obtenidos, tras aplicar estas técnicas, podremos concluir cual de los tres esquemas de modulación empleados en HTM es el que presenta mejores resultados. El estudio realizado en esta tesis se ha basado solamente en los resultados obtenidos de la forma de onda de la señal, sin explotar algunas características como la diversidad frecuencial de la OFDM. Otra tarea en la que se está trabajando es el análisis y la comparativa interanual de los datos de los sondeos de los 11 años, que corresponden con un ciclo solar.

El hecho de realizar las campañas de sondeos y test de nuevos esquemas de modulación durante un breve espacio de tiempo del verano austral provoca que el volumen de muestras obtenidas del estado de la ionosfera no sea muy elevado, por lo tanto, se puede dar el caso de que los resultados obtenidos en alguna de las campañas no sea significativo respecto a todo el ciclo solar. Nuestro grupo de investigación ha realizado un estudio que compara los resultados obtenidos del sondeo oblicuo de banda estrecha entre la Antártida y España y los resultados obtenidos de 5 observatorios que realizan sondeos verticales en puntos intermedios de la trayectoria de propagación que sigue la señal entre ambos puntos, obteniendo correlaciones entre los resultados de unas y otras [1]. Este estudio se está realizando en base a los resultados presentados en [2] empleando un número mayor de observatorios. Actualmente dicho análisis se está ampliando a todo el ciclo solar, teniendo en cuenta información de eventos atmosféricos y geomagnéticos a este estudio para obtener nuevas correlaciones entres los resultados de los sondeos oblicuos y dichos eventos. De esta manera se pretende obtener

nuevas correlaciones entre el comportamiento de la ionosfera y dichos eventos atmosféricos y geomagnéticos así como obtener una estimación de la bondad o grado de confianza de dichos sondeos con respecto al análisis de los resultados tanto de dichos eventos como de los sondeos verticales.

Se ha solicitado la concesión de un proyecto de investigación del plan nacional para seguir realizando tareas de investigación en la Antártida. Este proyecto persigue un objetivo muy ambicioso. Poder instalar una red de sensores en cualquier punto de la Antártida y comunicar con la ASJI mediantela tecnologia NVIS. Ello sera posible si la distancia entre dos sensores próximos no supera los 200 Km. Los sensores actúan de repetidor y llevan la señal desde la zona más remota hasta la ASJI. Desde el ASJI se enviarán los datos hacia España mediante el enlace oblicuo o empleando satélites.

Para este nuevo proyecto, se está trabajando en el diseño de un radio módem basado en la plataforma propietaria IRIS y una Raspberry Pi, ya que este sistema debe ser de bajo consumo y económico, ya que en algunos casos se instalará en sensores en los que no se podrá recuperar el equipo. En la fase actual del desarrollo *Hardware*, la plataforma IRIS actúa como un periférico del radio-módem, realizando esta las tareas de conversión de frecuencia de banda base a la frecuencia portadora deseada y vicebersa. La Raspberry Pi será el dispositivo en el que resida la inteligencia del equipo, ya que el hecho de albergar un sistema operativo basado en linux permite integrar fácilmente funcionalidades y comunicación con otros periféricos como Ethernet o acceso a disco duro (gestión de USB) para el almacenamiento de la información.

Con este nuevo sistema, la investigación española en la Antartida no quedará confinada a las proximidades de las dos bases antárticas, sino que podrá basarse en datos recogidos en zonas mucho más alejadas.

Referencias

1. A.G. Ads, P. Bergadà, J.R. Regué, R.M. Alsina-Pagès, J.L. Pijoan, D. Altadill, D. Badia, and S. Graells. Vertical and oblique ionospheric soundings over the long haul hf link between antarctica and spain. *Radio Science*, 50(9):916–930, 2015.

2. C. Vilella, D. Miralles, D. Altadill, F. Acosta, J.G. Solé, J.M. Torta, and J.L. Pijoan. Vertical and oblique ionospheric soundings over a very long multihop HF radio link from polar to midlatitudes: Results and relationships. *Radio Science*, 44(2), 2009.

Parte IV

Anexos

Anexo A

Spread Spectrum High Performance Techniques for a Long Haul HF Link

Spread Spectrum High Performance Techniques for a Long Haul HF Link

R.M. Alsina-Pagès, M. Salvador, M. Hervás, P. Bergadà, J.L. Pijoan, and D. Badia

Abstract. Skywave ionospheric communication systems offer a good choice to satellite communications when transmitting from the poles. For the last 10 years we have been sounding and testing modulations through a 12700 km HF link from the Spanish Antarctic Station (SAS) to Spain. Previous tests comparing DS-SS and OFDM showed that spread spectrum BER results outperformed OFDM at the expense of lower bit rates. In this paper we present three spread spectrum techniques for this long haul link that increase the bit rate and the spectral efficiency of the direct sequence while keeping the good BER performance obtained. Tests have been performed with several symbol periods as well as different bandwidth for each technique, so we can conclude which combination best suits this channel.

keywords. SC-FDE · OFDMA · SC-FDMA · PAPR · HF · Ionosphere

Source: IET Communications, Volume 9, Issue 8, 21 May 2015, p. 1048–1053
DOI: 10.1049/iet-com.2014.0807 , Print ISSN 1751-8628, Online ISSN 1751-8636

A.1 Introduction

Remote sensing communications are often solved with the use of satellites; however, communications from the poles to geostationary satellites are not always feasible since the visibility is very poor. Skywave ionospheric communication systems offer a good choice to satellite communications when the satellites have poor visibility or as a backup system of the satellite transmission. An example of remote sensing transmission applications solved using HF solutions can be seen in [1], this solution though, is not useful for our link because it needs channel information in the transmitter and our system is not duplex. Nowadays the data rates in the HF band for 3 kHz channels range from 75 to 4800 bps in robust mode or up to 12800 bps for uncoded operation with a 64-QAM constellation when the SNR conditions are extraordinarily good [2–4]. This standard is also not applicable in our system because these standards require higher SNR than the available in this link, although the bit rate would be enough for our throughput requirements.

The Research Group in Electromagnetism and Communications (GRECO), which has been unified to Research Group in Electronic Systems, Telecommunications and Data Analysis (GR-SETAD), has been working in advanced HF communication systems from the Spanish Antarctic Station (SAS) in Livingston Island (62.5^oS,60.4^oW) to Cambrils (41.04^oN,1.03^oE) since 2003 [5]. The goal of the project is to send geomagnetic data from the sensors in the SAS to Cambrils using a ionospheric long haul link of 12700 km. Exhaustive data about the impairments of this HF link have been gathered since 2003 and several performance parameters have been measured such as availability, SNR, delay power profile and Doppler spread [6–8]. At the same time channel characteristics have been studied and several proposals for a low-SNR physical layer have been investigated [9, 10].

The transmission power can not exceed 200 Watts due to power restrictions at the SAS, and the transmitter antennas have low efficiency due to environmental restrictions, consequently very low SNR is expected at the receiver. A first approach was testing DS-SS, as it is well known that spread spectrum techniques reject both narrowband interfering signals and noise [11], despite offering low bit rate data transmission [12, 10]. The goal of the work presented in this paper is to increase the transmitted bit rate and the spectral efficiency using signaling and quadriphase direct sequence spread spectrum techniques, which were proposed in [13]. The tests conducted in this work derive from the results obtained in [10], where a study about DS-SS and OFDM showed that, despite the better BER performance of DS-SS, the bit rate was too low even for the requirements of the remote sensors in the SAS. We are looking for a trade-off between BER and bit rate; therefore, we have designed some new tests maintaining good BER performance and improving data rate.

The remainder of this paper is organized as follows. Section A.2 details the link and the system, section A.3 describes the design of the tests, section A.4 shows the results of the comparison tests, and finally, section A.5 enumerates the conclusions.

A.2 Link and System Description

As it is well known, HF communications highly depend on ionospheric conditions, and in our case a minimum of 5 hops is needed to cover the distance between Antarctica and Spain [14]. The ionosphere reflection changes with sun radiation, which varies daily, annually and throughout a solar cycle, and also depends on sunspots and Earth's magnetic field [15]. Since the solar cycles have a duration of 11 years, channel sounding data has been collected and analysed since 2003. We use this data to optimize the channel model for our specific link. The first channel model, widely accepted for narrowband transmissions, was developed by Watterson[16]. Vogler and Hoffmeyer from Institute of Telecommunication Science (ITS) developed a wideband ionospheric HF channel model with non-Gaussian statistics and delay spread parameters [17]. Mastrangelo in [18] provided an HF channel simulation system that is well operative with both narrowband and wideband HF channel models. The variability of the channel, the high level of interference and the low SNR at the receiver side make the modulation design very challenging for remote sensing applications.

The system is capable of sounding the whole HF band every hour, 24 hours per day. We sound the channel during the first 40 minutes of every hour, so we are able to transmit modulation tests 10 minutes per hour. The other 10 minutes of each hour are dedicated to maintenance purposes. As the system is simplex we need to repeat the information several times in order to guarantee an acceptable quality at the receiver.

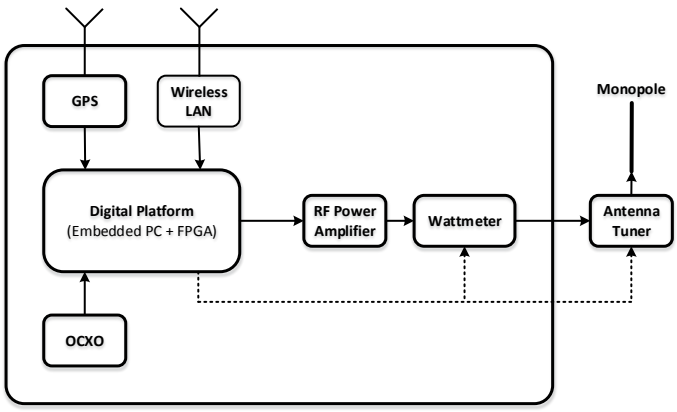

Fig. A.1 Block diagram of the transmitter hardware

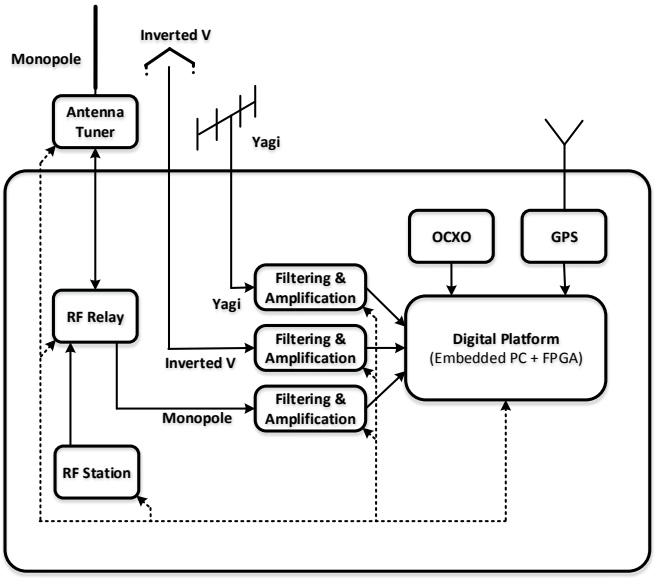

Fig. A.2 Block diagram of the receiver hardware

The core of the transmitter hardware consists of an embedded PC and a XTremeDSP-IV from Xilinx with three FPGAs: a Spartan-II a Spartan-IV and a Virtex-II (see Figure A.1). The Spartan-II is preconfigured and is responsible of the interface between the PCI bus and the Virtex-IV, the Virtex-II configures the clock, and the Virtex-IV, which is equipped with two 14-bit AD and DA converters and all the arithmetic and peripheral drivers, performs the digital radio procedures. The time synchronization accuracy is guaranteed by using a GPS unit with a PPS (Pulse Per Second) signal of $1\mu s$ of uncertainty, taking into account that GPS satellite do have enough coverage in the SAS. We use time synchronization with a GPS to guarantee the same time for both transmitter and receiver. For frequency synchronization we use Oven Controlled Crystal Oscillators (OCXO) of 100 MHz and (± 0.1ppb/^{o}C and ± 30 ppb per year). Moreover, the transmitter power amplifier can be switched off in case of severe impedance mismatch by means of a wattmeter that controls the forward and reverse transmitted power. All the transmitter hardware is deployed close to the antenna at the top of a hill near the SAS. The transmitting antenna is a 7.5m rugged monopole with 8° of take-off angle, with the possibility of adapting to transmit from 2MHz to 30MHz with a Standing Wave Ratio (SWR) lower than 2. All the electronics are inside a watertight sealed box, which provides electromagnetic shielding and protection against hard weather conditions. The system is remotely accessed by using a Wireless Local Area Network (WLAN) from the laboratory in the SAS. More information of the system performance and characteristics can be found in [8, 10].

The transmitter and receiver (see Figure A.2) system are equal but instead of one antenna the system is capable of receiving from three antennas at the same time. The antennas we are using in the receiver are a rugged monopole of 7.5 meters (the same as in the transmitter), a Yagi tuned at 14.5 MHz and an inverted V. The inverted V is a 28m folded dipole to cover also the entire HF band (2MHz-30MHz), please see [19] for more details. The main objective of receiving from three antennas is to maximize the amount of data we will be able to study, as well as to increase the robustness by using polarization diversity in the future.

A.3 Test Design

The tests designed in this work derive from [10] and the results showed therein from DS-SS and OFDM proposals. Results from this previous work showed a better BER performance when transmitting DS-SS symbols rather than multicarrier symbols, at the expense of low spectral efficiency. Although the bit rate required for the remote sensors data is very low, the results that showed a good BER performance in [10] did not have enough throughput. Therefore, three new modulation schemes introduced in [13] and based on DS-SS were designed: i) signaling (S), ii) quadriphase (Q) and iii) quasi-quadriphase (QQ). These three modifications are based on the fact that symbols not only carry information on the phase changes but also on the specific PN sequence used to spread the symbol in the frequency domain, and hence the whole family of Gold sequences may be used [20]. In this scenario, cross-correlation is key to minimize the error probability. Consequently we chose Gold sequences because of their good trade-off between cross-correlation and autocorrelation properties.

The data block length associated to each PN sequence is n where $n = log_2(N+1)$ and N the PN sequence length [21]. This technique improves the spectral efficiency and increases the bit rate in a factor of n. In the case of quadriphase, the improvement is even doubled, because the transmission uses both In-Phase and Quadrature components of the signal, where each component codes a different PN sequence. Therefore, the bit rate in quadriphase increases in a factor $2n$. Finally, an intermediate proposal (i.e. quasi-quadriphase) is addressed to avoid the phase conflicts that appear in quadriphase, at the expense of a reduced bit rate. Quasi-quadriphase uses both I and Q components as well, but the PN sequence family to be used is divided into two halves, which are solely used by one component at a time. Hence, no phase estimation is required and the bit rate increases in a factor $2(n-1)$. For more details about these three techniques, see [13].

PN length	BW [Hz]	bit rate Q [bps]	spectral eff.Q [bps/Hz]	bit rate QQ [bps]	spectral eff.QQ [bps/Hz]
31	250	81	0.324	64.5	0.258
31	500	161	0.322	129	0.258
31	1 k	323	0.323	258	0.258
63	500	95.2	0.190	79.4	0.158
63	1 k	190.5	0.190	158.3	0.158
63	2 k	380.8	0.190	317.5	0.158

Tabla A.1 Quadriphase and quasi-quadriphase tests

PN length	BW [Hz]	bit rate S [bps]	spectral eff.S [bps/Hz]	bit rate QQ [bps]	spectral eff.QQ [bps/Hz]
31	250	40.3	0.164	64.51	0.258
63	500	47.6	0.098	79.36	0.158
127	1k	55.11	0.057	94.48	0.094
255	2k	62.7	0.032	109.80	0.054
511	4k	70.45	0.018	125.25	0.031
1023	8.33k	81.46	0.009	146.62	0.017
2047	16.6k	89.56	0.005	162.83	0.009

Tabla A.2 Signaling and quasi-quadriphase bandwidth tests

A.3.1 Quadriphase and quasi-quadriphase bitrate test

This first test consists of sending the best combinations of symbol period and bandwidth in terms of BER, already obtained in [10], but using quadriphase and quasi-quadriphase techniques in order to increase the spectral efficiency. All the combinations used in the experiments are shown in table A.1.

A.3.2 Signaling and quasi-quadriphase bandwidth test

The second experiment transmits symbols with wider bandwidth, which enable higher throughput in signaling and quadriphase schemes as long as we are using longer PN sequences with equal time length. For this tests a symbol time of around 120 ms was chosen from the results obtained in [10] since it guaranteed a good BER performance. Table A.2 shows all PN sequence length combinations and the bandwidth that ranges from 250 Hz to 16.6 kHz. Wider bandwidths can not currently be tested due to hardware restrictions that will be solved for future works.

A.4 Test Results

As the SAS is only operative during the summer time in Antarctica, we can only run these tests during 3 months throughout the Austral summer, which restricts the amount of data for each test. The channel availability is very variable, so not all of the data received for each test can be properly used to get consistent results. The data used to evaluate these tests were sent on the 18th, 19th and 20th of February during the 2013 campaign. The work presented in this paper is based on 27 data blocks gathered from the three receiving antennas.

A.4.1 Data block design

The data blocks designed for these tests transmit equal number of bits for each modulation technique (i.e. 100 bits). A data set for each technique is transmitted sequentially. Since the number of bits per symbol depends on the PN sequence length and the use of phase and quadrature components, a 100 bits data set contains a variable number of symbols (e.g. 31 chips sequence encodes 5 bits, hence 20 symbols are transmitted per data set).

Each of the 27 received data blocks approximately contains 360 repetitions of the basic data set. A basic data set is composed of around 45 different blocks of 100 bits, with different PN sequence length, bandwidth and modulation technique. Therefore, each basic data set

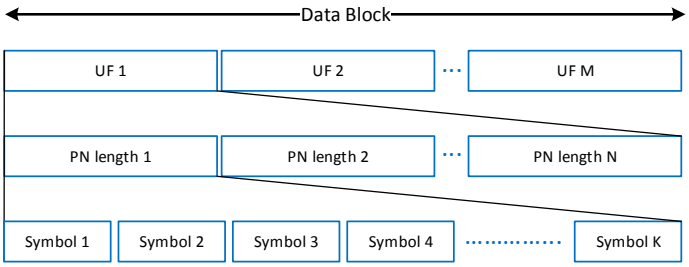

Fig. A.3 Detail of the data block format

contains one test for each possible combination, and this information is repeated in order to treat all the possibilities with similar channel conditions. A training set of PN sequences is sent at the beginning of each basic data set which guarantees a correct acquisition and synchronization, as well as several snapshots of the channel per data block. These training sequences consist of 3 m-sequences of 2047 chips each and an oversampling factor of 10.

A.4.2 Received blocks selection

An initial selection of the received data is needed to achieve meaningful results. The selection method is based on the synchronization quality computed by means of the training sequences.

As synchronization accuracy depends on these training sequences it would make no sense to take into account the results obtained if no proper synchronization was achieved. Three PN m-sequences length 255 with an oversample of 10 are sent before all data blocks, and are used to synchronize in the receiver. We consider a good synchronization when the pattern of the three sequences is found when correlating at the receiver, so demodulation can start guaranteeing a proper synchronization.

Only 27 out of 216 data blocks have been analysed to compute the results shown in this paper (see table A.3), using the criteria already described. This method by itself also considers the null availability during some hours of the day [8, 6] and the fact that the three antennas in the receiver side perform differently depending on the polarization. Table A.3 shows that the hours of the day and frequencies that perform properly are very similar one day to other, there is a certain pseudo periodicity [8]. It has to be taken into account that the sounding obtains the best transmission frequency performance depending on the hour of the day, so the frequency is not optional, and some of them perform better in one antenna than in the other. Poor HF channel conditions by means of SNR are shown in Figures A.4 (both right and left) as an example for signaling and quasiquadriphase. The SNR in this case is evaluated by symbol, and using the channel response obtained by means of correlation in the receiver and calculation of the scattering function. The SNR is evaluated computing the signal power contained in an area defined by the composite multipath spread and the composite Doppler spread [6], and the noise power outside this area. The Cumulative Density Function (CDF) of the SNR evaluated in both direct sequence modulations show the low SNR results already commented, and cause that only 12.5% of the received data can be used to obtain proper results. In this point it is important to remember that the described link pretends perform as a backup link or a low rate transmission data link for small meteorological and geomagnetic sensor data, so despite this low SNR results, the performance of the system is enough to transmit the required data.

A.4.3 Bit rate study: quadriphase and quasi-quadriphase outcomes

In [10], DS-SS showed the best results for digital transmission in the ionospheric channel from Antarctica compared to OFDM, but despite the good BER results the bit rate was too low for the requirements of remote sensing applications. The best combinations of PN sequence length and bandwidth for DS-SS tests are listed in table A.1 [10]. The same symbol period, PN sequence length and bandwidth have been used in quadriphase and quasi-quadriphase tests, in order to compare BER results as a function of bandwidth and bit rate. In Figure A.5.a, the CDF of BER for a PN sequence of length 63 are shown. Quasi-Quadriphase obtains the best possible combination of bandwidth and bit rate by means of the longest symbol period

Hour UTC	frequency [Hz]	antenna	data	modulation
00 UTC	8k	M	18/02/2013	Q
00 UTC	8k	V	18/02/2013	Q
00 UTC	8k	Y	18/02/2013	Q
10 UTC	19k	V	18/02/2013	Q
12 UTC	23k	M	18/02/2013	Q
12 UTC	23k	V	18/02/2013	Q
14 UTC	25k	M	18/02/2013	Q
14 UTC	25k	V	18/02/2013	Q
14 UTC	25k	Y	18/02/2013	Q
14 UTC	25k	V	19/02/2013	S
16 UTC	25k	V	19/02/2013	S
20 UTC	14.5k	Y	19/02/2013	S
22 UTC	10k	V	19/02/2013	S
00 UTC	8k	M	20/02/2013	QQ
00 UTC	8k	V	20/02/2013	QQ
00 UTC	8k	Y	20/02/2013	QQ
12 UTC	23k	M	20/02/2013	QQ
12 UTC	23k	V	20/02/2013	QQ
12 UTC	23k	Y	20/02/2013	QQ
22 UTC	10k	V	20/02/2013	QQ

Tabla A.3 Selected data blocks, with their transmission frequencies and received antennas (M stands for monopole, V stands for inverted V and Y stands for Yagi)

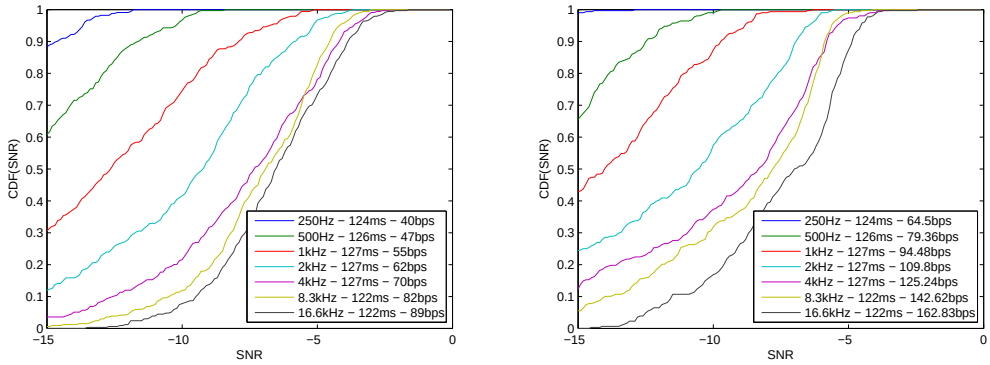

Fig. A.4 Cumulative Density Function of SNR for signaling (left) and quasi-quadriphase (right) for the tests detailed in table A.3

(i.e. 126 ms). The second best combination is also quasi-quadriphase with a shorter symbol period (i.e. 63 ms). The third best result corresponds to quadriphase with the longest symbol period (i.e. 126 ms). As quasi-quadriphase does not need any phase estimation process, BER results are substantially better than in quadriphase scheme. However, the bit rate is approximately 20% lower in quasi-quadriphase for the same symbol length. In this figure we can observe that in certain values of the CDF, some of the curves change slighty their slope and cross other results. Despite this occurs in high BER values, this slight variations are due to the small amount of data collected from each evaluated BER and modulation type.

As the spread bandwidth is slightly higher than the coherence bandwidth of the channel, the most significant parameter is the symbol period. The best results are associated to longer symbol periods as they correspond to lower bandwidths.

In Figure A.5.b the results for the CDF of BER when using a PN sequence length of 31 are shown. Similarly, the best results are given by quasi-quadriphase using the longest symbol period (i.e. 124 ms), followed by the second longest symbol period of quasi-quadriphase (i.e. 62 ms). The third best result is performed by the longest symbol period using quadriphase (i.e. 124 ms).

Table A.4 shows the CDF of BER for all the results given in Figure A.5, taking as a reference values for 5% and 10% of BER. As expected, the best modulation in terms of BER is quasi-quadriphase, while the bit rates are lower than the quadriphase results. The best results are achieved by the smallest bandwidth and the longest symbol period, as oversampling data improves low SNR in terms of $10 \cdot \log(k)$, where k is the oversampling factor. The symbols around 120 ms length present the best BER results because the longer the symbol period, the better the immunity against low SNR. The worst BER results correspond to quadriphase and to the wider bandwidth. The longer the Ts, the higher the oversampling

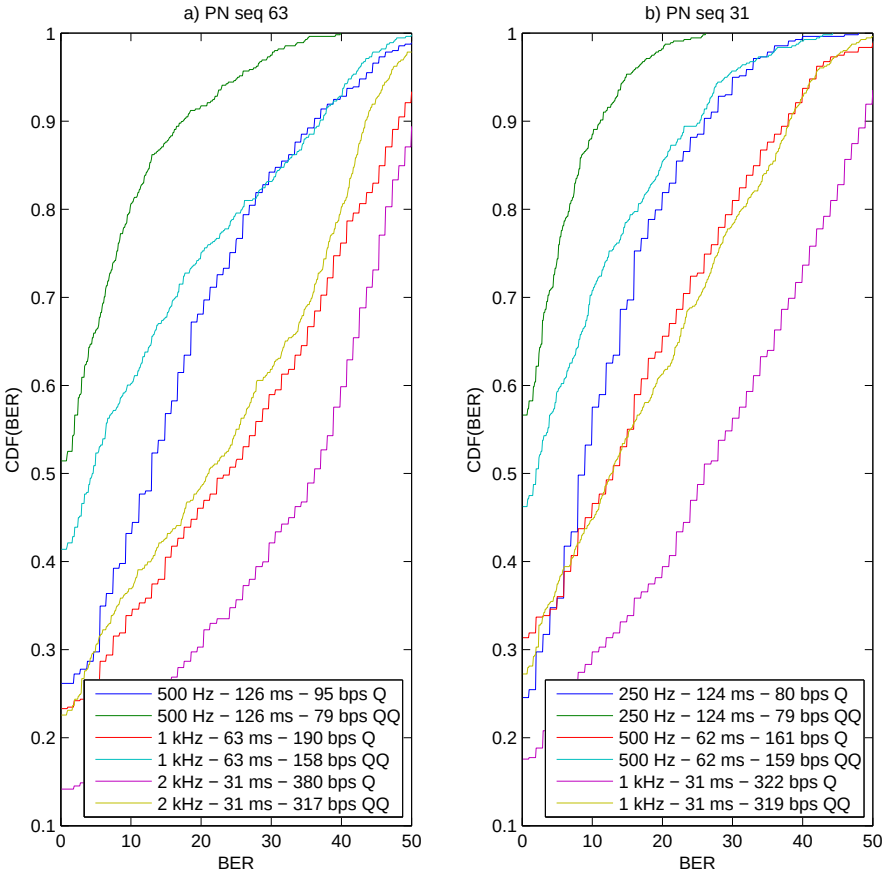

Fig. A.5 Cumulative Density Function of BER for PN sequence length 63 (a) and 31 (b) for the tests detailed in table A.1

factor, and hence the higher the reduction of uncorrelated noise. However, DS-SS performs better for wider bandwidth due to the higher process gain. Therefore in section A.4.4 several bandwidths are compared maintaining the same symbol period (around 120 ms for all tests).

A.4.4 Bandwidth study: signaling and quasi-quadriphase

The second test is a bandwidth analysis, in which the symbol period is kept constant and derived from the results in table A.4. These tests vary the PN sequence length and the bandwidth, assuming all the tests have the same symbol duration (around 120 ms). The detail of the tests is shown in table A.2. Our goal is to conclude whether a wider bandwidth performs better, assuming a non-variant symbol period.

PN length	T_s [ms]	BW	bit rate [bps]	modulation scheme	BER (5%)	BER (10%)
31	124	250 Hz	64.5	QQ	0.74	0.88
63	126	500 Hz	79.4	QQ	0.66	0.80
31	62	500 Hz	129	QQ	0.59	0.70
31	31	1 kHz	258	QQ	0.52	0.60
63	63	1 kHz	158.3	QQ	0.37	0.44
31	124	250 Hz	81	Q	0.36	0.57
31	62	500 Hz	161	Q	0.36	0.46
63	126	500 Hz	95.2	Q	0.29	0.43
63	31.5	2 kHz	317.5	QQ	0.30	0.36
63	63	1 kHz	190.5	Q	0.26	0.33
31	31	1 kHz	323	Q	0.24	0.29
63	31.5	2 kHz	380.8	Q	0.16	0.20

Tabla A.4 Cumulative density function results for 5% and 10% of BER value, sorted from the best (maximum probability) to the worst result (minimum probability), when transmitting with Q and QQ.

Figure A.6 shows the cumulative density function of BER for the signaling bandwidth study. As we expected, the best results correspond to the wider bandwidth (i.e. 16.6 kHz), and the results worsen proportionally as the bandwidth gets narrower, due to the decreasing process gain [22]. It is remarkable that the best BER results correspond to the higher bit rate, so, the fastest transmission technique is also the best in terms of BER.

As it was the first time we spread up to 16.6 kHz we chose the most robust modulation schemes for the bandwidth test. Hence, we have analysed both a signaling and quasi-quadriphase spread spectrum techniques. The quasi-quadriphase was chosen instead of quadriphase due to its better BER results. Figure A.7 plots the cumulative density function of BER for the quasi-quadriphase design detailed in table A.2. Similarly to the results shown in Figure A.6, the quasi-quadriphase and the signaling results follow the same behaviour: better performance for higher spreading factor. As occured in figure A.5, some of the data in the figure vary their slope slightly at certain moments and cross other curves; despite this precision punctual problem, the performance for each modulation can be clearly selected in terms of quality of the results.

Table A.5 shows the results in terms of the CDF(BER), sorted from best to worst, being the best results the greatest CDF values. Both 5% and 10% of BER are the chosen reference values again. The best BER performance is obtained by signaling at the expense of lower bit rates. The best quasi-quadriphase combination (i.e. 16.6 kHz and 162.83 bps) is similar to 2 kHz and 65 bps combination for signaling, with similar BER values but tripling the bit rate.

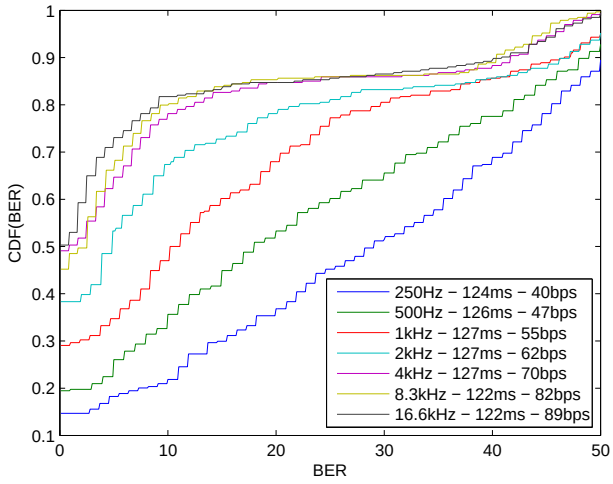

Fig. A.6 Cumulative density function of BER for signaling bandwidth study

Bandwidths higher than 2 kHz improve results when narrowband interference and coloured noise are present, which is a common situation in the Antarctic ionospheric channel.

We can observe that the BER distribution is not uniform. Indeed, both Figures A.6 and Figure A.7 present a fast increase for BER values below 10%, a flat zone between 10 and 35% and a final sharp increase from 35 to 50%. The performance of the long haul channel has shown in all these years of study that either performs with a BER around 5% or 10%, or presents synchronization problems due to lack of communication and the BER obtained is around 35% or even 40%. In our tests it is not common to find the intermediate BER values (around 25% or 30%).

A.5 Conclusions

In this paper we have presented the different modulation tests performed during the 2012/2013 campaign at the SAS, through the HF link from Antarctica to Spain (12700 km). The transmission power was 200 Watts, so we had to deal with very low SNR at the receiver. The tests conducted in this paper conclude that best BER results are achieved by modulations with the longest symbol period due to the high oversampling factor. Obviously, the best performance is a trade-off between BER and bit rate. When comparing the three modulation techniques, signaling is the most robust one with the best BER results, but the slowest in terms of bit rate. Quasi-quadriphase exhibits acceptable BER results and improves the bit rate; however, the best bit rate is achieved by quadriphase, but with the worst BER results. Consequently, if the system needs high reliability at the receiver, signaling is advised, while

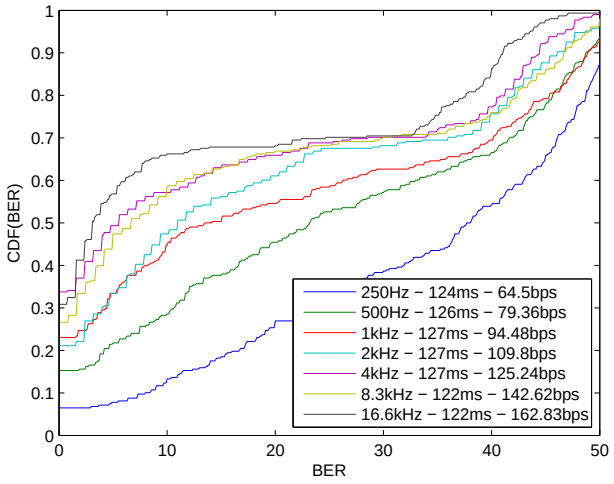

Fig. A.7 Cumulative density function of BER for quasi-quadriphase bandwidth study

the best trade-off between bit rate and BER corresponds to quasi-quadriphase. Finally, the bandwidth study demonstrates that whenever the oversampling factor is kept constant, higher bandwidth values lead to the best BER results at the receiver due to the higher process gain. Future work is focused on changing the hardware conditions that limit the bandwidth tests in order to increase the system capacity. Moreover, we are planning to decrease the symbol period in order to increase the bit rate as well as to apply channel codes and interleavers to reduce the BER at the receiver.

Acknowledgment

This work has been funded by the Spanish Government under the projects CGL2006-12437-C02-01, CTM2008-03536-E, CTM2009-13843-C02-02 and CTM2010-21312-C03-03.

PN length	T_s [ms]	BW	bit rate [bps]	modulation scheme	BER (5%)	BER (10%)
2047	123	16.6 kHz	89	S	0.73	0.81
1023	123	8.3 kHz	81	S	0.66	0.79
511	127	4 kHz	73	S	0.64	0.78
2047	123	16.6 kHz	162.83	QQ	0.56	0.66
255	127	2 kHz	65	S	0.53	0.67
511	127	4 kHz	125.24	QQ	0.49	0.57
1023	123	8.3 kHz	146.62	QQ	0.47	0.58
255	127	2 kHz	109.8	QQ	0.33	0.47
127	127	1 kHz	94.48	QQ	0.33	0.44
127	127	1 kHz	57	S	0.34	0.47
63	126	500 Hz	49	S	0.26	0.35
63	126	500 Hz	79.36	QQ	0.21	0.28
31	124	250 Hz	41	S	0.18	0.21
31	124	250 Hz	64.51	QQ	0.07	0.13

Tabla A.5 Cumulative density function results for 5% and 10% of BER, sorted from the best (maximum probability) to the worst results (minimum probability), for signaling and quasi-quadriphase results in the bandwidth test

Referencias

1. Lee, S., Park, S., Noh, G. *et al.*: Energy-Efficient Spectrum Access for Ultra Low Power Sensor Networks, IEEE Military Communications Conference, 2012.

2. MIL-STD-188-110B, 'Military Standard - Interoperability and Performance Standards for Data Modems', US DoD, 2000.

3. Furman, W.N., and Nieto, J.W.:Latest on-air testing of U.S. MIL-STD-188-110C appendix D wideband HF data waveforms, 12th IET International Conference on Ionospheric Radio Systems and Techniques, pp. 1-5, 15-17 May 2012.

4. NATO STANAG 4415:Characteristics of a robust, non-hopping, serial-tone modulator/demodulator for severely degraded HF radio links, Edition 1, 21 June 1999.

5. Pijoan, J.L., Altadill, D., Torta, J.M., *et al.*: Remote Geophysical Observatory in Antarctica with HF Data Transmission: A Review, Remote Sens. 2014, 6, 7233-7259; doi:10.3390/rs6087233.

6. Vilella, C., Miralles, D., and Pijoan, J.:An Antarctica-to-Spain HF Ionospheric Radio Link: Sounding Results, Radio Science, Volume 43, Issue 4, August 2008, doi: 10.1029/2007RS003812.

7. Vilella, C., Miralles, D., Altadill, D., *et al.*:Vertical and Oblique Ionospheric Soundings over a Very Long Multihop HF Radio Link from Polar to Midlatitudes: Results and Relationships, Radio Science, Volume 44, Issue 2, April 2009, doi: 10.1029/2008RS004001.

8. Ads, A., Bergadà, P., Vilella, C., *et al.*: A Comprehensive Sounding of the Ionospheric HF Radio Link from Antarctica to Spain, Radio Science, 2012, doi:10.1029/2012RS005074.

9. Bergadà, P., Deumal, M., Vilella, C., *et al.*:Remote Sensing and Skywave Digital Communication from Antarctica, Sensors, 2009, doi:10.3390/s91210136.

10. Bergadà, P., Alsina-Pagés, R.M., Pijoan, J.L., *et al.*:Digital Transmission Techniques for a Long Haul HF Link: DS-SS vs OFDM, Radio Science, Volume 49, Issue 7, pages 518–530, July 2014. doi: 10.1002/2013RS005203.

11. Proakis, J.:Digital Communications, McGraw Hill, 2000.

12. Alsina, P., Deumal, M., Bergadà, P., *et al.*:Multiresolutive acquisition technique for DS-SS long-haul HF data link, 11th International Conference on Ionospheric Radio Systems and Techniques, 2009.

13. Deumal, M., Vilella, C., Socoro, J., *et al.*:A DS-SS Signaling based System Proposal for Low SNR HF Digital Communications, 10th International Conference on Ionospheric Radio Systems and Techniques, 2006.

14. Perkiomaki, J.:HF Propagation Prediction and Ionospheric Communications Analysis,(2003-2013), *www.voacap.com*.

15. Davies, K.:Ionospheric Radio, Peter Peregrinus Ltd. on behalf of the Institution of Engineering and Technology, 1990.

16. Watterson, C.C., Juroshek, J., and Bensema, W.D.:Experimental configuration of an HF channel model, IEEE Transactions on Communication Technology, 18(6), pp. 792–803, December, 1970, doi:10.1109/TCOM.1970.1090438.

17. Vogler, L.E., and Hoffmeyer, J.A.:A model for wideband HF propagation channels, Radio Sci., 28(6), pp. 1131–1142, doi:10.1029/93RS01607.

18. Mastrangelo, J.F., Lemmon, J.J., Vogler, L.E., *et al.*:A New Wideband High Frequency Channel Simulation System, IEEE Transactions on Communications, 45(1), pp. 26–34, doi:10.1109/26.554283.

19. Barker & Williamson, "Broadband Frequency Agile HF Folded Dipole Antenna", https://www.bwantennas.com/instr/fdipole.pdf, accessed August 20th 2014.

20. Gold, R.:Maximal Recursive Sequences with 3-valued Recursive Cross-Correlation Functions, IEEE Transactions on Information Theory, 1968.

21. Enge, P.K., and Sarwate, D.V.:Spread-spectrum multiple-access performance of orthogonal codes: linear receivers, IEEE Transactions on Communications, vol. 35, no. 12, pp. 1309-1319, 1987.

22. Simon, M.K., Omura, J.K., Scholtz, R.A., *et al.*:Spread Spectrum Communications Handbook, McGraw-Hill Telecom Engineering, 2002.

Anexo B

Channel sounding and polarization diversity for the NVIS channel

CHANNEL SOUNDING AND POLARIZATION DIVERSITY FOR THE NVIS CHANNEL

M. Hervás, J. L. Pijoan, R. Alsina-Pagès, M. Salvador, D. Altadill
GRECO - La Salle, URL
Quatre Camins 30, Barcelona
Spain
mhervas@salle.url.edu, joanp@salle.url.edu, ralsina@salle.url.edu,
msalvador@salle.url.edu, daltadill@obsebre.es

SUMMARY

Near Vertical Incident Sky-Wave (NVIS) is a good alternative for long-haul links where no line-of-sight is available using near-vertical reflection at the ionospheric layers. The aim of our research is sounding the NVIS channel around the OE (*Observatori de l'Ebre*), in order to obtain the channel characterization as a slow fading multipath channel. Finally, polarization diversity techniques will be used in order to improve the performance of the system. As a first approach, we have used the raw data provided by the Digisonde DSP-4D, developed by the University of Lowell. In this paper, we evaluate the Doppler Spread, Doppler shift, Multipath Delay Spread and SNR for the NVIS channel. This study has been done for both ordinary and x-ordinary waves, for frequencies between 1 and 12MHz with steps of 500 KHz every 30 minutes for a full day. We have tested the use of phase-modulations beyond the 3 KHz bandwidth, in order to explore new techniques for future standards evaluating the advantages of the polarization diversity.

ACKNOWLEDGMENTS:

We would like to thank the help of the team of B. Reinisch at Lowell University. This work has been funded by the Spanish Government under the project CTM2010-21312-C03-03.

1 INTRODUCTION

One way to communicate through ionospheric reflection is Near Vertical Incidence Skywave (NVIS). In that operation mode, the antenna pattern should concentrate most of the radiation at angles above 45 degrees in the elevation plane and should be approximately omnidirectional in the horizontal plane. Then, communications over 300-400 Km without shaded areas can be achieved, since the signal comes from above. This is much larger than any VHF-UHF link, and line-of-sight is not needed, so it is a very useful technique to link remote areas with a central station. This is really interesting for military and humanitarian organizations, as well as for remote sensoring in places where no other infrastructures are available, e.g., the Antarctica [9].

NVIS propagation strongly depends on the operating frequency, and the highest useful frequency on a given point-to-point link is determined by the critical frequency of the region of the ionosphere where the propagating wave is refracted [3]. Some recent studies have been

done about the NVIS channel characteristics [2][3], showing that NVIS communications are highly reliable even when using low transmission power levels (10-20 W). The SNR may drop at some hours of the day for a certain frequency, but there are other parts of the HF band which increase it, so choosing the right frequency for every time of the day you may always guarantee a SNR greater than 10 dB.

As far as data transmission systems using NVIS are concerned, some experiments can be found in the literature. In [1], a 16 kbps data rate in a 3 KHz NVIS channel is obtained by using OFDM with a 256 QAM constellation on each subcarrier. In [4], the use of differential amplitude modulation using OFDM allows a 20,6 kbps data rate in a 3 KHz NVIS channel.

In this paper we study the use of narrow-band and spread spectrum modulations over out-of-standard bandwidths up to 30 KHz in a NVIS channel. As a first approach we have used the Digisonde DPS-4D developed by the University of Massachusetts Lowell Center for Atmospheric Research (ULMCAR) [5] and recently installed in Observatori de l'Ebre in Roquetes. This ionosonde transmits a digital Pseudo Random Sequence[10] in a bandwidth of 30 KHz so it is a very easy way to evaluate the behavior of spread-spectrum signals for NVIS communications. Thanks to the kind help of the engineers from ULMCAR, we could have access to the raw data stored by the Digisonde and evaluate the parameters presented in this paper.

In addition, the Digisonde has a couple of antennas (right-hand and left-hand circular polarization) able to separate the ordinary and extraordinary waves at the receiver. This allowed us to investigate the benefits of using polarization diversity in narrowband modulations.

This paper is organized as follows. In section 2, a brief description of the main features of the Digisonde is done. In section 3, an explanation about the channel sounding and demodulation scheme is described. In section 4, the results of channel sounding a signal demodulation applying polarization diversity are discussed. In section 5, the conclusions are explained.

2 MEASUREMENT SET-UP

The results presented in this paper are obtained from the raw data provided by the Digisonde DPS-4D developed by ULMCAR [5]. The main advantages of this new digital sounder are: coherent integration of several pulses at the same frequency, pulse compression for improvements in SNR, multiple receiver arrays, transmission and reception of circularly polarized signals and frequency multiplexing for an improved Doppler resolution.

The pulse compression radar allows fine-range resolution and long range detection radars without using short pulses with high peak power. Instead of those short pulses, phase-coded long pulses are transmitted with specific properties, and the received pulses are correlated to obtain short pulses with high power after the matched filter.

One of the most used codes in pulse compression radars are complementary codes [7][10]. For a pair of complementary codes with elements either 1 or –1, the sidelobes of the

compressed waveform from one code is the inverse of the ones from the other code. When the compressed waveforms from two codes are added together, the sidelobes will be totally canceled in the ideal case, and the magnitude of the main lobe will double.

In our case, the sounding is based on the transmission of a couple of even and odd complementary codes as shown in Figure 1.

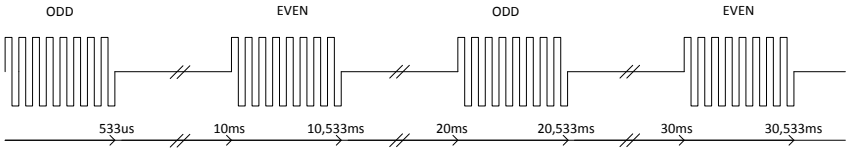

Figure 1: Example of 4 complementary pulses, as the ones transmitted in this system

Both the even and the odd code are 16-bit PN sequences, so the chip length is 33µs leading to a total bandwidth of 30 KHz.

Thanks to the simultaneous reception at both a right-hand and left-hand circular polarized antennas, the system is able to separate the ordinary wave from the extraordinary wave. The use of polarization diversity has been recently published in [6], in the context of a MIMO system in a one-hop HF link, but no other experiences have been found in literature in NVIS links.

3 TEST PROCEDURES

The Digisonde DPS-4D is one of the most well-known digital ionosonde among the observatories around the world. Figure 2 shows two ionograms obtained by Digisonde at the same time in two different seasons. The red line represents the ordinary wave reflections and the green one the extraordinary wave reflection. As you can see, there are substantial differences in terms of critical frequency (foF2), virtual height, number of reflections, etc.

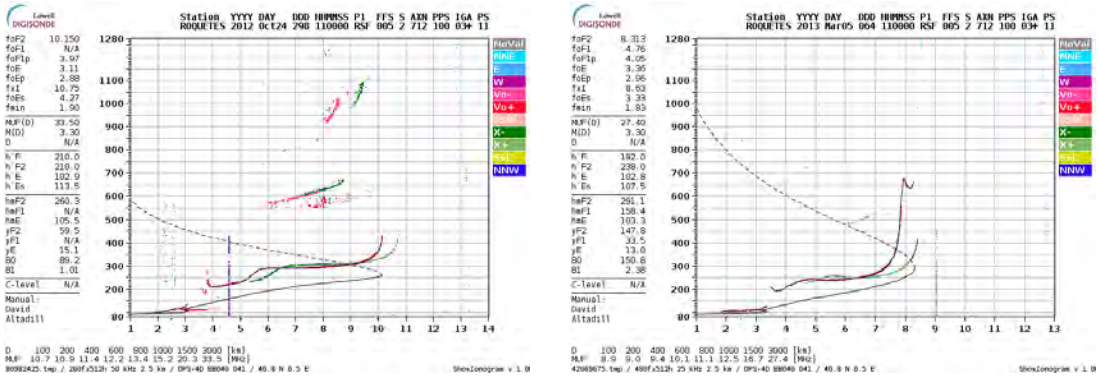

Figure 2: Ionograms of the two sounding days at 11 UTC obtained from Observatori de l'Ebre using DPS-4D Digisonde

The .RAW data saved by Digisonde DPS-4D allow us sounding the channel and study the effect of polarization diversity on the channel Bit Error Rate (BER). Those data are saved in IQ format. These studies have been done for both, ordinary and extraordinary wave, for different frequencies and seasons.

3.1 CHANNEL PARAMETERS

Our goal is to obtain the statistical behavior of the following channel parameters: Doppler Spread, Multipath Delay Spread, Doppler Shift and SNR. A block diagram of the whole process about the channel characterization calculations is shown in Figure 3.

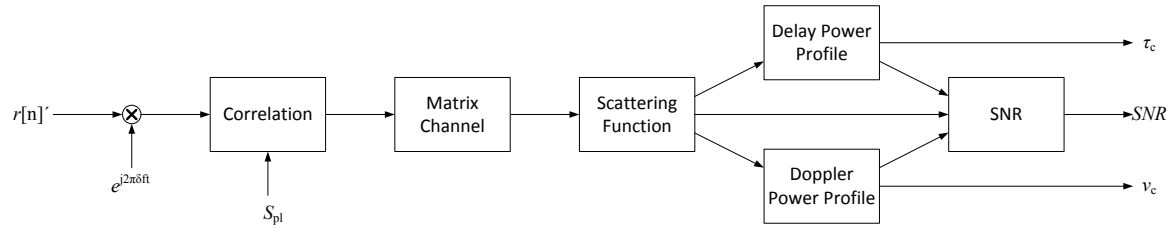

Figure 3: Block diagram of channel characterization calculus

All parameters have been obtained from the scattering function, which is easily computed measuring the channel impulse response, which can be calculated correlating the received signal and the transmitted PN sequence [8]. A process gain of 6 dB is obtained taking into account that the sequences are complementary codes. Then, the scattering function is calculated through the FFT of the channel impulse response in the time domain. In Figure 4, we can see an example of a scattering function calculated for an NVIS channel.

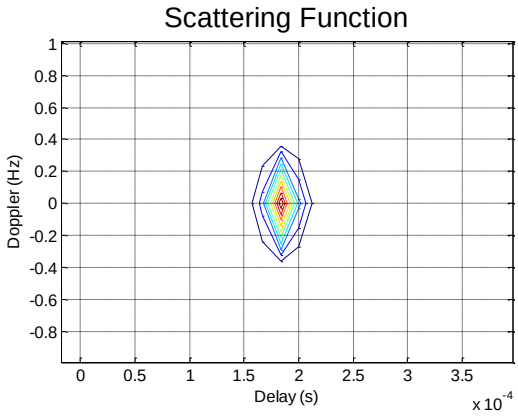

Figure 4: Scattering Function

The Multipath Power profile (1) and Doppler Power profile (2) are obtained integrating the Scattering function in the delay and Doppler domain, respectively.

$$\varphi(\tau) = \int_{-\infty}^{\infty} Rs(\tau, v)dv \quad (1)$$

$$\varphi(v) = \int_{-\infty}^{\infty} Rs(\tau, v)d\tau \quad (2)$$

Then, the Composite Multipath and Doppler Power Profiles are obtained by integrating the Multipath Power profile and Doppler Power profile in the time and frequency domain respectively. To avoid extra noise and interferences, a window around the Scattering Function's maximum is applied.

Finally, the Doppler and Multipath Spread is directly the difference (in x-axis) between the 10% and 80% of the Composite Doppler and Multipath Power Profile. A graphical example of these calculations can be found in Figure 5.

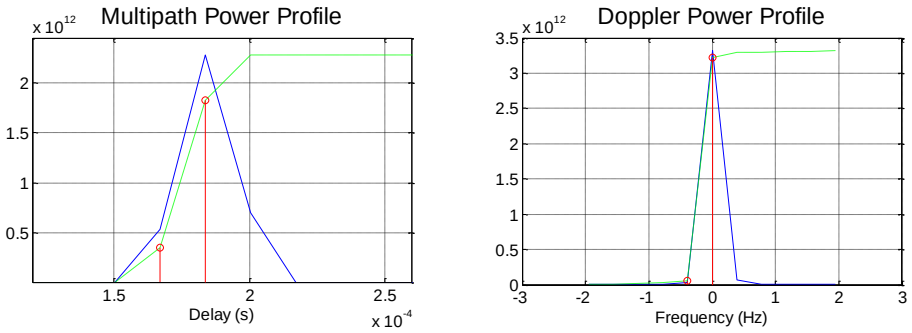

Figure 5: Multipath (left) and Doppler Power Profile (right) of NVIS channel

The SNR relationship is computed by means of the main path of the scattering function (see Figure 6). The rest of the scattering function is considered as the noise power.

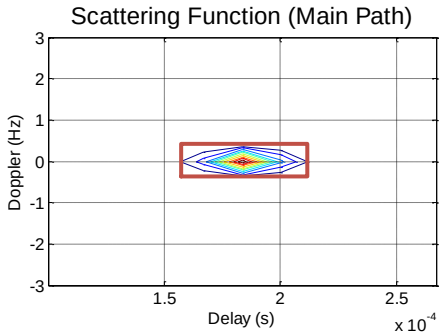

Figure 6: Main path of Scattering Function windowing for SNR evaluation

The SNR estimator used in this study is shown in (3) where P is the signal power, A_S is the area contained around Doppler Spread and Multipath Delay, A is the complete area of the scattering function and ρ_n is the noise per area unit. A complete development of the SNR estimator is shown in [8].

$$SNR = \frac{P|_{A_S} - \rho_n A_S}{\rho_n A}, \qquad where\ \rho_n = \frac{P|_{\overline{A_S}}}{\overline{A_S}} \tag{3}$$

The frequency value in the Doppler axis in which the scattering function is maximum, is known as the Doppler Shift. This parameter represents the effective shift of the received frequency, and is produced by the movement of the ionospheric layers.

3.2 MODULATION SCHEMES

As we use the signal sent and received by the Digisonde as a test signal, the signal properties cannot be changed in Digisonde. The transmitted signals are 2 complementary codes of 16-bits modulated in phase and up-converted to any carrier frequencies in the HF range (3-30 MHz). However, the received signal can be treated like a PSK modulated signal with a bandwidth of 30 KHz, which is much greater than the HF standard bandwidth of 3 KHz.

The aim of this work is to study the SNR as a function that depends on polarization (ordinary and extraordinary wave), hour of the day and frequency, and evaluate the improvement when polarization diversity is taken into account.

A block diagram of the receiver is shown in Figure 7. Phase and time synchronization have been performed through the correlation between the received signal and the sent PN sequence. The phase of the correlation output has been used to correct the phase of the received signal and demodulate properly the PSK data. The study has been done for both the ordinary and extraordinary wave.

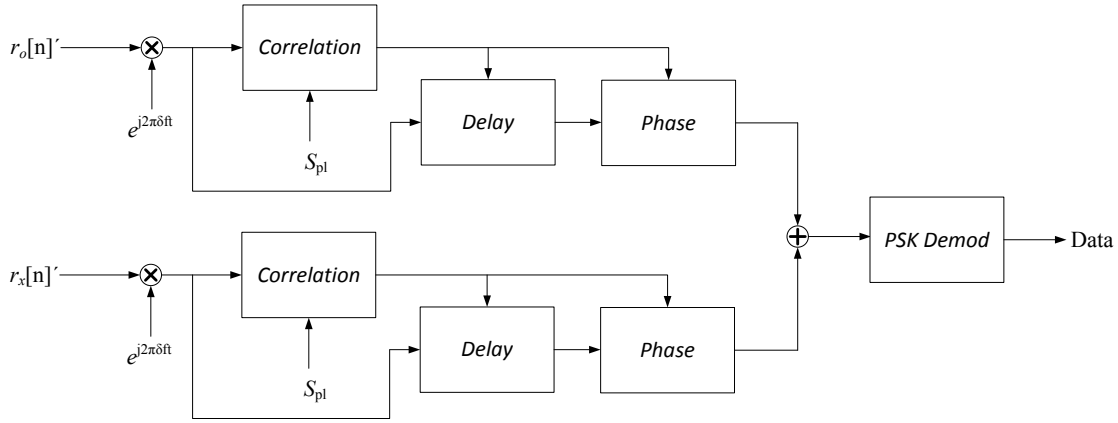

Figure 7: Demodulation scheme taking into account polarization diversity

Polarization diversity gain is obtained by adding in phase and temporarily synchronized the received signal of both ordinary and extraordinary waves. As the height where the reflection takes place depends on polarization, the correct synchronization time may be different for the ordinary and the extraordinary waves.

4 RESULTS

The results of this work are evaluated and shown in two parts, the channel sounding and the demodulation process applying polarization diversity.

4.1 CHANNEL SOUNDING

The channel sounding data has been obtained during two days at different seasons. The sounding took place every half hour, along a frequency range from 1 MHz to 12 MHz with a frequency step of 500 KHz.

The results in terms of Doppler Spread, Doppler Shift and Multipath Spread are summarized in Table 1. This information is used to evaluate the coherence time of the channel and the coherence bandwidth, and hence, to design the most suitable physical layer for a future communications system.

As the Digisonde is able to separately receive the ordinary and extraordinary wave, we have studied every parameter for both modes. From table 1 we can observe that the extraordinary

mode has a significant higher Multipath Spread, due to reflection at higher layers whereas the ordinary mode has a slightly higher Doppler spread in all cases.

		October 24th2012		March 5th 2013	
Parameters	Wave	Mean	Variance	Mean	Variance
Doppler Spread	Ordinary	0.6816 Hz	0.0940 Hz	0.3780 Hz	0.1994 Hz
	Extraordinary	0.1237 Hz	0.0956 Hz	0.0817 Hz	0.0617 Hz
Doppler Shift	Ordinary	-0.0888 Hz	0.5542 Hz	-0.0255 Hz	0.2081 Hz
	Extraordinary	-0.0735 Hz	0.4785 Hz	-0.0222 Hz	0.1769 Hz
Multipath Spread	Ordinary	710.71 µs	2.8301 µs	496.01 µs	2.0175 µs
	Extraordinary	921.41 µs	4.4577 µs	712.47 µs	3.1860 µs

Table 1: Summary of channel sounding results

The SNR for every hour and frequency is measured for both modes as it can be seen in Figure 8 and Figure 9. We can observe that the ordinary wave exhibits a greater SNR at lower frequencies (2.5-10.5 MHz) than the extraordinary wave during the daytime, while the extraordinary wave SNR is greater at higher frequencies (4.5-11 MHz) than the ordinary wave. Moreover, extraordinary waves suffer more attenuation from the D-Layer than ordinary waves during the daytime.

In optimal conditions we have measured SNRs up to 30-40 dB for a 30 KHz bandwidth. This a very promising result that can lead to high bit-rates for long distance NVIS links.

Finally, the SNR seems to be lower in March than in October, but the seasonal variation should be studied more deeply in future work as we only have data from one day of both months.

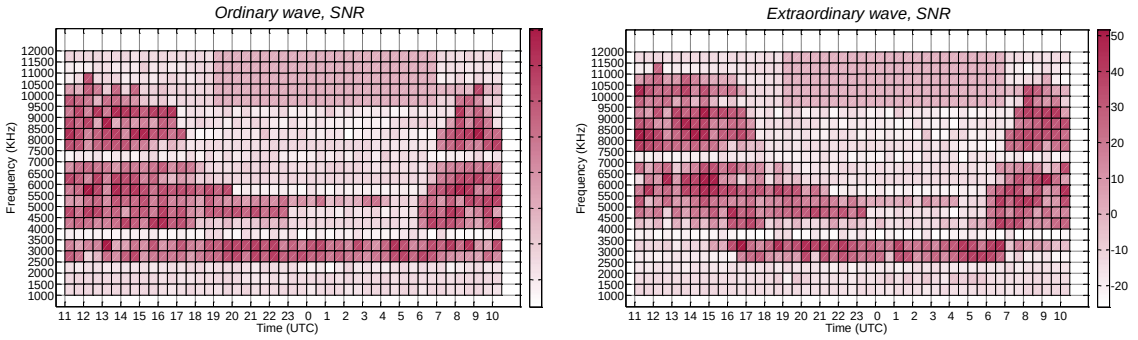

Figure 8: SNR relationship for Ordinary and Extraordinary waves in October 24th in 2012

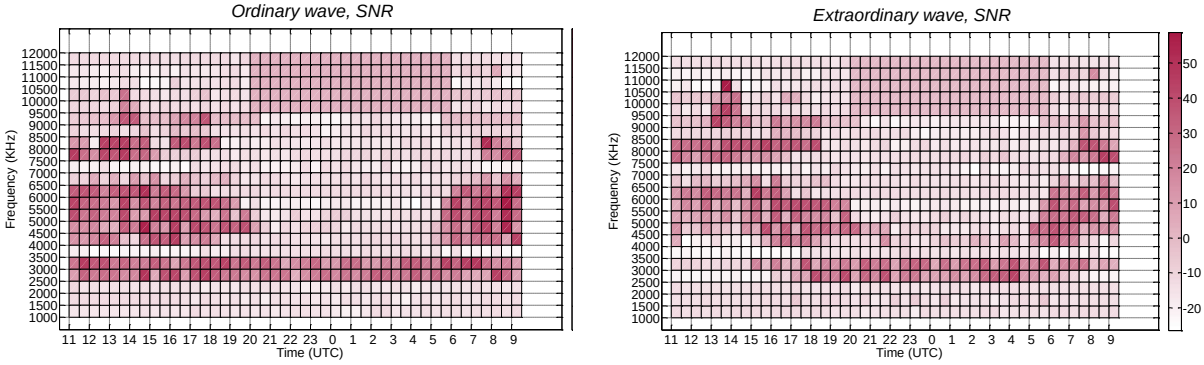

Figure 9: SNR relationship for Ordinary and Extraordinary waves in March 5th in 2013

4.2 MODULATION RESULTS

In Figure 10 and Figure 12, the BER (in %) for both modes as a function of the hour and frequency is calculated. The extraordinary mode performs poorly at low frequencies during daytime and the ordinary shows some bad performance frequencies at 2 and 4.5 MHz. After applying a simple strategy of polarization diversity, i.e., the addition in phase of both signals, a great outperformance is observed as shown in Figure 11 and Figure 13. As shown in figures, a wide range of frequencies can be used during daytime, while the performance at low frequencies is improved at nighttime.

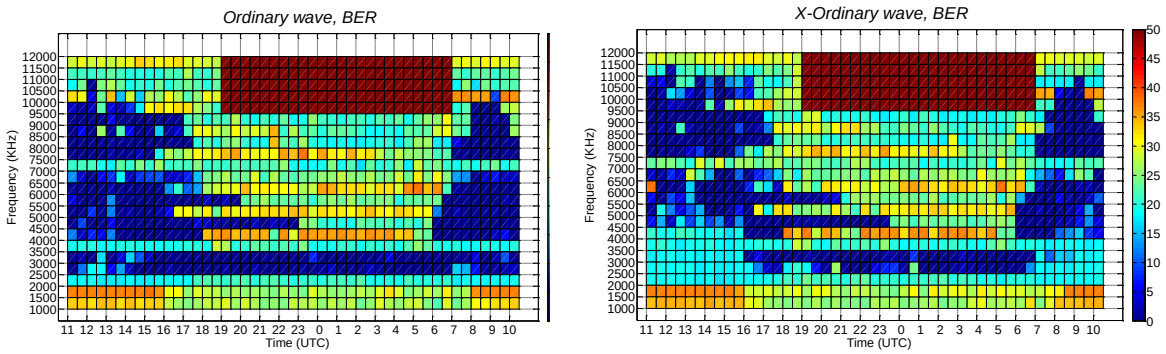

Figure 10: BER (%) for Ordinary and Extraordinary waves in October 24th in 2012

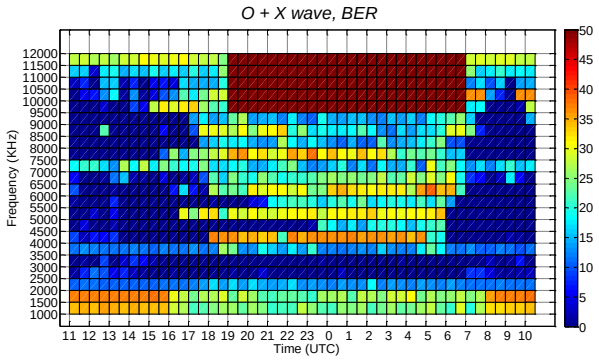

Figure 11: BER (%) applying diversity in October 24th in 2012

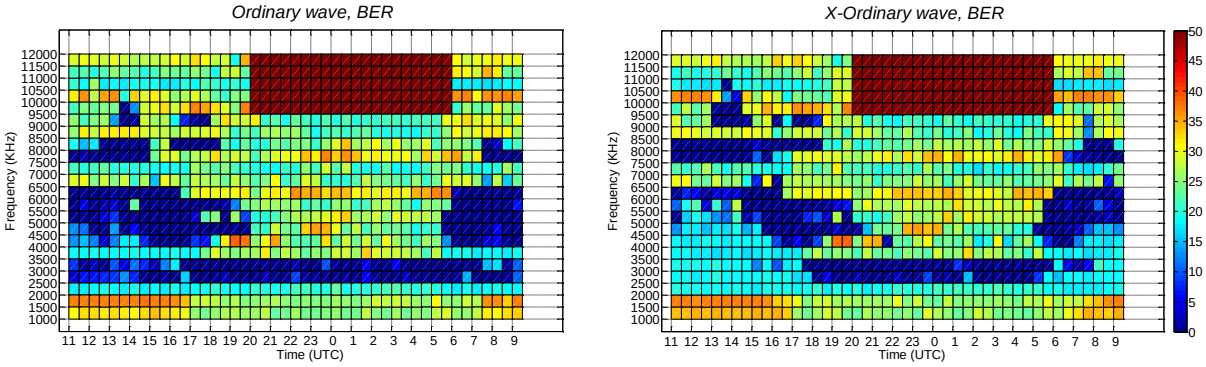

Figure 12: BER (%) for Ordinary and Extraordinary waves in March 5th in 2013

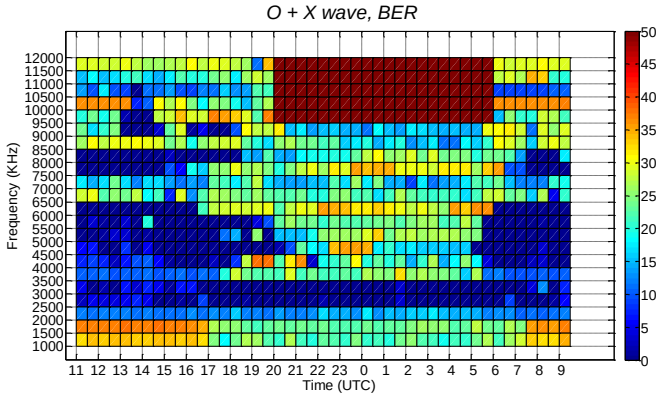

Figure 13: BER (%) applying diversity in March 5th in 2013

In order to evaluate deeper the performance improvement of polarization diversity, the variation of BER as a function of time for two specific frequencies (2 and 3.5 MHz) is shown in Figure 14. The left figure shows a decrease in terms of BER about 8% for both daytime and nighttime. In the right figure, the improvement can be shown when there is a BER lower than 20%, that represents an enough level of SNR to have a usable frequency. However, this improvement cannot be shown when the BER is larger than this 20%.

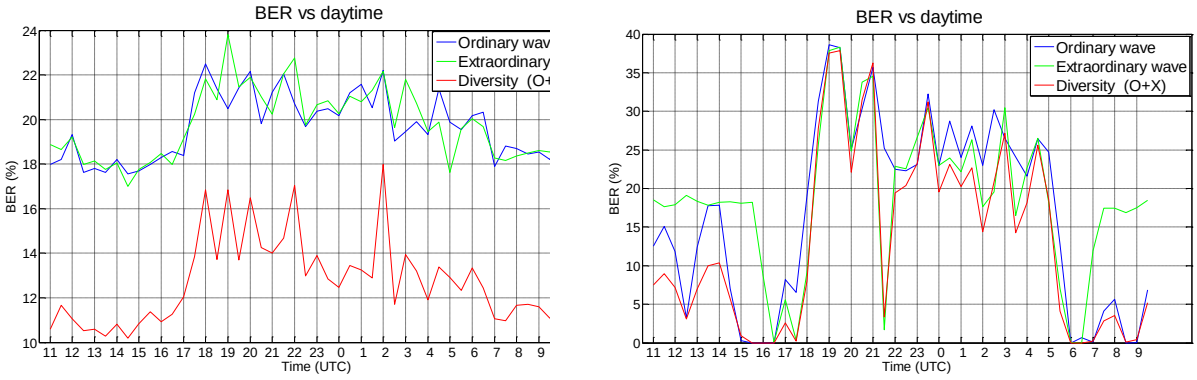

Figure 14: BER versus daytime for Ordinary, Extraordinary and O+X, for 2 (left) and 3.5MHz (right)

5 CONCLUSIONS

NVIS is a very promising communication system for links up to 300 Km without shaded areas. This cannot be achieved using neither VHF nor UHF band. In this paper we have shown a proof of principle of low power NVIS systems that show SNR up to 30-40 dB for a bandwidth of 30 KHz. With such a high SNR, the design of high bit rate physical layers makes sense.

As the ionosphere splits the incident wave into two modes with orthogonal polarization, it is possible to receive separately the ordinary and the extraordinary wave. In this paper we have showed that, using polarization diversity techniques, at least the range from 2 to 8.5 MHz can be used during daytime and 2 to 3.5 MHz during nighttime with low BER.

In future work, once the channel sounding is completed, a new physical layer will be defined. New modulations will be proposed and several polarization diversity approaches will be tested, as well as out-of-standard bandwidths beyond 3 KHz.

Moreover, a remote network sensor could be established taking into account the low power requirements in NVIS radio links, i.e. the Antarctic project, where several sensors are distributed around Livingston Island.

Finally, a 2x2 MIMO system can be envisaged with two transmitting and receiving antennas. This can duplicate the throughput, as you may send independent bit streams on every antenna.

6 REFERENCES

[1] Hoult, N. S.; Whiffen, J. R.; Tooby, M. H.; Arthur, P.C., *16 kbps modems for the HF NVIS channel*, IEE Eighth International Conference on HF Radio Systems and Techniques, (IRST 2000), pp.317-321, 2000

[2] Walden M., *A comparison of measurements and propagation simulations for mid-latitude HF NVIS links at 5 MHz during sunspot minima*, Proceedings of Nordic HF Conference, August 2010.

[3] Johnson, E.E., *NVIS Communications During the Solar Minimum*, IEEE Military Communications Conference (MILCOM 2007), pp.1-5, October 2007.

[4] Antoniou, S.; Christofi, L.; Green, P. R.; Gott, G. F., *High rate data transmission in the mid-latitude NVIS HF channel*, IEE Proceedings on Communications, vol.153, no.2, pp.272,278, April 2006,

[5] Reinisch, B. W., et al. *New Digisonde for research and monitoring applications*, Radio Science, vol 44, doi:10.1029/2008RS004115, 2009.

[6] Ndao, P. M.; Erhel, Y.M.; Lemur, D.; Oger, M.; Le Masson, J., *First experiments of a HF MIMO system with polarization diversity*, 12th IET International Conference on Ionospheric Radio Systems and Techniques (IRST 2012), pp.1-5, May 2012.

[7] Golay, M. J. E., *Complementary Series*, I.R.E. Transactions on Information Theory, pp. 82–87, 1961.

[8] Vilella, *C.; Comunicacions avançades d'HF entre la Base Antàrtica Espanyola i l'Observatori de l'Ebre: caracterització de canal i transmissió de dades*, PhD Thesis, 2010.

[9] P.Bergadà, M. Deumal, R.M. Alsina, J.L. Pijoan, *Time Interleaving Study for an OFDM Long-Haul HF Radio Link*, Ionospheric Radio Systems and Techniques, April 2009.

[10] Ming Yao et al.; *Comparison of Radar Waveforms for a Low-Power Vertical-Incidence Ionosonde,* IEEE Geoscience and Remote Sensing Letters, vol. 7, no.4, October 2010

Anexo C

IRIS: A software defined radio platform for educational purposes

IRIS: A software defined radio platform for educational purposes

MARCOS HERVÁS GARCÍA, ROSA MARIA ALSINA-PAGÈS, JOAN LLUÍS PIJOAN, MARTÍ SALVADOR and DAVID BADIA
GR-SETAD, La Salle, Universitat Ramon Llull (URL), Barcelona, Spain, c/Quatre Camins, 30, Barcelona, Spain. E-mail: mhervas@salleurl.edu

This paper presents the design of a scalable software defined radio platform based on a Spartan-6 FPGA as a core processor. The platform, named IRIS, has been developed for both educational and research purposes fitting the performance of the analog front-end, the processing core and unit cost to the requirements of the applications. The resolution and sampling frequency of the analog front-end are its main adjustable parameters. The requirements of the processing core involve the FPGA and the communication ports. The platform has five different peripheral ports for low and high speed communications ranging from 16 kbps to 2.5 Gbps. The communication ports allow our students to develop a high range of applications for both onsite and online courses applying teaching methodology based on learning by doing using a real system to help them to reach transversal competencies. Currently, the IRIS is used for educational purposes in practical applications of Software Defined Radio, as a collection of best practices for both Electromagnetic Compatibility and Signal Integrity courses, and the analysis to evaluate the performance of the analog front-end in the Software Radio course of BSc of Telecommunciations.

Keywords: Educational platform; Software Defined Radio (SDR); Field Programable Gate Array (FPGA); programable logic; signal integrity; Electromagnetic Compatibility (EMC)

1. Introduction

This paper presents the design of IRIS platform, based on a Software Defined Radio (SDR) architecture with programmable logic and its applications on education. It is well known that the SDR platforms have great versatility, because the system features can be modified just updating the firmware and changing a few components such as the antenna, the filters or the amplifier.
The IRIS platform was conceived to be used in both educational and research fields, so the design is scalable to satisfy both requirements. In order to fulfill the entire SDR design, in which MIMO and applications with different communications ports are desirable, the platform is design with 2 high speed
Analog to Digital Converters (ADCs), 2 high speed Digital to Analog Converters (DACs), and support several different clock input signals and different communication ports. Moreover, the IRIS has to be VITA 57 compliant in order to increase the feasibility of adding new hardware such as Digital Signal
Processors (DSP) through a Field Programmable Gate Array (FPGA) Mezzanine Card (FMC) connector. The platform has been designed following accurate Electromagnetic Interference (EMI) rules of design to obtain the best performance [1]. These rules have impact in the effective number of bits (ENOB) on a design with ADCs or DACs and in the signal integrity.
The students are provided with a lite version of the platform for educational purposes which they can use to develop real software radio applications taught in class. In the research field, the full version platform can be used with the higher features. We are currently setting up a research project line based on final master's thesis with the IRIS platform. Among them, we highlight the design of a broadband High Frequency (HF) radio-modem for both Near Vertical Incidence Skywave (NVIS) and single-hop oblique ionospheric transmissions. Once finished, this modem will be used to connect data loggers in remote placements to settle a remote sensing network, i.e. the Spanish Antarctic Station (SAS) in Livingston Island [2-5] in which data of the sensors are placed up to 300 km away from the SAS, and wherever remote data communication is needed. For educational purposes, this platform allows our student to apply Project-Based Learning (PBL) methodologies [6], such as, *i)* real SDR scenario implementation, *ii)* the best practices and design rules of this platform are detailed in the Electromagnetic Compatibility (EMC) courses and *iii)* the analog front-end including the ADC and DAC converters are measured to characterize the SDR system.

Finally, the platform is electrically and mechanically compatible with the proprietary robot known as LSMaker [7] for joint applications such as indoor location. The LSMaker is an educational platform which contains a microcontroller as a control processor, 4 motors, radio frequency (RF) connectivity and a display. This platform allows our students to learn about microcontrollers and how to program several applications in assembler and C code in different subjects distributed in 4 courses of the Telecommunications Engineering curricula.
In Sect. (2), the state of the art of standard platforms that satisfies our requirements is reviewed, Sect. (3) shows the system description of the IRIS, Sect. (4) and Sect. (5) present the applications on education and the conclusions, respectively.

2. Existing platforms

Current technology allows the design of high-performance radio-modems that work digitally with bandwidths up to 60 MHz. Therefore, the RF signal can be processed directly without an external mixer in the whole HF band.
The leading FPGAs manufacturers, Xilinx and Altera, mainly propose as high performance SDR system the use of evaluation boards [8] with additional subsystems based on the FMC VITA connectors [9] from third parties as Terasic, MVD Cores, 4DSP, HiTech Global and Nutaq Innovation, or other manufacturers as Analog Devices and Texas Instruments. This solution presents drawbacks in terms of scalability, size and unit cost. The cost can be up to some thousands of dollars which is prohibitive for educational purposes. Moreover the use of multiple boards makes the size bigger than integrated solutions.
Integrated commercial platforms can be divided into two categories: high performance SDR systems such as USRP, 4DSP or Nallatech in [10-12] or low cost educational SDR platform for amateurs and RF enthusiasts such as bladeRF [13]. These solutions have been developed by non-FPGA manufacturers and fit partially our requirements. They integrate the analog front-end, the processing core and some communication ports. The analog front-end is composed of high speed ADCs and DACs with a throughput ranging from 40 to 125 MSPS with a resolution ranging from 12 to 16 bits.
The higher performance platforms cover our needs of signal integrity and throughput for research applications but their price is too high for an educational platform. Moreover, these platforms have usually one PCIe communications port. Having other ports such as ethernet, Universal Serial Bus (USB) 2.0 On-The-Go (OTG) and UART allows us to have more flexibility for some applications such as connecting the platform to a laptop or to an ethernet network. The low cost SDR platform covers our requirements for educational applications with low throughput and low resolution converters, for example 40 MSPS and 12 bits. These platforms have a USB as communication port, and often ethernet and UART. The price of these platforms ranges from 450 $ up to 1000 $. However, these platforms are not supplied with a PCIe port for higher throughput applications and the ENOB is lower than the number of bits of the analog front-end because the lower cost solutions have not design accurately the Printed Circuit Board (PCB) taking into account the signal integrity.

3. Systems description

The IRIS platform design takes into account both the requirements of scalability in the performance and the unit cost, minimizing it for educational applications, and migrating to a higher performance design easily when the requirements of the application need it. For this reason, IRIS has been designed with pin-compatible components such as the FPGA, DAC, ADC and the clock input oscillators of the clock manager. To reduce the unit cost, the platform can be built without some additional hardware included in the design, i.e. the ethernet transceiver, the SDRAM memory, the secondary SPI flash memory which is used for specific applications or the USB OTG. In Fig. 1, the IRIS block diagram is shown.
The IRIS platform has two Serial Peripheral Interface (SPI) flash memories, one of them is used to store the FPGA bitstream program file, and the other memory is used to store additional information such as file system or Microblaze.
Microblaze [14] is an embedded microprocessor that can be configured as a part of its own hardware in Xilinx FPGAs. This embedded microcontroller allows us to control peripherals with an Intelligent Property (IP) core such as ethernet or USB OTG through C programming language with a stand-alone application or Linux operating system, which is easier than VHDL. Moreover, the system has a volatile SDRAM DDR3 memory, which is used to store and access data when the application is running at high speed.
The system has up to five communication interfaces: *i)* an USB to UART bridge, which can be used to send data at low speed or as a Microblaze console when it is configured on the board, *ii)* an ethernet transceiver

able to be configured as 10/100/1000 Mbps, *iii)* a USB OTG with a throughput of 480 Mbps, *iv)* a PCIe with a throughput of 2.5 Gbps, these interfaces can be used for higher throughput application requirements, and *v)* an additional UART can be attached to the LSMaker platform [7].
The analog front-end is composed of a dual ADC and a dual DAC, the input and output analog signals, respectively, are injected via SubMiniature version A (SMA) connector.

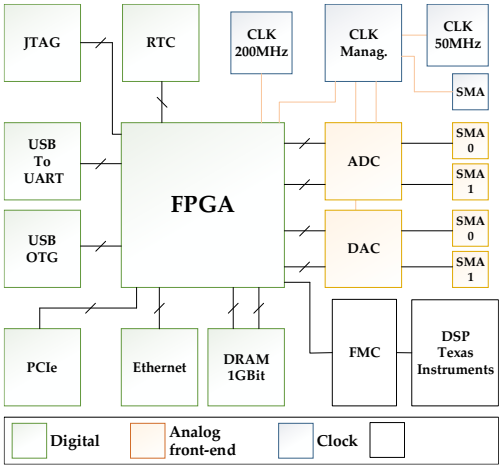

Fig. 1. Block Diagram of the IRIS platform

Both signals are single-ended, they are differentially coupled through operational amplifiers. The high performance analog front-end allows the processing of bandwidths of RF signals ranging from Direct Current (DC) up to 60 MHz.
The clock signal of the converters is distributed via a clock distributor, this solution minimizes the jitter and allows to divide the clock frequency of each output. The FPGA non-used pins are routed to the FMC connector for future applications.
The IRIS platform has been designed to be versatile, for this reason the platform has a Samtec FMC connector routed following the VITA 57 standard to connect the FPGA to an optional hardware, mainly a Texas Instrument DSP. The interface between the FPGA and DSP through a bus of 64 bits [15] is planned with 69 pins of 3.3 V CMOS routed to the FMC connector. DSPs are commonly used in radio-modems for operations such as Fast Fourier Transform (FFT), coding and applications at baseband.
All components having SPI port (AD, DA, distribution clock, SPI memories and FMC routed) have been multiplexed with 3 chip select signals minimizing the number of pins used. The platform has a Real Time Clock (RTC) connected to the FPGA through an Inter-Integrated Circuit (I2C) port, which has been routed to the FMC connector. These standard ports (I2C and SPI) to the FMC connector will allow us future communications between the FPGA and other components.

4. Applications on educations

Currently, the IRIS is being used as an educational platform in three main fields of the bachelor and the master of Telecommunications and Electronics: *i)* A practical SDR case in our Master of Telecommunications Engineering (MET), *ii)* as a collection of best practices and rules in the design of high performance PCB in EMC in the BSc of Electronic and Telecommunications and *iii)* the ADC/DAC performance analysis to evaluate the performance of the analog front-end in the Software Radio subject of BSc of Telecommunications.

4.1 Software Radio

The MET students use the platform to implement a real part of a SDR system. They simulate an ionospheric HF radio link with 4 hops between Antarctica and Spain [2]. The channel presents Doppler effect and intersymbol interference (ISI) due to the multipath caused by the ionospheric layers [3]. This particular 12700 km channel is studied because, not only GRSETAD has been studying it for more than 11 years, but also it has a similar behaviour to mobile communications channels in terms of time and frequency scattering. The channel characterization information is obtained from previous work [2]. The students design a wide-band modulation scheme such as OFDM or spread spectrum with a bandwidth up to 3 kHz

to compensate the effects of the channel, simulating the modulation scheme in Matlab software. Moreover, they implement an upconverter and a downconverter to modulate and demodulate the signal in the HF band. The communications port used to send and receive data to and from the PC is the UART with a throughput of 1 Mbps, which is enough for 3 kHz of bandwidth typically used in HF communication, the IP cores required to do this communication and the Matlab scripts have been supplied to the students. This one of the practical cases studied at MET, working in groups to improve not only the technical contents but also the transversal competencies.
The BSc of Telecommunications students use the platform to study basic concepts of VHDL and logic programmable oriented in the field of application of SDR. They are introduced to VHDL and FPGA devices, developing easy finite-state machines (FSM), FIR filters and correlations in both parallel and sequential structures. They observe that pipe-line structure obtains the higher speed using the maximum number of logic resources and sequential structures with lower speed using the lower logic resources. The students use Xilinx IP cores such as the Direct Digital Synthesizer (DDS) or FFT to understand the use of these well-known elements in SDR. Finally, they test the effect of the undersampling for frequency downconversion and implement practical cases such as an IQ modulator.

4.2 EMC and signal integrity design rules

This section summarizes the best practices applied in the PCB layout, which are part of the EMC courses. Special attention was given to EMC and signal integrity for a proper design of high speed and analog signals.

4.2.1 Power supply and filtering

The power supply has been separated in two groups, analog and digital sources. These power supply outputs have been filtered taken into account the maximum system frequency. Both analog and digital ground planes have been virtually separated, and all components have decoupling capacitors in all power supply pins. Switched regulators have been used for power supplying the FPGA and the digital parts because of their high current consumption. Capacitances are added, to work as decoupling capacitors, as close as possible to each input power of each integrated circuit, reducing both the inductance presented by the ground plane and the non-desirable noise effect produced by one integrated circuit upon another. Previous studies [1] demonstrate that using capacitors of the same value, the probability of having antiresonances in the decoupling network decreases, so this technique has been applied.
The linear regulator can reject the power supply ripple as a function of the load capacitance and the output current, as shown in [16]. In order to avoid crosstalk between integrated circuits in the power supply due to the current transient, the sensitive parts of the analog components have independent power linear regulator, such as the power supply pin of the internal clock circuit of the DAC. A full block diagram of the power supply can be seen in Fig. 2 where ADP5052 [17], LM2576 and LT3471 are switched regulators, ADP3333 [16], ADP3335 [18] and TPS51200 are linear regulators and LPF are the pi low pass band filter.

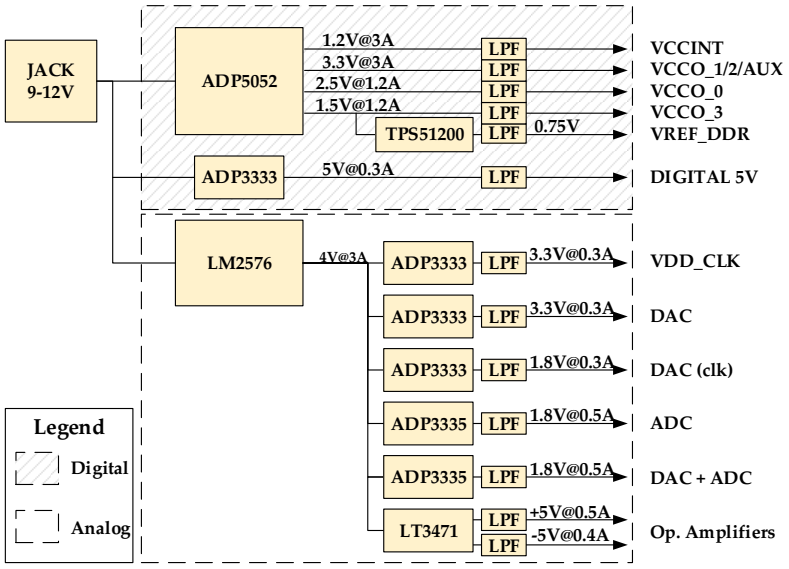

Fig. 2. Power supply diagram of the IRIS platform

4.2.2 Impedance matching

When the signal wavelength is comparable to the length of the track, it should be seen as a waveguide. Otherwise, difference in phase and reflexions are produced degrading the signal integrity [19]. The used waveguide microstrip 3a, stripline 3b, differential microstrip 3c and differential stripline 3d can be seen. The characteristic impedance of the tracks that work as a waveguide has been designed to be 50 Ω for single-ended and 100 Ω for differential pairs, knowing the dielectric characteristics. These routing consideration to design the tracks have taken into account for the GTP port, the USB OTG, the ADCs, the DACs, ethernet transceiver, the FMC and the DDR memory.

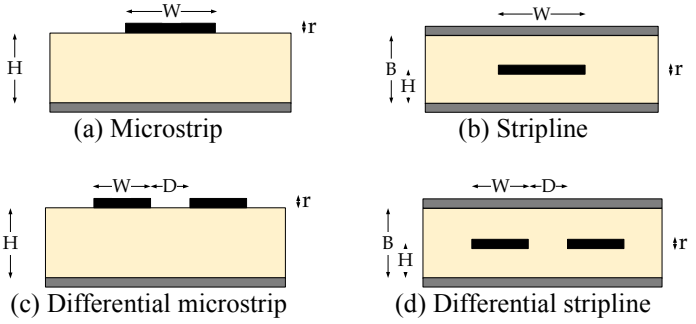

Fig. 3. The four waveguide used in the IRIS platform

4.2.3 Grounding

A proper ground design minimizes the noise and can provide protection against interference and emission. The impedance of a conductor depends on the frequency, as can be seen in $Z_g = R_g + jwL_g$. Any return current through the ground plane presents a potential difference, $V_g = I_g \cdot Z_g$. The copper impedance of a track or a plane is basically inductive, and as digital integrated circuits demand current peaks on each switching. These demands are converted into voltage differences, which are coupled to the rest of the circuit. The voltage difference, $V_L(t) = L_g \cdot \frac{dI_g}{dt}$, depends on both the inductance and the derivative of the current demanded. Therefore, an accurate ground design is supposed to minimize the impedance Zg, more precisely, the inductance Lg, and decrease the flow current Ig through a different path. The impedance Zg depends on the geometry of the track or plane, the wider the ground is, the lower the inductance. A full ground plane covering the PCB surface presents the lowest impedance, for this reason it was chosen for our design. All the ground connections have been done through via holes between the proximity of the pad and the ground plane.

4.2.4 PCB stack-up

The selection of the PCB stack-up number of layer has taken into account the following statements: *i)* internal signals have to be between full ground or power planes to be considered as striplines, *ii)* a full power plane in parallel with a ground plane add additional profitable capacitance for decoupling high frequency disturbances, *iii)* the higher frequency signals or the most susceptible ones to be disturbed can be routed on internal layers for non-desirable coupling effect reduction, minimizing the outer and the intern crosstalk, *iv)* at least 2 internal layers are needed to route some BGA components such as the FPGA, the DDR memory and the FMC connector and *v)* the PCB thickness has to be 62 mils or 1.6 mm for PCIe standard connectors. For these reason, a PCB stack-up of 8 layers has been chosen as it can be seen in Fig. 4. The internal Mid-Layer 1, Mid-Layer 4 and Mid-Layer 6 are ground planes, Mid-Layer 3 is the power plane and Mid- Layer 2 and Mid-Layer 5 are the internal layers for routing signals. Top and bottom layers were routed as microstrip tracks and internal layers as stripline tracks. The internal layers which are enclosed between 2 planes are isolated from external disturbances. The ground plane and the power plane are contiguous layers because the closer the parallel conductive surfaces are, the greater the desirable parasitic capacitance.

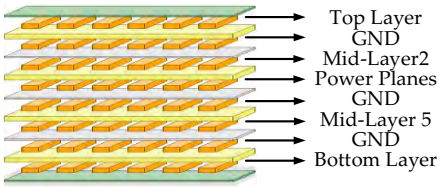

Fig. 4. PCB 8 layers stack-up

4.2.5 Track equalization

The design of a high speed digital bus such as the interface between the DDR memory and the FPGA has to ensure that all track lengths are equal. Differences in length between tracks at high frequencies represent a non-negligible delay between them. For this reason, as can be seen in Fig. 5, the smallest net length has been increased for both single-ended and differential signals up to be equal to the largest.

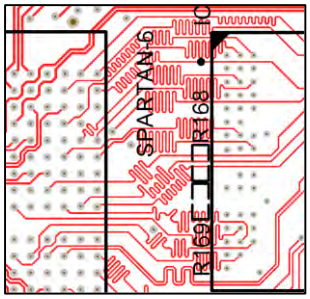

Fig. 5. Track equalization between the FPGA and DRAM

Measurements of the accuracy of the analog front-end have been conducted by the students. These measurements check the correct performance of the EMC and signal integrity criteria applied in the design and the quality of the SDR system. These measurements help them to learn in depth concepts previously studied in theoretical lessons such as intermodulation products, harmonics, distortion, aliasing and noise. A picture of the educational platform is shown in Fig. 6. The ADC is the model AD9204 and the DAC is the AD9745. Both ADC and DAC have been clocked at 50 MHz with a standard crystal oscillator of the manufacturer FOX. The parameters measured for the ADC are *i)* Signal to Noise Ratio (SNR) for both the carrier reference (dBc) and the converter full-scale reference (dBFS), *ii)* Spurious-Free Dynamic Range (SFDR) which is the difference between the full-scale of the converter and the powerful interference, *iii)* ENOB, *iv)* Signal to Noise And Distortion Ratio (SINAD), *v)* Total Harmonic Distortion (THD) and *vi)* Total Harmonic Distortion plus Noise (THD+N) which is equal to the SINAD measuring from DC to half sampling frequency. These six parameters are defined and considered as basic measures of the ADC dynamic performance in [20]. The only parameter measured for the DAC is the FSDR because the source of signal has a level of SNR lower than the desired 73 dB, which is the quantisation error of the converter. The source of signal is a DDS inside of the FPGA.

Fig. 6. Picture of IRIS platform

4.2.6 ADC performance measurement

The ADC sampling measurements are carried out with the RF signal generator 8642B from HP. It has been used to inject the input signal to the system. This RF generator has a much better performance than the ADC AD9204 and guarantee nonharmonic distortion power below -100 dBc and a phase noise of -138 dBc/Hz at an offset of 20 kHz from the carrier. These measures are higher than the approximately 60 dB of SNR able to measure the ADC by the fact of having a resolution of 10 bits.
All parameters have been calculated from the results obtained in Fig. 7 with Matlab where the full scale, the quantisation noise level and the process gain have been drawn. The quantisation noise is $6.02 \cdot Nbits + 1.72 = 61.92\ dB$ lower than the full-scale. The performance parameters are measured for a bandwidth of 25 MHz which is half of sampling frequency. The noise power N0 has been calculated integrating the noise over a non-distorted bandwidth by any spurious and extrapolating it for the 25 MHz of bandwidth and the distortion D integrating the 8 most powerful spurious.

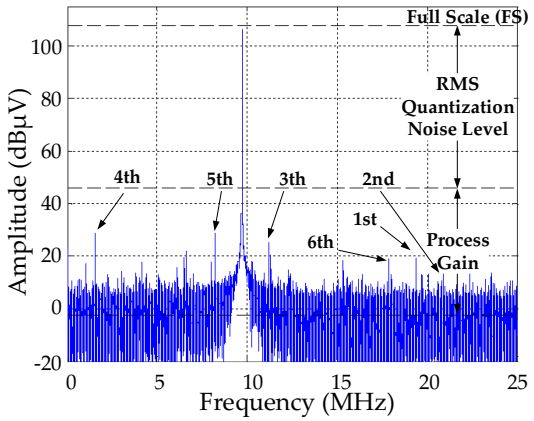

Fig. 7. Signal analysis of the digital signal convertered by the ADC

The values obtained are *i)* SNR=60.9 dB / 59.3 dBc *ii)* THD=-72.5 dB, *iii)* SINAD=60.66 dB, *iv)* ENOB=9.78 Bits and *v)* FSDR=79.2 dBc. The ENOB and the real number of bits of the converter are very similiar, 9.78 and 10. It demonstrates that the analog front-end has been designed accurately.

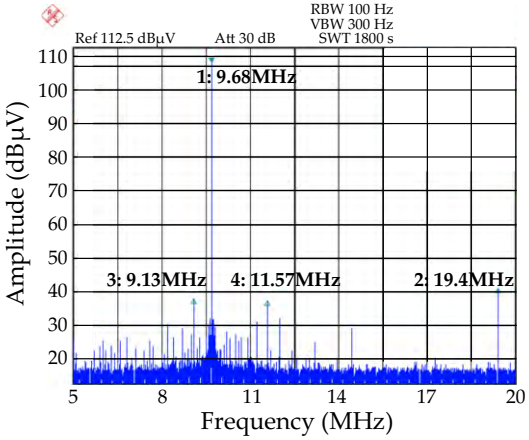

Fig. 8. A DDS signal injected by the DAC

4.2.7 DAC performance measurement

The measurement of the DAC performance has been carried out with the DDS xilinx IP core and a spectrum analyzer. The FSDR has been calculated as the ratio between the signal power and the integration of the powerful spurious. The analysis to obtain results have been done from Fig. 8, the FSDR calculated is 68 dBc and 69.15 dBFs and the quantisation noise is $6.02 \cdot Nbits + 1.72 = 74\ dB$, which is 5 dB greater than the FSDR, near to 1 bit in terms of ENOB. Some peaks observed on the DAC are generated by the DDS. The peak power of these distortions are higher than quantisation noise, then the accuracy of the converter cannot be measured precisely.

5. Conclusions

The IRIS is a compact and integrated SDR platform with a high grade of scalability and connectivity that follows all the requirements mentioned for educational and research purposes.
The platform has an accurate design in terms of signal integrity and EMC as we have been able to observe previously in the ADC performance measurements. These results show us that the platform outperforms similar ones presented in the literature, with the same unit cost or comparable performances with less unit cost. The XtremeDSP Development Kit - Virtex-4 Edition with ADCs and DACs resolution of 14 bits has a cost of thousands of dollars. The analog front-end presents better performance than the IRIS platform with an ENOB of 12.3 bits which improve our educational version of 10 bits of resolution in 2.5 bits. However, the cost of our platform, which is about 300 $, is much lower. The USRP N200/N210 from Ettus Resarch, with dual ADCs and DACs of 14 and 16 bits of resolution, respectively, has an ADC FSDR of 88 dBc and DAC FSDR of 80 dBc, which is higher than our 79.2 for ADC and 68 for DAC. However, the cost of this Ettus version is much higher than the IRIS platform for educational purposes.
Currently, the IRIS is being used as educational platform for putting into practice concepts reviewed in the lectures for both BSc and MSc of Telecommunications. The feedback obtained from the students is very positive since they have the chance to work with a real platform and implement real-time algorithms. The great connectivity allows the students to work from out of the class with only a PC and the IRIS. From the scholar point of view, it allows us to deploy SDR courses and the MET in online format using a real system, because the IRIS allows to work from home. The system may be connected using the ethernet transceiver or the USB OTG.
The IRIS platform can be used for both on-site and online programs. The platform was created to apply teaching methodology based on learning by doing or PBL [6] using a real system that the students can use along the year in school or at home. Some schools use virtual labs, however, working with a real system helps students reach transversal competencies and increase their knowledge.
Finally, for future application the system can be expanded through the FMC connector, by adding some subsystems such as a DSP to our system. It can be attached to the LSMaker proprietary robot with a UART to communicate between a microcontroller and the Spartan-6.

Acknowledgment- The authors would like to thank the Spanish Government by funding this work under the project CTM2010-21312-C03-03.

References

1. H. W. Ott, *Electromagnetic Compatibility Engineering*, John Wiley & Sons, 2011.
2. C. Vilella, J. Socoro, J. Pijoan, Gutierrez, I., Altadill, D., An Antarctica to Spain HF Link. Oblique Sounding Results, *Ionospheric Radio Systems and Techniques*, 2006.
3. A. Ads, P. Bergadà, C. Vilella, J. Regué, J. Pijoan, R. Bardají, A Comprehensive Sounding of the Ionospheric HF Radio Link from Antarctica to Spain, *Radio Science,* **48**, 2016, pp. 1-12.
4. J. Pijoan, D. Altadill, M. Torta, R. Alsina-Pagès, Remote Geophysical Observatory in Antarctica with HF Data Transmission: A Review, *Remote Sensing,* **6**(8), 2014, pp. 7233-7259.
5. P. Bergadà, R. Alsina-Pagès, J. Pijoan, S. M., J. Regué, D. Badia, S. Graells, Digital Transmission Techniques for a Long Haul HF Link: DS-SS vs. OFDM, *Radio Science,* **49**(7), 2014, pp. 518-530.
6. F. M. Richard and K. S. Linda, Learning and teaching styles in engineering education, *Engineering education,* 1988, pp. 674-681.
7. J. Albo-Canals, D. Vernet, X. Canaleta, X. Vilasis-Cardona, LSMaker: A Robotic Platform for Engineering Education, *IEEE International Symposium on Circuits and Systems (ISCAS)*, 2013.
8. Xilinx inc Spartan6 EK, http://www.xilinx.com/products/boards-and-kits/EK-S6-SP605-G.htm, Accessed 28 April 2014.
9. 4DSP FMC176, FMC176, http://www.4dsp.com/FMC176.php, Accessed 28 April 2014.
10. Ettus Research, http://home.ettus.com/, Accesed 26 May 2014.
11. 4DSP AD350, http://www.4dsp.com/AD350.php, Accessed 28 April 2014.
12. Nallatech, XtremeDSP, http://www.nallatech.com/Development-Kits/virtex-4-xtremedsp-development-kit.html, Accessed 28 April 2014.
13. Nuand LLC, http://www.nuand.com/, Accessed 16 May 2014.

14. Xilinx inc., Microblaze Processor Reference Guide, UG081, http://www.xilinx.com/support/documentation/sw_manuals/xilinx12_1/mb_ref_guide.pdf, Accessed 6 June 2014.
15. Xilinx inc., Interfacing Xilinx FPGAs to TI DSP Platforms Using the EMIF, XAPP753, http://www.xilinx.com/support/documentation/application_notes/xapp753.pdf, Accessed 6 June 2014.
16. Analog Devices inc., ADP3333: High Accuracy Ultralow IQ, 300 mA, anyCAP Low Dropout Regulator, ADP3333 datasheet, http://www.analog.com/media/en/technical-documentation/data-sheets/ADP3333.pdf, Accessed 6 June 2014.
17. Analog Devices inc., ADP5052: 5-Channel Integrated Power Solution with Quad Buck Regulators and 200 mA LDO Regulator, ADP5052 datasheet, http://www.analog.com/media/en/technical-documentation/data-sheets/ADP5052.pdf, Accessed 6 June 2014.
18. Analog Devices inc., High Accuracy Ultralow IQ, 500 mA anyCAP Low Dropout Regulator, ADP3335 datasheet, http://www.analog.com/media/en/technical-documentation/data-sheets/ADP3335.pdf, Accessed 6 June 2014.
19. H. Johnson and M. Graham, High-Speed Digital Design, a handbook of black magic, Prentice Hall PTR, 1993.
20. W. Kester, Understand SINAD, ENOB, SNR, THD, THD+N, and SFDR so you don´t get lost in the noise floor, *Analog Devices Support*, http://www.analog.com/media/en/training-seminars/tutorials/MT-003.pdf, Accessed 6 June 2014.

Marcos Hervás received the BSc degree in Telecomunications engineering from Universidad de Alicante (UA), Alicante, Spain, the MSc in Telecomunications engineering from Enginyeria La Salle, Universitat Ramon Llull (URL), Barcelona, Spain, in 2008 and 2011, respectively. Currently is a PhD candidate and member of the research group GRSETAD. His current research interest include the areas of wireless communications and the corresponding digital signal processing and its electronics, especially for OFDM, SCFDMA and the implementation of software defined radio communication systems in FPGA devices.

Rosa Ma Alsina-Pagès received her BSc and MSc in Electronics and Telecommunications in La Salle, Universitat Ramon Llull (URL) in 1999, 2001 and 2004 respectively. She obtained her PhD in Telecommunications Engineering with Cum Laude in 2012, also in La Salle (URL). She has several papers in communications and signal processing journals. Her current research interests include digital signal processing, physical layer modulation and code design, and ionospheric HF communications.

Joan Lluís Pijoan received his MsC degree in Telecommunications from the Polytechnical University of Catalonia (UPC) in 1994 and the PhD degree from Ramon Llull University in 2000. Joan Llus Pijoan has been the leader of several research projects concerning low power advanced HF communications with Antarctica and multicarrier modulations applied to low voltage and high voltage systems, with a strong cooperation in European Actions COST 262 Spread Spectrum Systems and Techniques in Wireless and Wired Communications and COST 289 Spectrum and Power Efficient Broadband Communications.

Martí Salvador received his BSc and MSc in Telecomunications from Universitat Ramon Llull (URL) in 2013 and 2014 respectively. He has been working in the Electronic and Communications area of the URL where he has received a research internship for three years. His study fields during these years were mainly Mobile Communications, HF and Ionospheric Communications. He worked for 6 months in the Robotics and Mechatronics Department of the DLR in Germany, and he is actually working for Samsung Research America in the US.

David Badia received the BSc degree in Telecommunications engineering from EUETT La Salle, associate to Universitat Politècnica de Catalunya, the MSc degree in electrical engineering, and the PhD degree from Enginyeria La Salle, Universitat Ramon Llull (URL), Barcelona, Spain, in 1990, 1995 and 2012, respectively. He is a lecturer of the Communications and Signal Theory Department since 1987, and member of the new research group in electronic systems, telecommunications and data analysis GR SETAD. His research topics are EMC, electronic instrumentations systems and innovative teaching.

Anexo D

Narrowband and Wideband Channel Sounding of an Antarctica to Spain Ionospheric Radio Link

OPEN ACCESS

1st International Electronic Conference on Remote Sensing
22 June - 5 July 2015

Conference Proceedings Paper – Remote Sensing

Narrowband and Wideband Channel Sounding of an Antarctica to Spain Ionospheric Radio Link

Marcos Hervás[1,*], Rosa Ma Alsina-Pagès[1], Ferran Orga[1], Joan Lluís Pijoan[1] , David Badia[1] and David Altadill[2]

[1] GR-SETAD La Salle, Universitat Ramon Llull, Quatre Camins 30, 08022 Barcelona, Spain; E-Mails: ralsina@salleurl.edu (R.M.A.-P.); forga@salleurl.edu (F.O.); joanp@salleurl.edu (J.L.P.); david@salleurl.edu (D.B);

[2] Observatori de l'Ebre, (OE), CSIC - Universitat Ramon Llull, Horta Alta 38, 43520 Roquetes, Spain; E-Mail: daltadill@obsebre.es (D.A.);

* Author to whom correspondence should be addressed; E-Mail: mhervas@salleurl.edu (M.H.); Tel.: +34-932902445; Fax: +34-932902385.

Published:

Abstract: La Salle and Ebro Observatory have been involved in several joint projects about remote sensing in Antarctica for the last 11 years (approximately one solar cycle). The Ebro Observatory has been monitoring and analyzing the geomagnetic and the ionospheric activity in the Antarctic Spanish station Juan Carlos I, ASJI, (62.7ºS, 299.6 ºE) for more than eighteen and ten years respectively. La Salle has two main goals in the project. The first one is the data transmission and reception from Antarctica to Spain to obtain a historical series of measurements of channel sounding of this 12760 km ionospheric HF radio link. The second one is the establishment of a stable data low power communication system between the ASJI and Cambrils, Spain, (41.0ºN, 1.0ºE) to transmit the data from the remote sensors located in the island. In this paper, both narrowband and wideband soundings have been carried out to determine channel availability performed using a frequency range from 2 to 30 MHz with 0.5 MHz step during the 24 hours of the day, encompassing wider channel measurements than previously done, in terms of hours and frequency. This paper presents the results obtained for the austral summer in 2014, using a monopole antenna at the transmitter and an inverted V on the receiver side.

Keywords: geomagnetism; remote sensors; HF; ionosphere; channel sounding; Antarctica

1. Introduction

Analyzing the ionosphere and the magnetic field in the Antarctica is an important contribution to understand of Earth's phenomenons concerning the geophysical science. Knowledge acquired on the characteristics of the channel does not only improve the performance of high frequency (HF) radio-communication systems, but also develops ionospheric science. Vertical and oblique sounding techniques are frequently used to obtain the characteristics of the ionospheric channel for a given radio-link. The geomagnetic observatories have been collecting for years the magnetic field variations in fixed locations having a wide range of time scales, from seconds to centuries, to make possible the understanding of the behavior of the magnetic field of the Earth.

The Antarctic Spanish Station Juan Carlos I (ASJI) is located in the Livingston Island, a place of great interest because it monitors the sub-auroral zone [1]. The ASJI has a geomagnetic observatory with the International Association of Geomagnetism and Aeronomy code LIV. LIV is remotely managed by the Ebro Observatory Institute (EO) in Spain and it is aimed to monitor the magnetic field variations of that region. ASJI is only attended by scientist and technicians during the austral summer, typically from December to February. As ionospheric exploration by vertical soundings is one of the most commonly used to observe the vertical structure of the ionosphere, a VIS (Vertical Incidence Sounder) was installed at the ASJI during the summer expedition of 2004–2005 by OE. In 2003, an OIS (Oblique Incidence Sounder) was also installed in the ASJI by La Salle with a double objective: *i)* to measure the characteristics of the ionospheric channel from ASJI to Spain, taking into account days, annual and solar cycle variations and *ii)* to settle a robust hardware and software platform for an HF radio-communication system from ASJI to Spain. The later system should be able to operate under hard environmental conditions, with the best digital modulations designed for a low power and high interference communications system. The OIS covers a long haul ionospheric link (see Figure 1), of around 12760 km, from the ASJI (62.7ºS, 299.6 ºE) to Cambrils (41.0ºN, 1.0ºE).

In previous works, both narrowband and wideband soundings had been analyzed [2], but both carrier frequencies and the time of transmission were limited. Since 2008, an enhanced transmitter and receiver were installed [3], and the oblique sounding observations can be widely recorded. The results presented in this paper give light to the knowledge of this long haul link, but also help us to design the physical layer characteristics remaining from the previous studies [4,5], where less carrier frequencies were used and the tests were not performed during the entire day.

Figure 1. Geographical link characteristics. The transmitter is located in the ASJI, in Livingston Island (62.7ºS, 299.6 ºE) and the receiver is placed in Cambrils (41.0ºN, 1.0ºE).

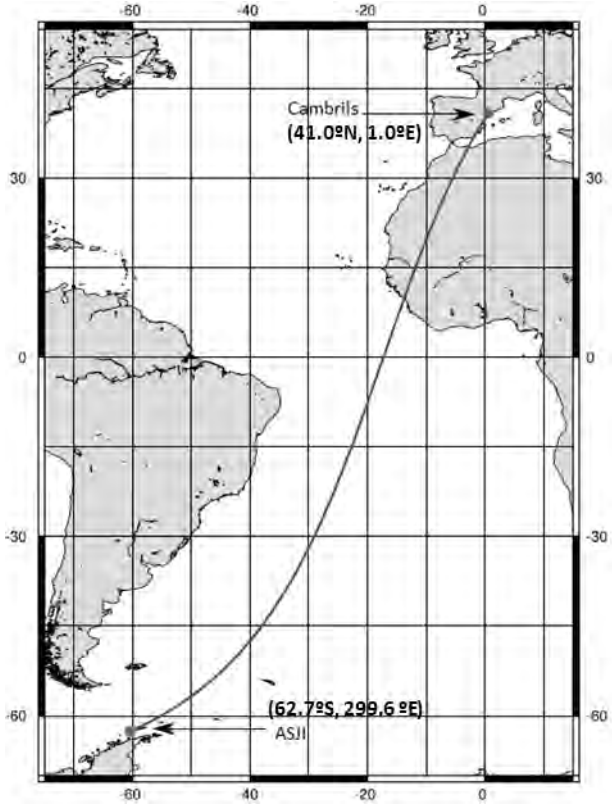

This paper is organized as follows. Section 2 describes all the measured parameters. Section 3 gives details of the communications hardware equipment between the Remote Geophysical Observatory and Spain. Section 4 explains the test design for narrowband and wideband sounding measurements through a long-distance HF link in 2014 campaign. Section 5 presents the results of the sounding measurements. Finally, section 6 contains the conclusions and the future work.

2. Measured Parameters

This section describes the main sensors located at the ASJI and its measurements.

2.1. Measurements of Geomagnetic Parameters

Measuring geomagnetic parameters is a complex task due to the fact that the physical magnitude to be measured is a vector. This requires an accurate determination of the magnitudes with respect to a fixed reference frame and skilled staff from both technical and scientific point of view.

The geomagnetic vector can be given in either three of coordinate systems based on a geographic reference: *i)* Cartesian: where X, Y, Z are the geographic north, east and altitude projections respectively. *ii)* Cylindrical: where H and Z are the horizontal and altitude projections and D is the declination angle between the geographic north and the magnetic field, establishing that the positive is towards east. *iii)* Spherical: where F is the total vector magnitude, D is the declination and I is the inclination angle between the horizontal projection and the magnetic vector itself, establishing positive downwards.

As far as the geomagnetic sensors are concerned, a D/I fluxgate theodolite (see Figure 2) is mounted in the first hut of the ASJI. This sensor permits a manual measurement of the Declination and Inclination angles of the vector magnetic field in absolute terms, which permits to discuss about the uncertainties of this instrument [6]. It consists of a fluxgate magnetometer bar mounted on the telescope of a non-magnetic theodolite.

Figure 2. The manual D/I fluxgate theodolite being manipulated by a specialist.

A variometer type δD/δI vector magnetometer (see Figure 3) is mounted in the second hut to measure automatically the variations of the magnetic field vector once per minute. It consists of two perpendicular pairs of Helmholtz coils the polarization of which allows measuring the Declination and Inclination variations with a Proton magnetometer located at their center [7]. The Proton magnetometer measures the total magnetic field intensity, F, when the coils are not polarized.

Figure 3. The δD/δI vector magnetometer deployed at the ASJI with the two perpendicular pairs of Helmoltz coils and the Proton magnetometer allowing to measure the variations of D and I.

The last of these three huts houses the electronic system controlling this automatic instrument. A new three-axis fluxgate magnetometer (see Figure 6) was added during the 2008 expedition. It is able to measure automatically the magnetic field variations from an analogue output sampling at both 1 and 0.1 Hz by the corresponding Analog to Digital Converter, ADC.

Figure 4. The three-axis automatic fluxgate magnetometer was added in 2008.

Once the raw data is processed, the definitive data set is sent to the World Data Centers becoming accessible to the scientific community. Nowadays, a real-time access to the data is provided through a satellite link thanks to the International Real-time Magnetic observatory (INTERMAGNET). Nevertheless, a reliable skywave link designed by La Salle and the Ebro Observatory is active as a backup. A future project is motivated to separate our sensor data from the INTERMAGNET link and transmit only through the autonomous skywave link which, besides, is becoming another interesting sensor of the ionosphere due to the capability of measuring the ionosphere performance.

2.2. Vertical incidence soundings of the ionosphere

A Vertical Incidence ionospheric Sounder (VIS) was installed at the ASJI (Figure 5) during the 2004-2005 survey to provide information of the ionospheric characteristics in this region. Data provided by the VIS is used to characterize the climatology of the ionosphere and to investigate the ionospheric effects caused under geomagnetically disturbed periods.

Figure 5. The VIS installed at the ASJI is the Advanced Ionospheric Sounder (AIS) developed by the *Instituto Nazionale di Geofisica e Vulcanologia* (INGV) of Rome, Italy. For more details about the ionosonde see [8].

The VIS located at the ASJI records a vertical incidence ionogram every 10 minutes. A ionogram is a graph that represents the time-of-flight for every radio frequency transmitted vertically and received after its reflection in the ionosphere. Figure 6 shows an example of a ionogram recorded by the VIS at the ASJI where the particular layers of the ionosphere can be seen clearly. For more details about the VIS soundings see [9].

Figure 6. An example of a ionogram recorded by the VIS at the ASJI where one can see clearly the particular layers of the ionosphere.

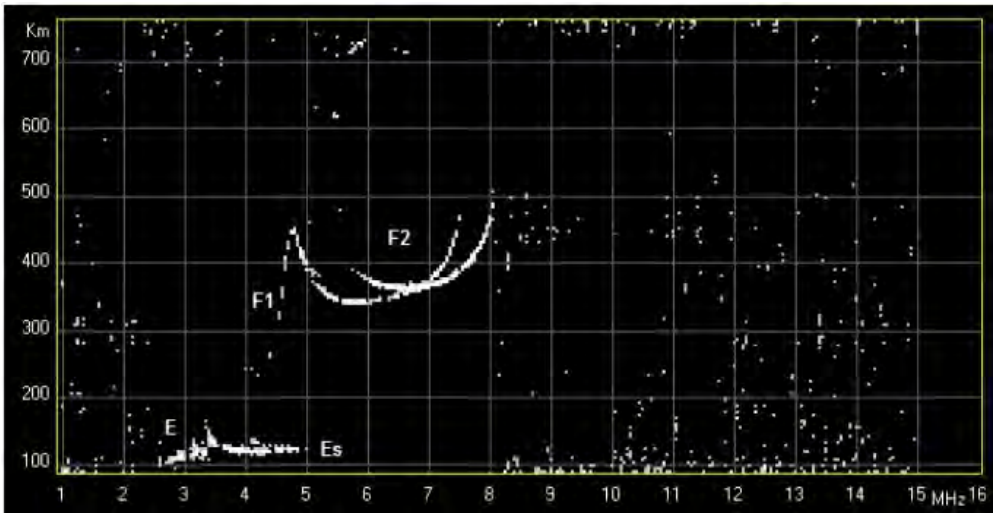

2.3. Oblique incidence soundings of the ionosphere

The oblique ionosonde is developed by La Salle to analyze and characterize the ionospheric channel between Antarctica and Spain [2]. It is used to obtain useful and key parameters for modeling the HF radio link; i.e, link availability, power delay profile of the channel and frequency dispersion. The soundings are carried out during the austral summer, when the ASJI is operative, the transmitter antenna is located at the ASJI (see Figure 7), and the receiver is located in Cambrils, Spain. More details of the HF data transmission are given in the section 4.

Figure 7. The antenna of the oblique ionosonde transmitter in the ASJI.

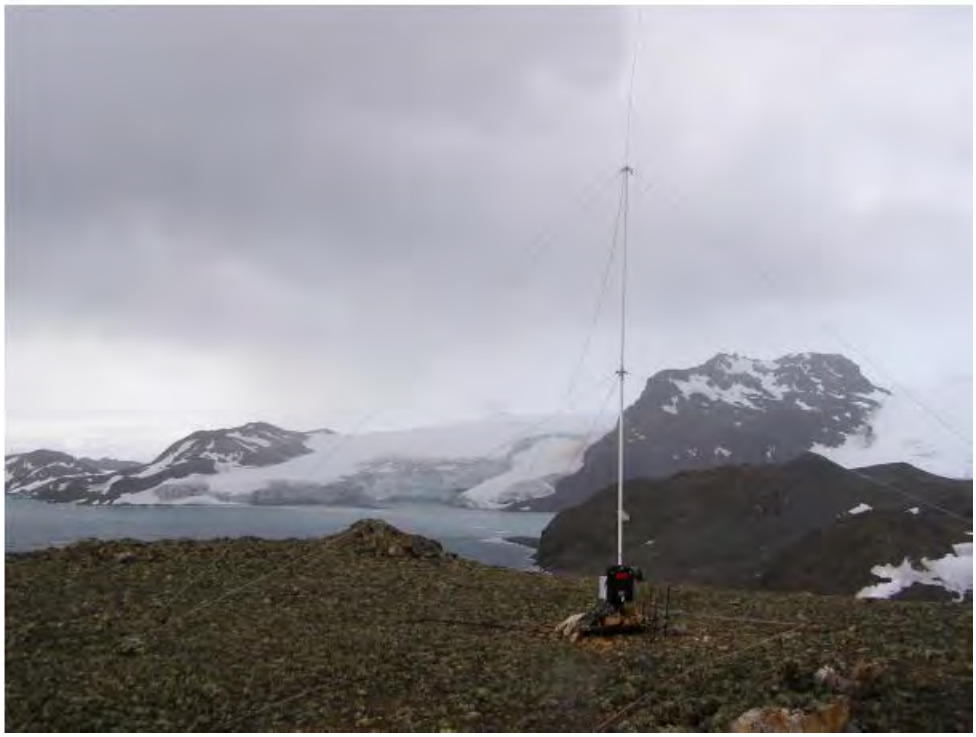

3. System Description

The hardware of the ionospheric channel sounder jointly with the oblique ionosonde and data transmission system has been designed in order to have an extended frequency range and to get the best frequency and time accuracy. Moreover, the whole transmission system has been entirely redesigned compared to the initial system deployed on the survey 2003-2004 [2]. It was upgraded with faster and more reliable equipment during the 2009-2010 expedition. As a result of the last improvement, the system is able to operate at a higher bandwidth up to 40 KHz and to sample at 100 ksps. Also the system was redesigned to be more flexible concerning the frequency and bandwidth selection for the soundings.

The main features of the transmitter and receiver hardware are described below.

3.1. Hardware of the Transmitter

The core is composed by an embedded PC with a Digital Signal Processing (DSP) unit inside which performs the tasks of controlling and configuring the system parameters. The main DSP unit is the XTremeDSP-IV from Nallatech and it includes 3 Xilinx FPGA[1] described below: *i)* a Virtex-II is responsible for clock configuration, *ii)* a Spartan-II handles the interface between the PCI bus and *iii)* a Virtex-4 which performs the software radio procedures. In order to perform these software radio operations, the Virtex-4 is equipped with two 14-bit ADC, two 14-bit DAC and all the arithmetic and peripheral drivers. Figure 8 shows a block diagram of the transmitter.

Figure 8. Scheme of the transmitter that consists of an embedded digital platform and different peripherals used to control the system and to improve the synchronization.

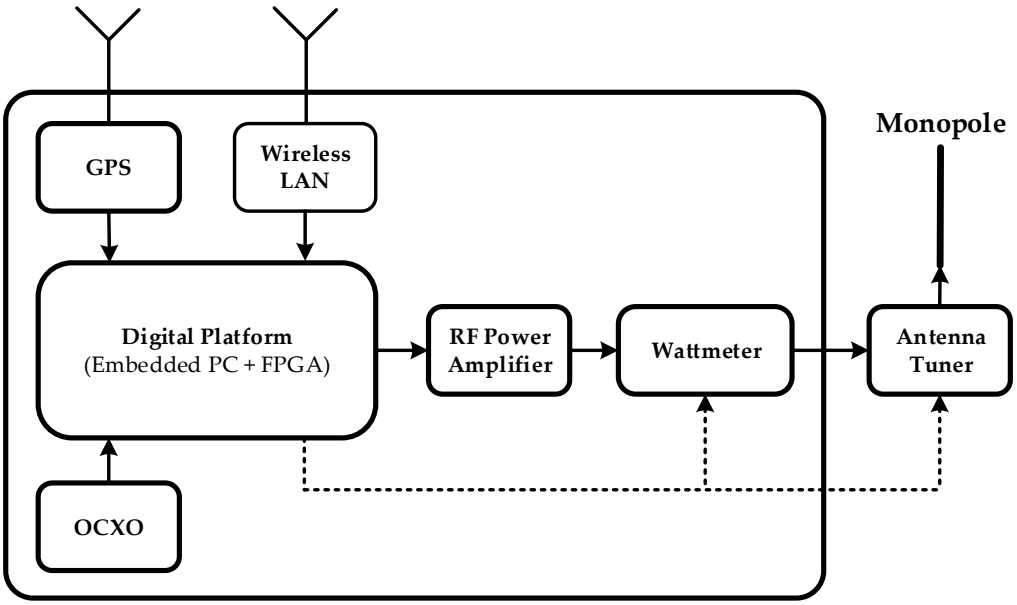

Moreover, a GPS unit is placed to make possible the time synchronization using the Pulse Per Second (PPS) signal, which makes possible to measure the propagation time of the wave with an accuracy of 1

[1] FPGA stands for Field Programmable Gate Array, and it is an integrated circuit to be configured after manufacturing.

μs. Also, a 100 MHz Oven Controlled Crystal Oscillator (OCXO) is installed in both transmitter and receiver in order to increase the frequency synchronization accuracy. The Wattmeter measures the forward and reverse transmitted power in order to notice severe impedance mismatch. And the FPGA is capable, thanks to its peripheral drivers, to switch off the amplifier in case of malfunctioning. The Antenna Tuner is used to tune semi-automatically the monopole antenna, which transmits the signal.

As far as the deployment is concerned, all the transmitter hardware is close to the antenna at the top of a hill near to the ASJI. All the electronics is sealed inside a watertight box which protects against severe weather conditions and provides electromagnetic shielding. The system is remotely accessed through a Wireless Local Area Network (WLAN) from the laboratory in the ASJI.

3.2. Hardware of the Receiver

An inverted-V antenna is used to get the signal in the receiver. As shown in Figure 9, the radio frequency signal is passed through a certain filtering and amplification process, and given next to the digital platform, which works the same way as the transmitter described above.

Moreover, the receiver also has an OCXO and a GPS to improve both frequency and time synchronization. A block diagram of the receiver is shown in Figure 9.

Figure 9. Scheme of the receiver that consists of several filtering stages and a digital platform with peripherals to improve synchronization.

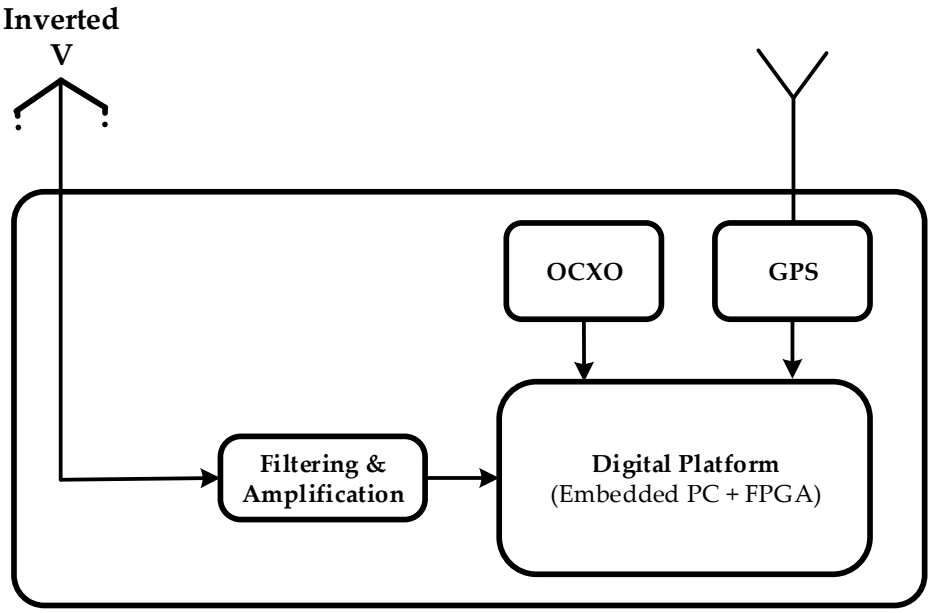

4. Data analysis

This section presents a detailed explanation of the test description and the analysis algorithms for narrowband and wideband oblique sounding.

4.1. Tests Description

The analysis of the sounding channel has been carried out in both narrowband and wideband. While the narrowband analysis focuses on channel availability and Signal to Noise Ratio (SNR), the wideband calculates the scattering function from the estimated channel impulse response, and then evaluates the multipath delay spread and Doppler spread.

The soundings are carried out during 24 hours a day (sessions) for a frequency carrier ranging from 2 to 30 MHz with steps of 500 Hz which corresponds to 57 sub-sessions. Every sub-session is divided into a frame to subdivide the time into two experiments, using 40 s for both of them. Finally, every session has a time slot of 22 minutes (called 'others' in the figure) to transmit the data from the sensors, and to test also new modulations schemes. The structure of the periodic experiment conducted during the 2013-2014 campaign can is described in Figure 10. These soundings were carried out for 25 days, between January 25th and February 18th.

The idle intervals are included in all frames to ensure the system to guarantee synchronization. The antenna tuning of 20W is required because the transmitter antenna is a monopole. The channel sounding is carried out in the processes called 'tone' and 'PseudoNoise (PN) sequence' during 10 s each.

Figure 10. Frame structure of the channel sounding.

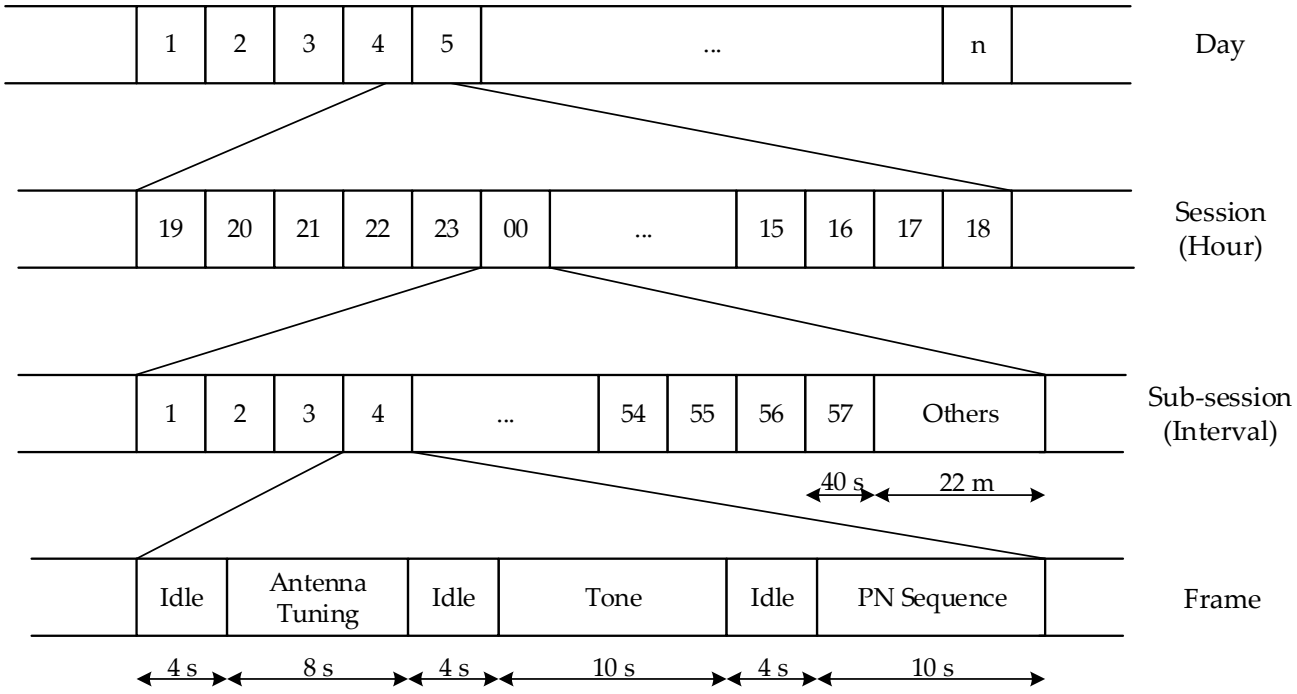

The narrowband analysis is necessary to characterize the channel in terms of SNR and availability, using a sine wave as the transmitted signal. This tone is transmitted during 10 s. The configuration parameters are detailed in Table 1.

Table 1. Configuration parameters and setup for the narrowband sounding in 2013-2014 survey.

Parameter	Value
Signal	Sine wave
Duration	10 s
Silence	4 s

The wideband analysis is necessary to characterize time and frequency dispersion in the channel. The transmitted signal for the wideband analysis is a PN sequence [10] with the configuration parameters detailed in Table 2.

Table 2. Configuration parameters and setup for the wideband sounding in 2013-2014 survey.

Parameter	Value
Sampling frequency	100 kHz
PN sequence length	127
Family of sequences	m-sequence
Chip frequency	5 kHz
Number of sequences per test	300

4.2. Narrowband Analysis

The narrowband analysis focuses on SNR and channel availability computation. The channel availability is defined as the probability of a link to reach a minimum SNR value and therefore achieving a certain quality of service (see [11] for more details). A minimum SNR value of 6 dB was specified to estimate the channel availability in a bandwidth of 10 Hz [2]. In order to improve the reliability of the detection system, due to the probability of high noise and interference, several techniques were developed in [3]. SNR is computed with the comparison between the received power measured during the tone intervals and the noise power measured during the idle periods.

The first step is to filter the signal to obtain a usable power profile, conducted in frequency domain with the Fast Fourier Transform (FFT). Afterwards, a windowing is applied to *i)* remove the non-desirable signals out of the reception frequency and *ii)* avoid creating transients from the impulsive interferences falling far away from the reception frequency [3] when an ideal filter is used. Previous tests showed that the Kaiser window presents a better smooth response [3].

The measurements of SNR can be distorted easily because of high level of interferences. To overcome this problem a time framing technique is used, consisting on dividing the tone interval in 10 smallest sub-intervals of 1 s each, and observing the evolution of the SNR along the whole interval (see in Figure 11).

Figure 11. Diagram of time framing technique for narrowband sounding.

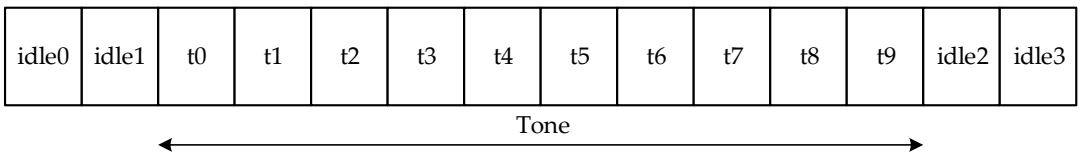

According to previous experiments, two SNR threshold values are defined, $Th_{Low} = 3dB$ and $Th_{HIGH} = 6dB$. Only those measurements that fulfill $SNR \geq Th_{Low}$ over 70% of the segments or $SNR \geq Th_{HIGH}$ over 50% of the segments are taken into account to estimate the SNR and channel availability. An estimation of the SNR result of February 17th is shown in Figure 12.

Figure 12. SNR of February 17th (in dB) over a bandwidth of 10 Hz, in which the regions of day, night, sunrise and sunset can be appreciated

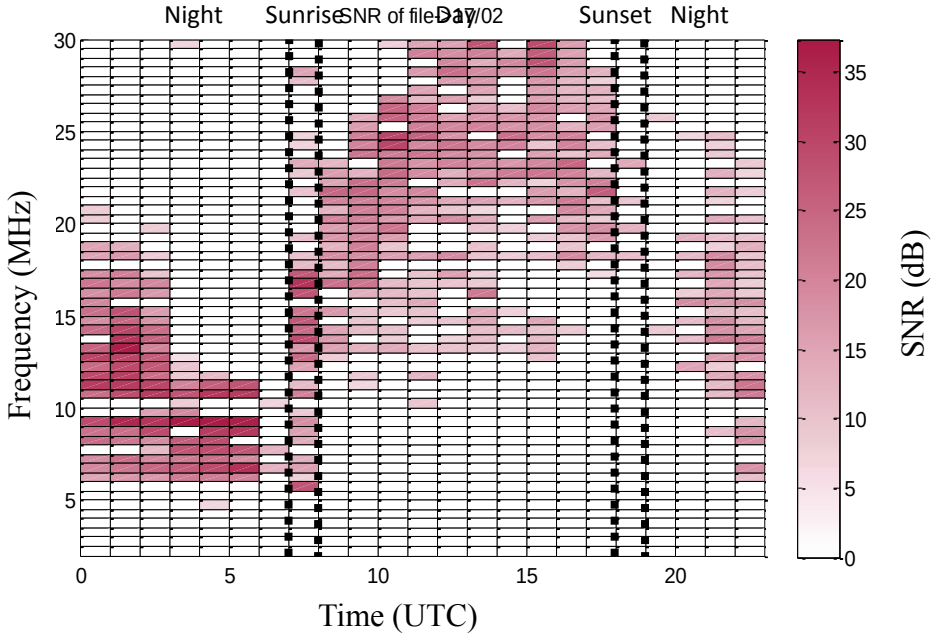

4.3. Wideband Analysis

The wideband analysis is performed sending PN waveforms with good cyclic cross-correlation characteristics, therefore using M-sequences [12]. The computation process for the wideband sounding is detailed in Figure 13.

Figure 13. Diagram of the computation process for wideband channel sounding.

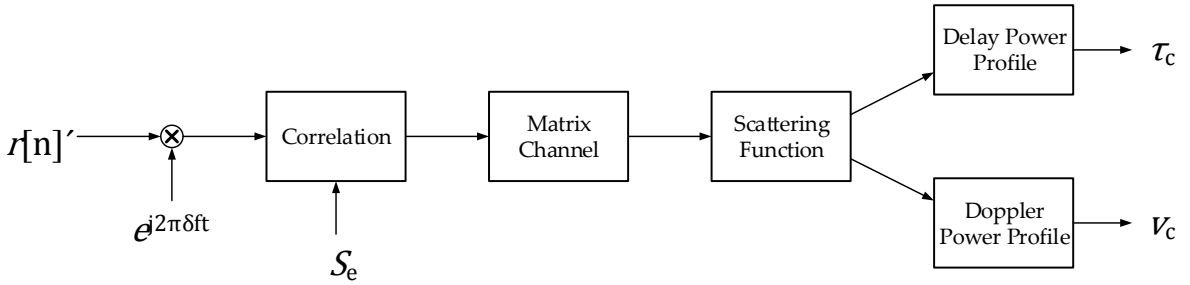

The wideband analysis is crucial to characterize time and frequency dispersion in the channel. First, the received signal *r[n]* (with the characteristics described in 4.1) is correlated with the original PN sequence S_e. The correlation function is calculated as

$$\phi_{r,S_e}[n] = \sum_{k=0}^{N_e-1} r[n+k]S_e[k] \quad (1)$$

where N_e is the length of the PN sequence. Hence, the channel impulse response $h[n,\tau]$ can be written as:

$$h[n,\tau] = \phi_{r,S_e}[nlN_c + \tau] \quad (2)$$

where τ is the delay variable, l is the number of chips and N_c is the number of samples per chip. From equation 2, the following parameters are calculated: scattering function, composite multipath spread and composite Doppler spread. The scattering function $R_s[\tau,\upsilon]$ is calculated as the FFT of the channel impulse response [12].

$$R_h[\xi,\tau] = \sum_{\xi} h^*[n,\tau]\, h[n+\xi,\tau] \quad (3)$$

$$R_s[\tau,\upsilon] = \sum_{\xi} R_h[\xi,\tau]e^{-j2\pi\xi\upsilon} \quad (4)$$

Both the composite multipath spread and the composite Doppler spread are calculated from the data obtained in the scattering function $R_s[\tau,\upsilon]$. Let $[\tau_1,\tau_2]$ be the multipath observation window, and $[\upsilon_1,\upsilon_2]$ the Doppler spread observation window. Consequently, both multipath power profile is defined as

$$\phi[\tau] = \sum_{\upsilon=\upsilon_1}^{\upsilon_2} R_s[\tau,\upsilon] \quad (5)$$

And the Doppler power profile is defined as

$$\phi[\upsilon] = \sum_{\tau=\tau_1}^{\tau_2} R_s[\tau,\upsilon] \quad (6)$$

In this work, the window have been set to [-3.5,3.5] (ms) and [-2.5,2.5] (Hz) respectively, due to maximum delay and Doppler spread values obtained in previous tests [2].

Next, the spread parameters are calculated. The multipath spread is measured from the multipath power profile as the 80% of the power spread [2]. This parameter is named composite multipath spread (t_{eff}) and was defined in [13]. The same way, the Doppler spread is measured from the Doppler power profile as the 80% power spread. It is named composite Doppler spread (u_{eff}), and it was defined in [14].

In Figure 14 we can observe the performance of the wideband sounding of the February 1st 2014, at 00 UTC for 13 MHz of carrier frequency. In Figure 14.a the channel response $h[n,\tau]$ is plot, and the channel variations along time can be observed. In Figure 14.b, the scattering function has been calculated using $h[n,\tau]$, and $R_s[\tau,\upsilon]$ is obtained after performing the FFT. In Figure 14.c, the multipath power profile is observed for the previously defined time window, and finally, in Figure 14.e, the Doppler power profile is plotted for the previously defined frequency window.

Figure 14. Wideband channel response and measures for February 01st 2014 at 07 UTC with 13 MHz of carrier frequency: **(a)** normalized channel response $h[n,\tau]$, **(b)** normalized scattering function $R_s[\tau,\upsilon]$, **(c)** multipath power profile (in ms), **(d)** the integral of the multipath power profile to calculate delay spread (in ms), **(e)** Doppler power profile (in Hz), and **(f)** the integral of the Doppler power profile to calculate Doppler spread (in Hz).

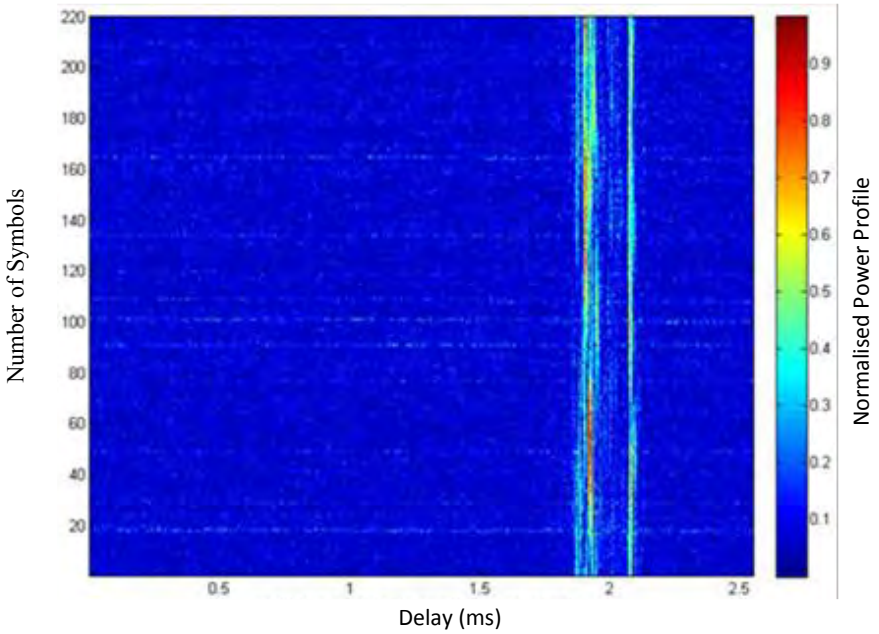

(a)

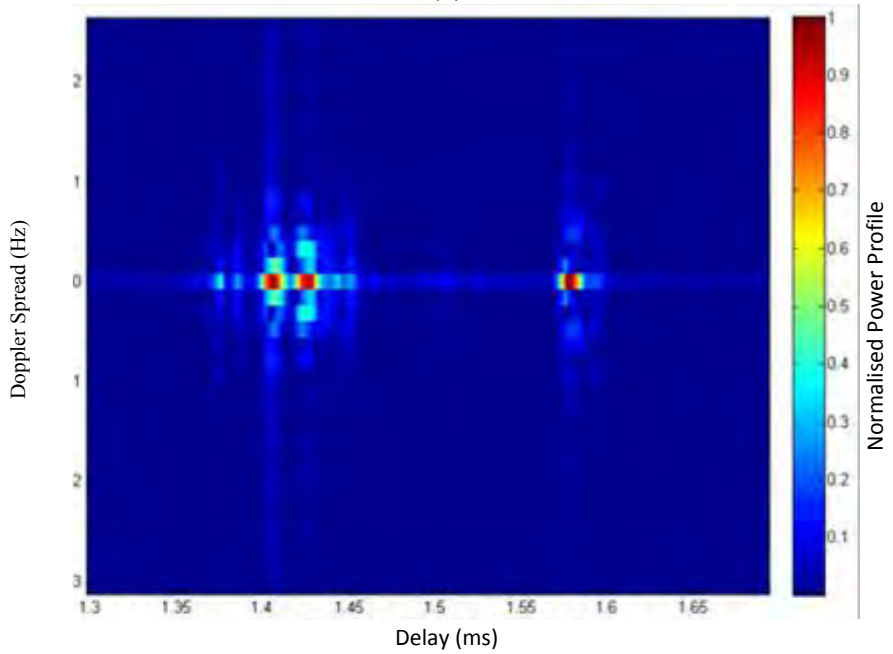

(b)

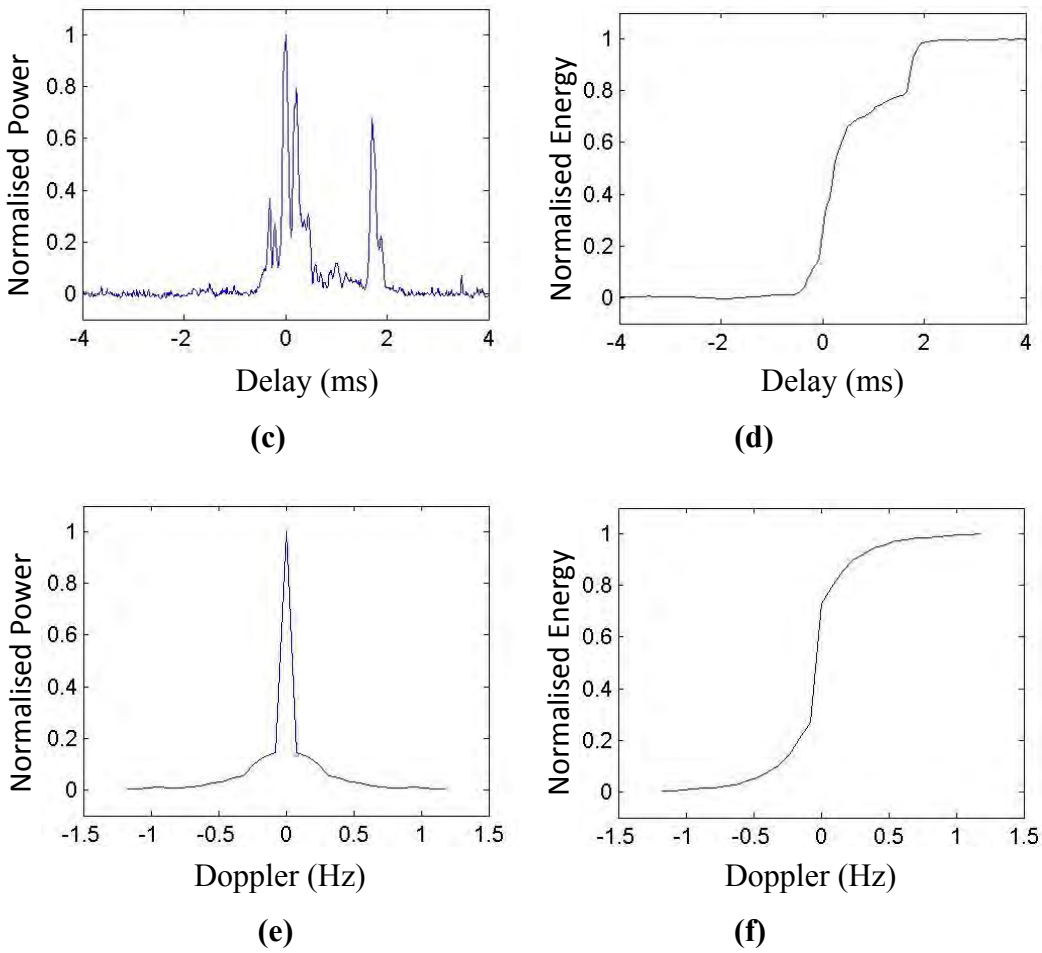

5. Results

5.1. Narrowband Results

The results of narrowband analysis shown in Figure 15 represent the average plot of the channel availability for the survey. Figure 15 depicts the channel availability for frequencies ranging from 2 to 30 MHz as function of time. The Frequency of Largest Availability (FLA) for a particular time is shown as dashed line. Four different zones can be distinguished: day, night, sunrise and sunset.

During the day interval, from 08 UTC to 17 UTC, the frequencies ranging from 20 to 30 MHz present the better performance in terms of SNR. For the sunset period, around 18 UTC, the interval of frequencies that performs best falls linearly with the time between 20 and 30 MHz to 10 and 20 MHz. The night period is defined from 19 UTC to 06 UTC and the frequencies ranging from 6 to 15 MHz show the best results. Finally, for the sunrise, which is the period defined around 07 UTC, its best operation frequencies increase linearly with the time from frequencies between 6 and 15 MHz to frequencies ranging from 20 to 30 MHz.

In consequence, we can conclude the best reflective frequencies during the daytime are the highest frequency range, the nighttime the lowest one, and sunrise and sunset are regions of switching between these periods of time performing in an unstable condition for all frequencies. It is worth noticing a drop in the FLA after sunrise (9-10 UT) and a post sunset jump (20-21 UT) of the FLA. These effects deviate from the expected smooth transition of the FLA from nighttime to daytime conditions and vice versa.

Figure 15. Channel availability of the campaign 2014 measured during the austral summer, from January 25th to February 18th.

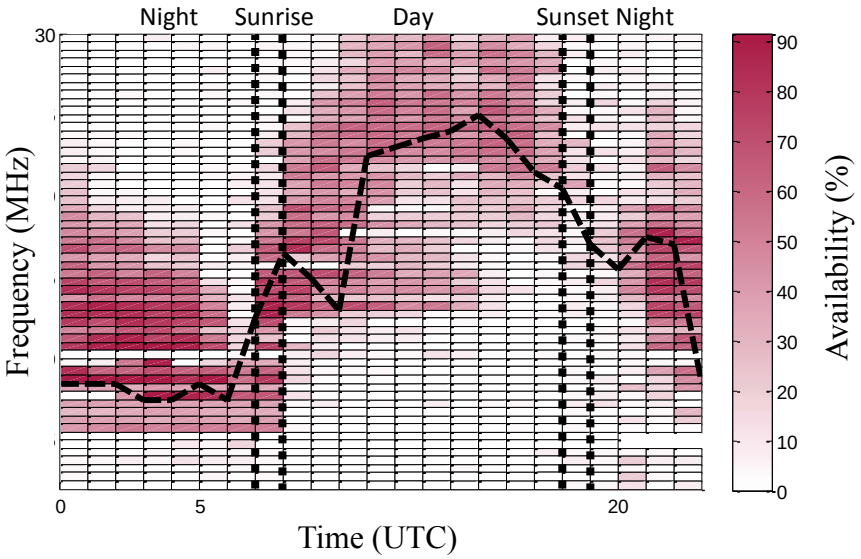

5.2. Wideband Results

The results of wideband analysis are shown in Figure 16. Figure 16.a and Figure 16.c, present the mean delay spread and the mean Doppler spread, from which one can distinguish four different performance zones also: day, night, sunrise and sunset [13]. Figure 16.b and Figure 16.d show the standard deviation for the delay spread and the Doppler spread respectively.

During day interval, from 08 UTC to 17 UTC, high frequencies ranging from 20 MHz to 30 MHz show the higher delay spread and Doppler spread of all measures. This means that the channel is available for a wide range of frequencies but its channel response is varying and unstable, and the intersymbol interference caused by a long channel response will be an important parameter for the modulation design.

Sunset time, around 18 UTC, presents an irregular performance when comparing high frequencies and low ones, but low frequencies start performing better while high frequencies decrease its availability. Also sunrise, around 07 UTC shows unstable performance in terms of wideband availability.

Nighttime, shown both on the right and on the left of Figure 16, ranging from 19 UTC to 06 UTC, present the best measurements in terms of channel availability and parameters. Best frequencies are around 10 MHz, despite channel is available until 20 MHz. Delay spread mean values are around 2 or 3 ms, with low deviation, and maximum Doppler spread values are around 0.7 Hz.

Figure 16. Mean value for the Delay Spread in ms **(a)**, standard deviation for Delay Spread in ms **(b)**, mean value for Doppler Spread in Hz **(c)** and standard deviation for Doppler Spread in Hz **(d)**.

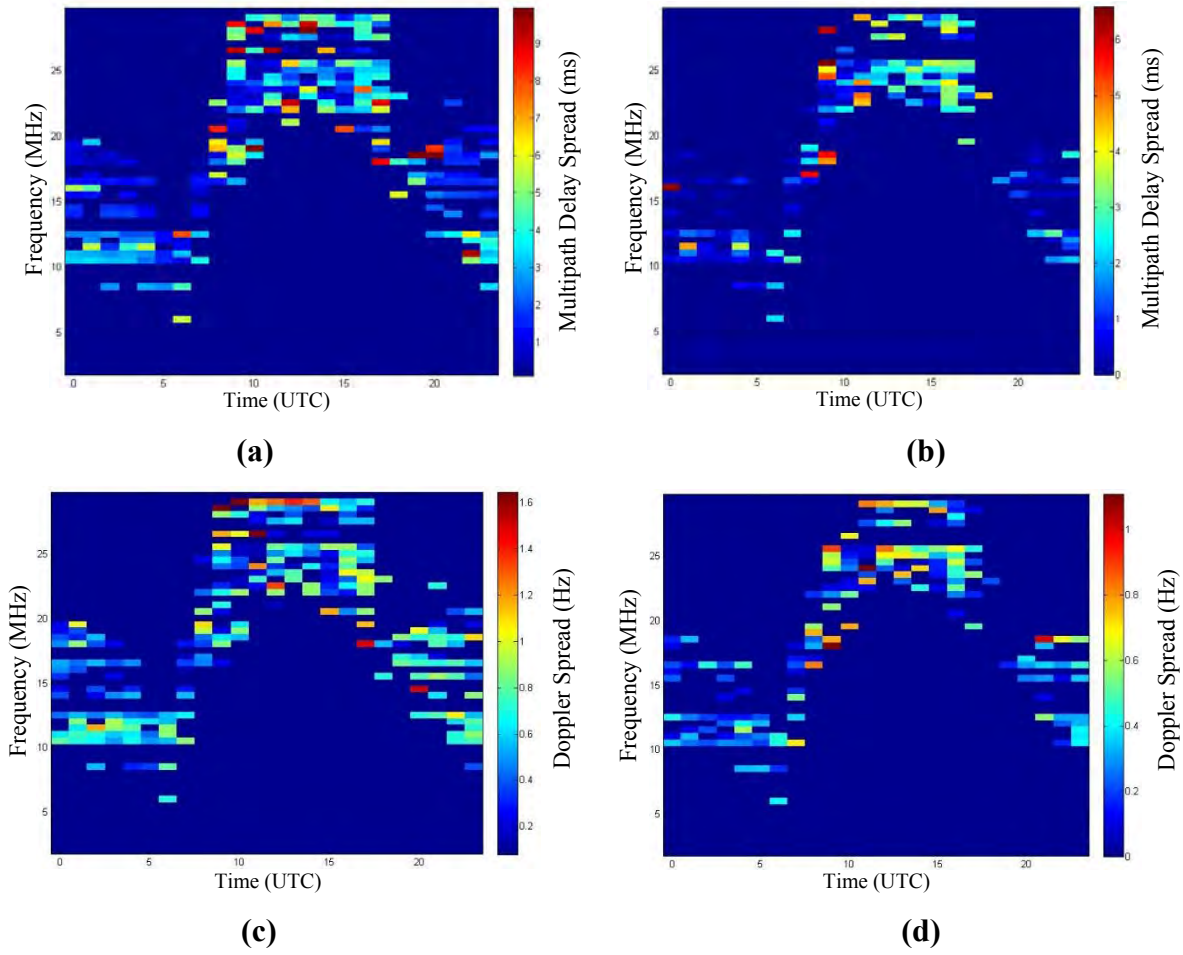

5.3. Discussion

Narrowband and wideband analysis conducted show similar results in terms of availability depending on the hour of the day. Nighttime is the best reception time, using frequencies from 8 MHz to 20 MHz. Narrowband presents its best SNR results while wideband shows its smaller delay spread and Doppler spread measurements.

These results allow us to conclude that for the best hours and frequencies, high throughput modulations like OFDM should be used, in order to increase the bit rate of the communication. Delay spread and Doppler spread won't worsen the results in a severe way, according to the measured values. Despite of that, the OFDM modulation should be designed taking into account coherence time and coherence bandwidth calculated using the measured parameters of Doppler spread and delay spread. Finally, at sunrise, sunset and daytime, a more robust modulation should be used. Direct sequence spread spectrum could be a good option assuming lower throughput, but assuring a more robust communication against channel variations or fadings.

6. Conclusions

This paper presents the main results of the oblique sounding measurement recorded during the campaign of 2014 with a transmitter placed in the Remote Geophysical Observatory of the ASJI and the receiver located in Cambrils (Spain). The sounding has been carried out for both narrowband and wideband to characterize the channel in terms of SNR, availability, multipath delay spread and Doppler spread. These measurements of the long haul link improve the knowledge of the performance of the ionospheric channel 12760 km long, and allow us to fully define the physical layer to send the data of the remote sensors deployed among the island from the Antarctica to Spain.

The values measured of narrowband and wideband confirm that both soundings show similar results in terms of availability depending on the hour of the day and of the frequency. Furthermore, the wideband analysis present results of the period of the day that is more suitable for data transmission, because the channel shows a good performance (with low Doppler spread and low delay spread). It also describes the hours of the day when the channel measurements, despite showing some availability, present worst results. This leads us to design a proper robust modulation for those hours, while the best transmission hours and frequencies use high throughput modulation techniques.

The future work is focused on two main goals. The first one is the study of the historical series of Doppler spread, delay spread and SNR for the entire solar cycle (around 11 years), using part of the data we have already measured. We are also working in including the number of paths in the receiver as a channel measurement in the wideband analysis. The second goal is to end the design of the HF modem; the channel characteristics shown in this paper are crucial for a proper design of the modulation, coding and interleaving of the physical layer of the modem.

Acknowledgments

This research has been supported by the Spanish Government under projects CTM2010-21312-C03-03 and –C03-01. In addition to the authors of this paper, the following people have been part of the research groups of these projects: Ahmed Ads, Raúl Bardají, Estefania Blanch, Oscar Cid, Juan José Curto, Simó Graells, Miguel Ibáñez, Joan Mauricio, Santiago Marsal, Joan Ramon Regué, Xavier Rosell, Martí Salvador, Antoni Segarra, José Germán Solé and Joan Miquel Torta.

Author Contributions

Marcos Hervás analyzed and wrote the part of the paper related with the narrowband soundings. Dr Rosa Ma Alsina-Pagès had the idea to write this paper, and analyzed and wrote the wideband sounding study in this paper. Ferran Orga wrote the introductory part, the measured parameters and the system description of this paper. Dr Joan Lluis Pijoan has been the principal investigator of project –C03-03, he has been involved in the part of channel sounding and testing of advanced modulations and reviewed the paper. Dr David Badia installed the transmission system in Antarctica, installed the receiver system in Spain and reviewed the paper. Dr David Altadill has been the principal investigator of project –C03-01 and coordinator of both projects and he has reviewed the paper.

Conflicts of Interest

The authors declare no conflict of interest.

References and Notes

1. Torta, J.M.; Gaya-Piqué, L.R.; Riddick, J.C.; Turbitt, C.W. A Partly manned geomagnetic observatory in Antarctica provides a reliable data set. *Contrib*. *Geophys*. *Geodesy Geophys*. *Inst*. *Slov*. *Acad*. *Sci*. **2001**, *31*, 225–230.
2. Vilella, C.; Miralles, D.; Pijoan, J.L. An Antarctica-to-Spain HF ionospheric radio link: Sounding results. *Radio Sci*. **2008**, doi:10.1029/2007RS003812.
3. Ads, A.G.; Bergadà, P.; Vilella, C.; Regué, J.R.; Pijoan, J.L.; Bardají, R.; Mauricio, J. A comprehensive sounding of the ionospheric HF radio link from Antarctica to Spain. *Radio Sci*. **2012**, doi:10.1029/2012RS005074.
4. Hervás, M.; Pijoan, J.L.; Alsina-Pagès, R.M.; Salvador, M.; Badia, D. Single-carrier frequency domain equalization proposal for very long haul HF radio links. *Electron*. *Lett*. **2014**, 17, 1252-1254, doi: 10.1049/el.2014.1184.
5. Bergadà, P.; Alsina-Pagès, R.M.; Pijoan J.L.; Salvador, M.; Regué, J.R.; Badia D.; Graells, S. Digital transmission techniques for a long haul HF link: DS-SS *vs.* OFDM. *Radio Sci*. **2014**, doi:10.1002/2013RS005203.
6. Marsal, S.; Torta, J.M. An evaluation of the uncertainty associated with the measurement of the geomagnetic field with a D/I fluxgate theodolite. *Measur*. *Sci*. *Technol*. **2007**, *18*, doi:10.1088/0957-0233/18/7/046.
7. Marsal, S.; Torta, J.M.; Riddick, J.C. An assessment of the BGS δDδI vector magnetometer. *Publs*. *Inst*. *Geophys*. *Pol*. *Acad*. *Sci*. **2007**, *99*, 158–165.
8. Zuccheretti, E.; Bianchi, C.; Sciacca, U.; Tutone, G.; Arokiasamy, J. The new AIS-INGV digital ionosonde. *Ann*. *Geophys*. **2003**, *46*, 647–659.
9. Bergadà, P.; Deumal, M.; Vilella, C.; Regué, J.R.; Altadill, D.; Marsal, S. Remote sensing and skywave digital communication from Antarctica. *Sensors* **2009**, doi:10.3390/s91210136.
10. Golomb, S. *Shift Register Sequences*; Holden-Day: San Francisco, USA, 1967.
11. Goodman, J.; Ballard, J.; Sharp E. A long-term investigation of the HF communication channel over middle- and high-latitudes paths. *Radio Sci*. **1997**, 32, 1705–1715, doi:10.1029/97RS01194.
12. Proakis, J. *Digital Communications*, 4th ed.; McGraw Hill: Boston, MA, USA, 2000.
13. Angling, M.J.; Davies N.C. An assessment of a new ionospheric channel model driven by measurements of multipath and Doppler spread. In Proceedings of the 1999 IEEE Colloquium on Frequency Selection and Management Techniques for HF Communications, London, UK, 29–30 March 1999.
14. Warrington, E.M.; Stocker A.J. Measurements of the Doppler and multipath spread of the HF signals received over a path oriented along the midlatitude trough. *Radio Sci*. **2003**, *38*, doi:10.1029/2002RS002815.

Anexo E

QPSK demodulation using Cellular Neural Networks

QPSK demodulation using Cellular Neural Networks

Rosa Ma Alsina-Pagès, Marcos Hervás, Xavier Vilasís-Cardona, Mireia Vinyoles-Serra,
GR-SETAD, La Salle, Universitat Ramon Llull, Barcelona, Spain 08022
Email: xvilasis@salle.url.edu

***Abstract*—We show how QPSK signals can be demodulated using a simple discrete time two neuron CNN, on real data of a long haul radio link to Antarctica.**

I. Introduction

The two neuron cellular neural network (CNN) is the simplest CNN system considered has shown a rich complex behaviour (see for instance [1] and [2] and references therein). Under suitable conditions, the dependence of the steady state of the oscillator upon the external inputs suggests its use as a classifier. This paper aims at presenting an application for this particular feature: the demodulation of the QPSK digital encoding for hostile transmission channels. In effect, demodulation can be understood as a classifing problem in the in-phase/quadrature space, in which the coding for each of the four symbols has to be identified. Usually, this classification is very simple and so no sophisticated method is required, but for hostile channels, in which noise, interference and multipath delay spread may prevail over signal, it becomes a challenging problem. An adequate tuning of the two neuron system parameters, allows for a very simple demodulation algorithm in the form of a digital multi-input multi-output filter. The tuning may be devised to be time-varying in order to make the system adaptive to cope with the channel characteristics.

This note includes an essencial recall of the convergence map of the two neuron oscillator, a description on the long haul HF link to Antarctica, a recall of QPSK modulations and some results on the CNN demodulation.

II. Two neuron CNN

Two neuron Cellular Neural Network consists on two different cells locally connected each other via some parameters usually called weights. The state of each neuron is defined by the system equations (Eq. 1). It determines the state of a cell depending on its initial state $x_i(0)$, a linear combination of the external inputs u_0, u_1, a threshold I, and the output values y_0, y_1, and the external influence is described by the B-transformation (2). This dynamical system, yet simple, has an interesting behavior from the convergence point of view. Depending on the system parameters $(s, p_+, p_-, I, b_+, b_-, b_0)$ and the external inputs u_i, the final outputs y_i can take binary values, can be closed curves or even can behave in a chaotic manner. Nevertheless, we are interested now in the binary outputs because we want to relate CNN with hypothesis testing. If inputs are constant in time and $p_+ = p_- = p$, there exist a Lyapunov function [3] and if $s > 1$, outputs are binary, and belong to the set $\mathcal{S} = \{(+1,+1),(+1,-1),(-1,-1),(-1,1)\}$.

978-1-4799-6007-1/14/$ 31.00

For our application, a discrete time implementation is preferred [4],

$$\begin{cases} x_0(k) = sy_0(k) + p_+ y_1(k) + u'_0, \\ x_1(k) = sy_1(k) + p_- y_0(k) + u'_1, \end{cases} \tag{1}$$

with $y_i(k+1) = \mathrm{Sgn}\ x_i(k)$, $i = 0, 1$ and

$$\begin{pmatrix} u'_0 \\ u'_1 \end{pmatrix} = \begin{pmatrix} b_0 & b_+ \\ b_- & b_0 \end{pmatrix} \begin{pmatrix} u_0 \\ u_1 \end{pmatrix} + \begin{pmatrix} I \\ I \end{pmatrix} \tag{2}$$

The final outputs depend on the values of the u's defining the so called convergence map (Fig 1).

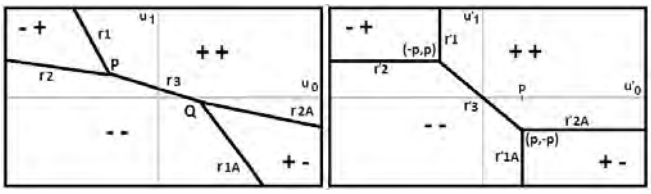

Fig. 1. Convergence map for a positive parameter p in the u-plane and u'-plane respectively.

III. Long Haul Antarctic HF Link and QPSK modulation

Our group has been investigating the HF channel between the Spanish Antarctic Station (SAS) on Livingston Island (62.5S, 60.4W) and the Ebre Observatory (EO) in Roquetes (40.8N, 0.5E) in Spain for more than 10 years. It is a very long transmission path (12700 km, with 4-5 hops [8]) with a transmitted power of only 200W and very simple antennas both at the transmission and reception side, due to enviromental restrictions. These facts results in very low or even negative Signal to Noise results (SNR) at the receiver [6], [7]. The data link is established by means of the ionosphere, a layer of the upper atmosphere that is ionized by solar radiation.

PSK modulations are digital modulations that convey data by changing the phase of the reference signal, i.e. the carrier wave [5]. QPSK uses four points on the constellation diagram, all in a circle. With four different phases, QPSK can encode two bits per symbol.

QPSK modulation is used in the Antarctic link to increase the bitrate compared to PSK in SC-FDE (Single Carrier Frequency Domain Equalization) modulations, which is a frequency-division multiple access scheme. The choice of SC-FDE is due to its low PAPR (Peak to Average Power Ratio) and great robustness against fadings. In the past, other wideband modulations as DS-SS or OFDM were already tested [10].

SER (max 1)	prob MMSE	prob ZF	prob CNN
0.00	0.6154	0.4872	0.5385
0.03	0.8462	0.6667	0.7179
0.06	0.9231	0.7949	0.8205
0.1	1	0.9231	0.9487

TABLE I

IV. Tests and results

Tests have been run over a SC-FDE modulation using a QPSK scheme, to double the transmitted bits with the same bandwidth. The modulation and link characteristics are the following: 12700 km ionoshperic link, 200 W power transmission, maximum multipath power spread of 3.5 ms, maximum Doppler spread of 2.5 Hz and average coherence time 300 ms, equal to around 120 symbols QPSK. The bandwidth used in the modulation is 400Hz and block time is 30 ms, symbol time is 1/400 s. Conventional demodulation [5] would apply equalization schemes below the coherence time (every 200 ms approx.), in order to correct channel variations over the signal, and demodulate afterwards. Our proposal focuses in demodulating without applying an equalization scheme to divide the in-phase/quadrature space with the CNN convergence map into regions corresponding to the four different symbols. We expect to save computational load and errors when the pilot symbols used to equalize get bad receptions. We compare the results of the CNN demodulation scheme with two frequency linear equalizers: MMSE (Minimum Mean Square Error) estimator and ZF (Zero Forcing) equalizer [5]. The study of the mean and the variance of the received data characteristics lead us to define the B-tranformation to be a rotation (Figure 2 left). This rotation puts the mean of each received symbol in the center of a quadrant, as the original QPSK design. The results compare the error in symbols when demodulation using MMSE equalization, ZF equalization and CNN QPSK demodulation scheme.

The symbol error rate for an ideal scenario (A) is zero, no symbol is incorrectly identified. The symbol error rate (SER) for MMSE and ZF is 0.0250 and 0.1125 respectively. This is an example of the situation where equalization force symbol changes due to channel performance and the error in demodulation increases.

Figure 2 shows scenario B results: the received QPSK data on the left, and the phase rotation and symbol separation using the CNN on the right, with the symbols received during 200 ms. Scenario B has more dispersion of measured values at the receiver than scenario A. The mean for the training set is less representative of all the received data and the variance is higher. The CNN adjustes the classifier for these new parameters and the obtained SER is 0.0250, against the same value for MMSE (0.0250) and 0.0750 for ZF equalization.

The symbol error rate comparison between the two equalizers and the CNN demodulation are shown in table I for a coherence time considered of 200 ms. The CNN demodulator has been tested in several data tests performed in February 22nd 2013 in order to compare its performance to two baseline

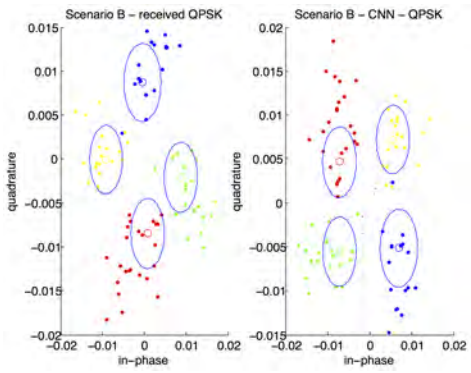

Fig. 2. Sc. B. Each color corresponds to a different symbol. The small circle is the mean value for the training set, and the big one responds to its variance.

linear equalizers aforementioned. Table I shows the probability of obtaining a SER better or equal to each value in the left column for the three methods. The best performance is presented by MMSE estimator, followed by the CNN demodulator and last the ZF equalizer. Despite that the best results correspond to MMSE estimator, the computational charge for the CNN demodulator is lower, and presents a real alternative to the classic equalization technique.

V. Discussion

These preliminary results are just a proof of concept for the idea and how competitive can it become. In fact, the ionospheric channel is time varying. This time variation can easily be accomodated in the CNN algorithm by tracking the center positions and adapting the CNN parameters, by means of evaluating quality measurements of the QPSK constellation received. Besides, a full system devised to work on the CNN principle can be devised and shall deliver much better accuracy results, besides the gain in computing power.

Acknowledgments

This work has been funded by the Spanish MINECO under the project CTM2010-21312-C03-03.

References

[1] Vilasís, X. & Vinyoles, M. [2010] "Two neuron CNN : search for limit cycles", *Int. J. of Bifurcation and Chaos* Vol 20, pp. 1137-1173.
[2] Vilasís, X. & Vinyoles, M. [2011] "Classifying with a two neuron CNN", *Int. J. of Bifurcation and Chaos* Vol 22, pp. 1-28.
[3] Chua, L.O & Yang, L. [1998] "Cellular Neural Networks: Theory," *IEEE Trans. Circ. Syst.*, Vol. 358.
[4] Harrer, H. & Nossek, J.A. [1992] "Discrete Time Cellular Neural Networks" *Int J. of Circuit Theory and Applications* Vol 20, pp. 453-457.
[5] Proakis, J. [2000], *Digital Communications*, McGraw Hill.
[6] Vilella, C. Miralles, D. and Pijoan, J. [2008] "An Antarctica-to-Spain HF Ionospheric Radio Link: Sounding Results", *Radio Science*, *43*.
[7] Vilella, C. *et. al.* [2009], "Vertical and Oblique Ionospheric Soundings over a Very Long Multihop HF Radio Link from Polar to Midlatitudes: Results and Relationships", *Radio Science*, *44*.
[8] Perkiomaki, J. [2003-2013], HF Propagation Prediction and Ionospheric Communications Analysis, *www.voacap.com*.
[9] Ads, A. et. al., [2013], "A Comprehensive Sounding of the Ionospheric HF Radio Link from Antarctica to Spain", *Radio Science*, *48*.
[10] Bergada, P. et. al., "Digital Transmission Techniques for a Long Haul HF Link: DS-SS vs. OFDM", *to appear in Radio Science*.

Universitat Ramon Llull

Aquesta Tesi Doctoral ha estat defensada el dia ____ d _____ de ____

al Centre **Escola Tècnica Superior d'Enginyeria Electrònica i Informàtica La Salle**

de la Universitat Ramon Llull

davant el Tribunal format pels Doctors sotasignants, havent obtingut la qualificació:

President/a

_____

Vocal

_____

Vocal

_____

Vocal

_____

Secretari/ària

_____

Doctorand/a

Marcos Antonio Hervás García

C. Claravall, 1-3
08022 Barcelona
Tel. 936 022 200
Fax 936 022 249
E-mail: urlsc@sec.url.es
www.url.es